Modeling and Simulation of Solar Chimney Power Plant with and without the Effect of Thermal Energy Storage Systems

THESIS SUMMITTED TO

THE SCHOOL OF GRADUATE STUDIES

ADDIS ABEBA INSTITUTE OF TECHNOLOGY

IN PARTIAL FULFILMENT OF THE REQUIREMENT FOR DEGREE OF

MASTERS OF SCIENCE IN MECHANICAL ENGINEERING

(WITH SPECIALIZATION IN THERMAL ENGINEERING)

Thesis Advisor: Dr.-Ing. Abebayehu Assefa

By: Robera Daba

September 2011

Addis Ababa Institute of Technology

School of Graduate Studies

Mechanical Engineering Department

Modeling and Simulation of Solar Chimney Power Plant with and without the Effect of Thermal Energy Storage Systems

BY

Robera Daba

Approved by the Examining Board:

_____ _____

Chairman, Department's Graduate Committee

_____ _____

Advisor

_____ _____

External Examiner

_____ _____

Internal Examine

Table of Contents

LIST OF FIGURES

LIST OF TABLES

ACKNOWLEDGMENTS

First of all I would like to praise God for His help and guidance throughout my life. I would like to express my sincere gratitude to my advisor Dr.-Ing Abebayehu Assefa for giving me the opportunity to work on this project and for his guidance and encouragement without which this work could have not been completed. He has been a constant source of inspiration throughout my study period.

I am also grateful to Ato Getachew Shunki for the kind support rendered to me on different occasions.

Last but not list, I would like to thank my family and my lovely friends Askalech Daba, Yohanis Mitiku and Abera Berecha who are always beside me and played a great role in the completion of my work.

ABSTRACT

A solar updraft tower power plant – sometimes also called 'solar chimney' or just ‘solar tower’ – is a solar thermal power plant utilizing a combination of solar air collector and central updraft tube to generate a solar induced convective flow which drives pressure staged turbines to generate electricity.

Several technologies exist that can convert solar energy into electrical energy. The solar chimney is part of the solar thermal groups of solar conversion technologies. Of these technologies the solar dish has the highest energy efficiency (the current record is a conversion efficiency of 30% of solar energy). Solar trough plants have been built with efficiencies of about 20%. The solar chimney has an efficiency of less than 2%. However, due to its greater scale and simplicity, the solar chimney may have an economic efficiency approaching or exceeding that of the other methods.

To improve efficiency of the plant thermal storage system is used. Thermal storage system improves the power output by re-shaping the profile of the power output. The most commonly suggested method for creating energy storage is to place extra thermal mass under the collector in the form of black containers of water.

In this paper both the solar chimney power plants: the plant with and without thermal storage system are simulated for the case of Afar region using Fluent and the effect of turbine position is also analyzed. The cost of the power output per kilowatt-hour is reduced while using the thermal storage system. It also regulates the power output. The power output increases as the turbine is positioned at higher position but the cost of the chimney so the plants cost increases very much.

Solar chimneys are very suitable for use in remote communities where there is high solar energy capacity; such as Afar and Somalia, as a power source for both residential and industrial use, based on reliability, cost, and operational factors. They can provide a suitable energy source in many remote areas of Ethiopia, including areas that are not currently supplied by conventional means.

CHAPTER ONE

INTRODUCTION

Overview of the Thesis

Energy is central to sustainable development and poverty reduction efforts. It affects all aspects of development - social, economic, and environmental - including livelihoods, access to water, agricultural productivity, health, population levels, education, and gender-related issues. None of any development goals can be met without major improvement in the quality and quantity of energy services in any country. But there are a number of problems related to energy, especially in developing countries. Let me first discuss the world energy demand and then proceed to the renewable energy resources. [1]

1.1 The world Energy demand

Following IEA (2004), in the absence of new government policies, world primary energy demand is projected to expand by almost 60% between 2002 and 2030, with an average annual growth rate of 1.7%, which is lower than in the past three decades (2% per year; see Table: 1-3). Moreover, the transport and power-generation sectors will absorb a growing share of global energy in line with past trends (see Table: 1-2). Let us consider each fuel separately.

Fossil fuels (oil, natural gas and coal) dominate the global primary energy mix with a share about 80% (see Table: 1-3, total fossil fuels). Moreover, according to IEA (2006a), fossil fuels will account for around 83% of the increase in world primary demand over the period 2004-2030.

Oil is the largest fuel in global primary energy mix (see Table: 1-3), with annual growth rate of its demand about 1.6% per year (see Table: 1-1). However, IEA (2006a) predicts a decline, from 35.5% in 2002 to 33% in 2030. Oil use is concentrated in the transport sector, which is the main fuel in road, sea and air transportation. Indeed, IEA (2004) predicts that transport will account for two-thirds of the increase in total oil use.

Natural gas is the third energy source in the world primary energy demand, with 21% of the total demand in 2002 (see Table: 1-3). However, IEA (2004) forecasts that natural gas will be the second largest energy source after 2020 (24% in 2020, and 25% in 2030), overtaking coal.

Moreover, it is the fossil fuel with the highest growth rate (2.3% per year; see Table: 1-1). The power sector will account for 60% of the increase in gas demand.

Coal is the second energy source, with 25.42% in 1971 and 24.75% in 2002 (See Table: 1-3). However, IEA (2004) projects slower annual growth rate (1.5%) than both oil (1.6%) and natural gas (2.3%) (See Table: 1-1). Indeed, as it was just observed, coal will be overtaken by natural gas as the second largest energy source. Most of the increase in coal demand comes from power stations, but this will decrease in all OECD countries. However, industry, households and services will use more coal in non-OECD countries.

Nuclear fuels are exclusively used in power stations. However, the weight of nuclear power remains lower than fossil fuels (6.37% in 2004; see Table 3). Indeed, according to the IEA (2004), it will progressively decline because nuclear power has to compete with other technologies, and many countries decide to phase out nuclear power. However, IEA (2004, 2006a) also observes that these projections are subject to great uncertainty. Indeed, at this moment, the European Union (EU) shows great interest in nuclear power as a way to reduce both its dependence on imported natural gas and CO_2 emissions. The EU observes that nuclear fuels are more widely distributed than oil or natural gas, and they are CO_2-free.

Finally, let us briefly describe the size of renewable resources in the primary energy mix. Table: 1-3 (total renewables) shows that the weight of renewable resources in the world primary energy demand is much lower than non-renewable resources (14.36% in 1971 and 13.16% in 2004). According to IEA (2004, 2006a), this trend will remain the same, with a share around 13% in 2030. The group called “other renewables” represents the energy source with the highest growth rate (see Table: 1-1). Indeed, the IEA (2004) projects an annual growth rate of 5.7% until 2030. However, the share of these renewable resources remains very low (0.07% in 1971 and 0.51% in 2004) because they start from a very low level.

- Summarizing, this section concludes that, regarding to energy, there is clear dependence of the world economy on non-renewable resources. Indeed, as it was shown before, non-renewable energy resources represents 86.84% of the world primary energy demand in 2004, with a share of fossil fuels about 80% (see Table 1-3, total non-renewables and total fossil fuels).

Table 1-1: Average annual growth rate of world primary energy demand (%)

Energy	**1971-2002**	**2002-2010**	**2010-2020**	**2020-2030**
Coal	1.70	1.8	1.6	1.5
Oil	1.4	2	1.8	1.6
Natural gas	2.9	2.7	2.6	2.3
Nuclear	10.8	1.5	0.6	0.4
Hydro	2.5	2.6	2	1.8
Biomass and waste	1.6	1.5	1.4	1.3
Other renewable [a]	8.5	8	6.2	5.7
Total primary energy	**2**	**2.1**	**1.9**	**1.7**

[a] Geothermal, solar, wind, tidal and wave energy. Source: World Energy Outlook. IEA (2004)

Table 1-2: Sectoral shares in world primary energy demand (%)

Energy	**1971**	**1990**	**2002**	**2004**	**2010**	**2020**	**2030**
Power-generation	21.88	32.07	36.38	36.89	37.83	39.08	40.21
Industry	27.19	24.44	21.41	22.41	21.14	20.82	20.46
Transport	15.46	16.43	17.57	18.29	18.29	19.13	19.85
Own use and losses	9.50	10.05	9.50	9.87	9.87	9.77	9.61
Others	25.98	17.01	13.63	12.87	12.87	11.21	9.86
Total	100	100	100	100	100	100	100

Source: World Energy Outlook. IEA (2004, 2006a)

Table 1-3: World primary energy demand (%)

Energy	**1971**	**1990**	**2002**	**2004**	**2010**	**2020**	**2030**
Coal	25.42	25.00	23.09	24.75	22.66	22.17	21.84
Oil	43.59	36.43	35.53	35.17	35.53	35.22	34.97
Natural gas	16.11	19.24	21.17	20.55	22.17	23.96	25.05
Nuclear	0.52	6.01	6.69	6.37	6.38	5.39	4.63
Hydro	1.88	2.12	2.17	2.16	2.26	2.23	2.21
Biomass and waste	12.41	10.57	10.82	10.50	10.37	9.91	9.73
Other renewables[a]	0.07	0.64	0.53	0.51	0.83	1.12	1.55
Total primary energy	100	100	100	100	100	100	100
Total fossil fuels[b]	85.12	80.66	79.80	80.46	80.16	81.35	81.86
Total non-renewables[c]	85.64	86.67	86.49	86.84	86.54	86.73	86.50
Total renewables[d]	14.36	13.33	13.51	13.16	13.46	13.27	13.50

[a]Geothermal, solar, wind, tidal and wave energy.
[b]Coal + oil + natural gas.
[c]Fossil fuels + nuclear.
[d]Hydro + biomass and waste + other renewables.
Source: World Energy Outlook. IEA (2004, 2006a)

1.2 Problems related to the usage of non-renewable energy resources

As the previous section just observed, the world economy has high dependence on non-renewable energy resources. However, a key feature of non-renewable energy resource is that their stocks (reserves) are finite. Therefore, the usage of non-renewable energy resources calls attention to the "survival" (*i.e.*, economic growth and development) of the economic system due to the limited availability of these resources.

- The reserves of oil and natural gas will last, respectively, 41 and 64 years at current rates. Moreover, the coal reserves will last around 155 years. Hence, since the world economy shows a high dependence on fossil fuels, one concludes that the usage of non-renewable energy resources (in particular, fossil fuels) rises the

question of the maintenance of economic growth and development in medium and long-term. **[3]**

- Even if enough energy is somehow indefinitely conjured up for everyone who wants it, without risking conflict and mayhem in bringing it back home, there would still be an enormous problem - how to use the energy without causing unacceptably high levels of damage to the natural world.

- The most obvious threat is the prospect that burning fossil fuels is intensifying natural climate change and heating the Earth to dangerous levels. Carbon emissions - thought to be a major cause of global climate change - are set to increase by 60%. As developing countries' share of world energy demand surges from 38% to a predicted 48%, poor countries are expected to contribute two-thirds of the projected increase in carbon emissions.

- Not only greenhouse effect is a problem but also there are still real costs that go with the quest for and use of energy: air and water pollution, impaired health, acid rain, deforestation, and the destruction of traditional ways of life. It is one of the most vicious circles the planetary crisis entails.

- In general, the world's energy use is unsustainable. One alternative way of coming out of this energy crisis is to use renewable energy which is obtained from inexhaustible natural sources.

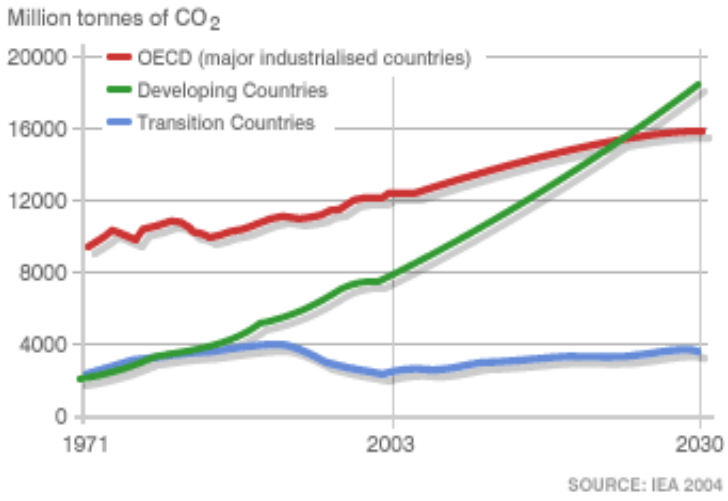

Figure 1-1: World CO_2 emissions in the next 20 years

- Renewable energy sources (RES) capture their energy from existing flows of energy, from on-going natural processes, such as sunshine, wind, flowing water, biological processes, and geothermal heat flows.

Solar energy is viewed as the clean and renewable source of energy for the future. Solar energy can be derived directly in many methods. In one particular method, sunlight hits the absorber surface of a solar thermal collector and the surface warms. The heat energy is carried away by a fluid flow to the place where the energy is required. The solar chimney power plant, whose modeling is done in this thesis, works in this method. **[1]**

1.3 Objectives

The general objective of this thesis is to model a solar chimney power plant with and without thermal storage system and compare the power outputs and the economical benefits gained because of using thermal storage systems.

The specific objectives of this thesis are, therefore,

- Developing a model for both solar chimney power plants with and without thermal storage system,
  - Analysis of the model using Computational Fluid Dynamics (CFD) software,
  - Making economic analysis of the model.
  - Comparison of the models

1.4 Literature Review

- The Solar Chimney technology for electricity generation was inspired by several engineers in the first decades of 20th century. In 1926 Prof Engineer Bernard Dubos proposed to the French Academy of Sciences the construction of a Solar Aero-Electric Power Plant in North Africa with its solar chimney on the slope of the high height mountain.

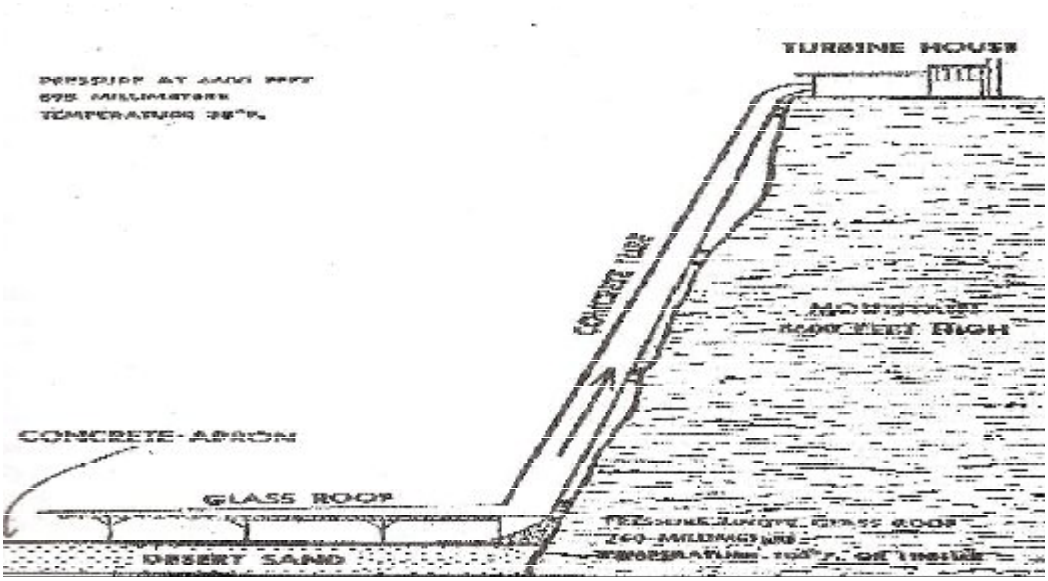

Figure 1-2: Figure and data from the book: ”Engineer’s Dream”, Willy Ley, Viking Press 1954 for solar chimney [6]

- The collected operational data were in accordance with the theoretical results
- Prof. Jorg Schlaigh proposed in his book huge reinforced concrete solar chimneys of heights 500m-1000m. These solar chimneys are very expensive constructions. Therefore the investment cost per produced KWh on the solar chimney technology with concrete chimneys is higher than the competitive solar thermal technologies (SCP for example).
- However the solar chimney technology has an important benefit in comparison to the other renewable technologies (Wind, SCP, PV). This is the ability of its Power Plants, equipped with thermal storage facilities of negligible cost, to produce electricity for 24h/day, 365days/year.
- The solar chimney concept was originally proposed by Professor J. Schlaich of Stuttgart in the late 1970s. Less than four years after he presented his ideas at a conference, construction on a pilot plant began in Manzanares, Spain, as a result of a joint venture between the German government and a Spanish utility.

A 36 kW pilot plant was built which produced electricity for seven years, thus proving the efficiency and reliability of this novel technology. The chimney was 194.6 m high and the collector had a radius of 122 m. It produced an upwind velocity of 15 m/s under no-load conditions. Operating costs of this chimney were minimal. Fundamental investigations for the Spanish system were reported by Haaf et. al. (1983) in which a brief discussion of the energy balance, design criteria, and cost analysis was presented. In a later study, Haaf

(1984) reported preliminary test results of the plant built in Spain. Dimensions of solar chimneys for different power generating capacity were reported by Haaf et. al. (1983).

Mullet (1987) presented an analysis to derive the overall efficiency of the solar chimney.

Governing differential equations were developed by Padki and Sherif (1988) to describe the chimney performance. Other related studies include an investigation of the viability of solar chimneys for medium-to-large scale power production (Padki and Sherif, 1989) and power generation in rural areas (Padki et. al., 1989). Yan et. al. (1991) reported on a more comprehensive analytical model in which practical correlations were used to derive equations for the airflow rate, air velocity, power output and the thermo fluid efficiency.

More recently, however, Padki and Sherif (1992) discussed in brief the effects of the geometrical and operating parameters on the chimney performance.

In the past few years, the solar chimney technology has found widespread applications especially in areas such as crop drying and ventilation. Barrozzi et. al. (1992) performed numerical modeling of solar-chimney-based ventilation for a house in Nigeria. Similar experiments were carried out in Algeria as reported by Bouchair (1994). Bansal et. al.(1993) also tried to model the solar chimney for room ventilation purposes.

Other objectives included developing a mathematical model that could predict the performance characteristics of solar chimneys and validate model results against experimental data.

The solar chimney offers a method for a large-scale generation of electricity from solar energy.

There are proposals for the construction of commercial plants of up to 200 MW in India, South Africa, Australia and other countries. The capital cost is high but running costs are very low, the fuel is free and the power station has a long lifetime. The technology could become the cheapest method for the large scale generation of solar electricity.

Figure 1-3: Manzanares solar chimney power plant [7]

Currently Australia is having a large scale power generation using this solar chimney mechanism, full-scale plant under evaluation by Enviro-Mission in Australia needs to be 5km across and 1 km high to achieve 200 MW of electricity generating capacity. This capacity can power 200,000 homes. The plant will cover an area of at least 20 square kilometers, and it will be Australia's, and the world's, tallest and largest engineered structure.

Solar chimney power stations could make important contributions to the energy supplies in Africa, Asia and Australia, because there is plenty of space and sunlight available.

Solar chimney power stations are particularly suitable for generating electricity in deserts and sun-rich lands. Their efficiency increases with the height of the chimney, not linearly, but exponentially. For the power stations to generate electricity economically, not only large glass or plastic roof surfaces are necessary, but also a very high chimney. The height is needed simply from the fact that the updraft is proportional to the height, and also to make best use of the heat available.

Solar chimneys will have a superior level of greenhouse abatement by producing only clean green sustainable electricity, no coal or gas fired electricity generator is able to compete with the clean emission free credentials of a solar chimney.

To replace a typical 2000 MW black coal-fired power station, about 10 solar chimneys of the capacity of the proposed test plant would need to be built (depending on scale and capacity). This would also abate more than 14 million tones of greenhouse gases from

entering the atmosphere annually. So an area of 100 km² is required and this can only replace one coal-fired power station. This makes this technology useful only for some countries and lands.

Several technologies exist that can convert solar energy into electrical energy. The solar chimney is part of the solar thermal groups of solar conversion technologies. There are two other designs that work in the same way. The first is the solar trough design and the other is the solar dish/stirling design. Of these technologies the solar dish/stirling has the highest energy efficiency (the current record is a conversion efficiency of 30% of solar energy). Solar trough plants have been built with efficiencies of about 20%. The solar chimney has an efficiency of less than 2%. However, due to its greater scale and simplicity, the solar chimney may have an economic efficiency approaching or exceeding that of the other methods.

1.5 The Working Principles of Solar Chimney Power Plant

Two basic principles are behind power generation in solar updraft towers, the greenhouse effect and buoyancy-driven flow. Solar irradiation passes through the glass of the collector, is absorbed by the ground below, and re-emitted to the air under the greenhouse. Convective effects from the ground also account for some of the air heating. The high-temperature, lower density air is funneled toward the tower. The buoyancy of the air creates a pressure difference in the column of the tower, driving the air from the base of the tower to its upper outlet. The kinetic energy of the air is captured by the turbine system, which is typically located at the base of the tower.

Components of Solar Updraft Tower

The three primary components of a solar updraft tower are the solar collector, the tower or chimney, and the turbine. The following sections describe the important components, their role in the tower, and their materials and construction.

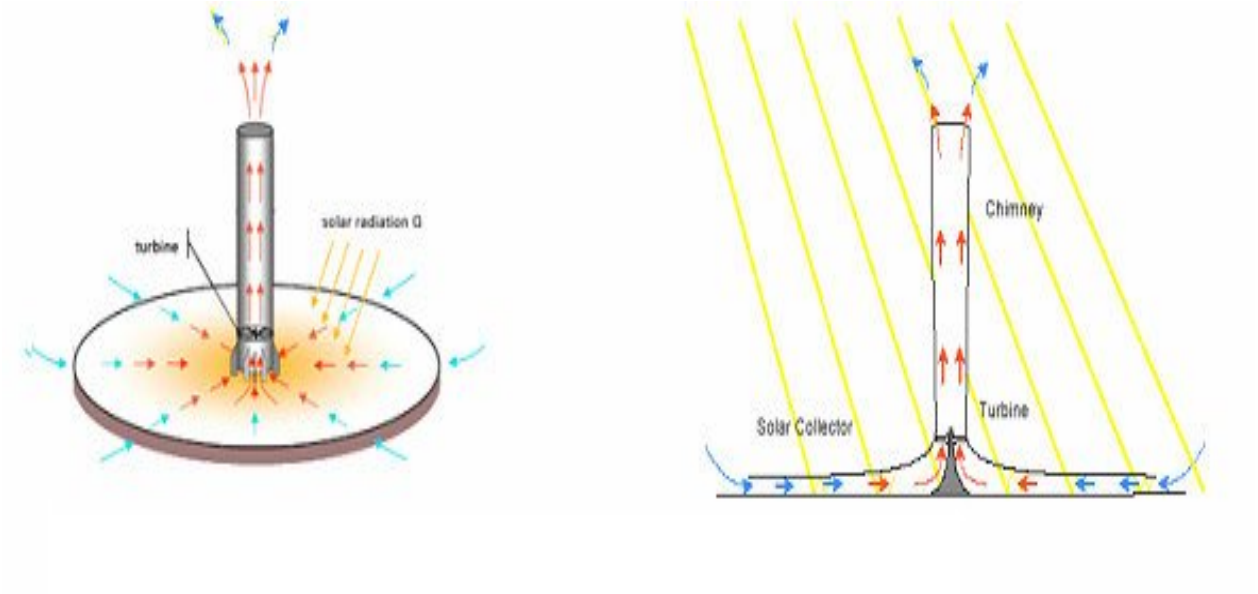

a) 3D View b) 2D View

Figure 1-4: Working principle of the plant [13]

1.5.1 Collector

The solar tower uses a greenhouse-like collector to heat the air that drives the power plant. The collector surface gradually rises closer to the tower, to direct the heated air towards the tower, and then curves up sharply at the base of the tower in order to transition the air flow up the tower. The tower material can be any glasslike material, with high transparency to the solar spectrum but with low transparency to the infrared radiation emitted from the warmed ground.

The collector of the prototype plant built at Manzanares is shown in Figure: 1.5. The Manzanares plant's collector was constructed from a combination of glass and plastic materials, designed to explore the durability and effectiveness of a variety of materials. The glass panes were spaced on a 1m by 1m lattice, and the plastic sections were arranged in 6m by 6m sections. The shape of the collector is typical of solar updraft tower design. The outer edge of the collector is roughly 2 meters off the ground.

Figure 1-5: The collector at the Manzanares plant in Spain (Schlaich 2005) [18]

The Manzanares plant provided a useful evaluation of the performance of the greenhouse. The roof proved to be insensitive to dust accumulation, with the infrequent rains in the area providing sufficient for self-cleaning (Schlaich 1995).

The durability of the glass roof proved to be exceptional, with none of the panes from the collector of the test plant broken during the seven years of operation, while some portions of the plastic roof ripped as early as the first year of operation. An additional benefit of the collector is that the ground area under the collector can be used as a greenhouse for growing plants or as a drying area for plant material.

1.5.2 Chimney

The chimney (or tower) of a solar updraft tower is the thermal engine of the plant. The heated air from the collector is funneled into the chimney, where the buoyancy difference between the heated air and the surrounding atmosphere creates a pressure difference that drives the air up the chimney.

Several factors contribute to the physical design of the chimney. The chimney should be designed to minimize the frictional losses and to maximize the pressure difference in the tower. The pressure difference in the tower is proportional to its height, so maximizing the height of the tower is critical to improving the efficiency of the tower. Schlaich suggests that reinforced concrete would be a cost effective way to create a stable tower with a lifespan of up to 100 years (Schlaich 1995). Other possible construction options include reinforcing frames covered in various membranes, including cable-net or corrugated sheet, and supporting guy wires. The prototype plant at Manzanares was constructed as a framed, guyed tower, approximately 195 m tall and 10 m in diameter, covered with corrugated sheeting approximately 1.25 mm thick. The tower was erected

without any large equipment; the tower was hydraulically lifted from below as each 4 m tall segment was placed under the tower and attached to the existing structure.

1.5.3 Turbine

The solar thermal updraft tower uses a turbine or array of turbines to generate power. The turbine or turbines operate as cased pressure-staged generators, similar to a hydroelectric plant. Turbines are placed near the bottom of the tower, for ease of access for maintenance and easy connection to the generating equipment. A single turbine can be mounted on vertical axes inside the chimney, while multiple turbines can be placed either in the chimney or in the transition area between the chimney and collector, as shown in Figure: 1-6.

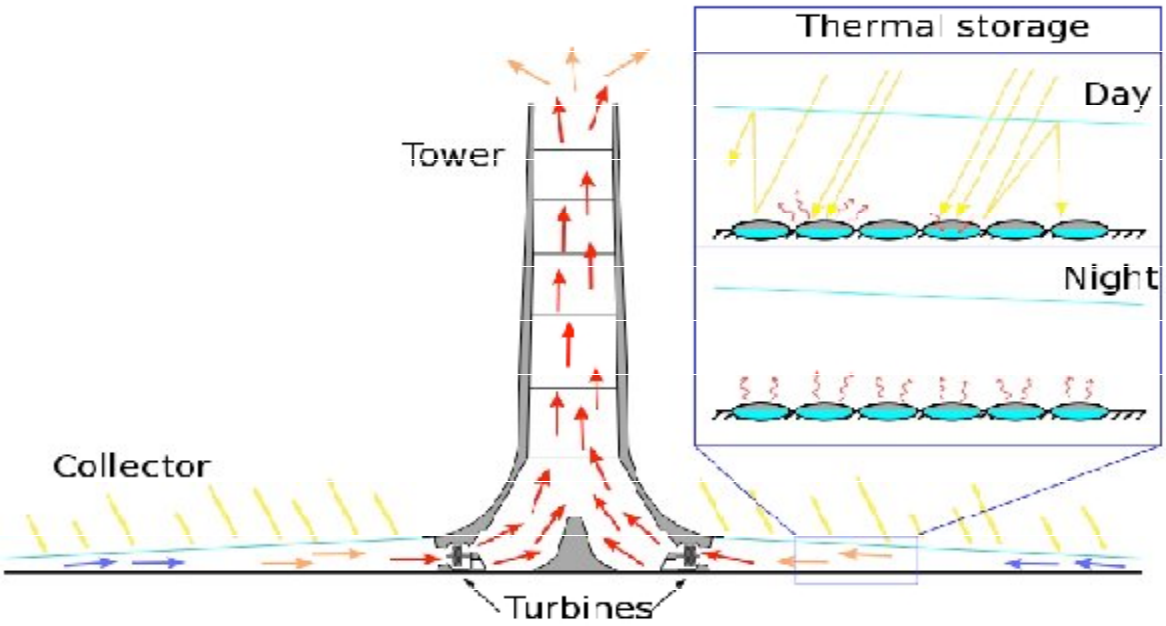

Figure 1-6: Schematic of a tower with horizontally mounted turbines [8]

The turbines are subjected to relatively steady airflow compared to those of wind generator plants, and thus subject to less physical stress. The blades of the turbine feather to adjust to different levels of airflow and pressure drop. As the only component of the system with moving parts, the turbine's reliability is critical. The manufacturer examined the turbine from the Manzanares power plant; it showed little wear after seven years of almost continuous operation (Schlaich 1995).

1.6 Characteristics of the Plant

Apart from working on a very simple principle, solar chimneys have a number of special features

1. The collector can use all solar radiation, both direct and diffuse. This is crucial for tropical countries where the sky is frequently overcast.

2. Due to the soil under the collector working as a natural heat storage system, updraft solar chimneys can operate 24 h on pure solar energy, at reduced output at night time. If desired, additional water tubes or bags placed under the collector roof absorb part of the radiated energy during the day and release it into the collector at night. Thus solar chimneys can operate as base load power plants. As the plant's prime mover is the air temperature difference (causing an air density difference) between the air in the chimney and ambient air, lower ambient temperatures at night help to keep the output at an almost constant level even when the temperature of natural and additional thermal storage also decreases without sunshine, as the temperature difference remains practically the same.

3. Solar chimneys are particularly reliable and not liable to break down, in comparison with other power plants. Turbines and generators - subject to a steady flow of air - are the plant's only moving parts. This simple and robust structure guarantees operation that needs little maintenance and of course no combustible fuel.

4. Unlike conventional power stations (and also some other solar-thermal power station types), solar chimneys do not need cooling water. This is a key advantage in the many sunny countries that already have major problems with water supply.

5. The building materials needed for solar chimneys, mainly concrete and glass, are available everywhere in sufficient quantities. In fact, with the energy taken from the solar chimney itself and the stone and sand available in the desert, they can be reproduced on site.

6. Solar chimneys can be built now, even in less industrially developed countries. The industry already available in most countries is entirely adequate for solar chimney requirements. No investment in high-tech manufacturing plants is needed.

7. Even in poor countries it is possible to build a large plant without high foreign currency expenditure by using local resources and work-force; this creates large numbers of jobs while significantly reducing the required capital investment and thus the cost of generating electricity.

Nevertheless, solar chimneys also have features that make them less suitable for some sites:

1. They require large areas of flat land. This land should be available at low cost, which means that there should be no competing usage, like e.g. intensive agriculture, for the land.

2. Solar chimneys are not adequate for earthquake prone areas, as in this case chimney costs would increase drastically.

3. Zones with frequent sand storms should also be avoided, as either collector performance losses or collector operation and maintenance costs would be substantial there.

1.7 Limitations of the paper

This paper uses the data of four different months of a year and concludes for the power output of a year; which could be considered as the limitation of the paper.

CHAPTER TWO

MODEL SIMULATION PROGRAM

2.1 Introduction

FLUENT is a state-of-the-art computer program for modeling simulation flow and heat transfer in complex geometries. FLUENT provides complete mesh flexibility, including the ability to solve your flow problems using unstructured meshes that can be generated about complex geometries with relative ease. Supported mesh types include 2D triangular/ quadrilateral, 3D tetrahedral/hexahedral/pyramid/wedge, and mixed (hybrid) meshes. FLUENT also allows you to refining or coarsen your grid based on the flow solution.

FLUENT is written in the C computer language and makes full use of the flexibility and powered offered by the language. Consequently, true dynamic memory allocation, efficient data structures, and flexible solver control are all possible. In addition, FLUENT uses a client/server architecture, which allows it to run as separate simultaneous processes on client desktop workstations and powerful computer servers. This architecture allows for efficient execution, interactive control, and complete flexibility between different types of machines or operating systems.

All functions required to compute a solution and display the results are accessible in FLUENT through an interactive, menu-driven interface. **[2]**

2.2 Program structure

FLUENT package includes the following products:

- FLUENT, the solver.
- GAMBIT, the preprocessor for geometry modeling and mesh generation.
- TGrid, an additional preprocessor that can generate volume meshes from existing boundary meshes.
- Filters (translators) for import of surface and volume meshes from CAD/CAE packages such as ANSYS, CGNS, I-deas, NASTRAN, PATRAN, and others.
- Figure: 2.1 show the organizational structure of these components.

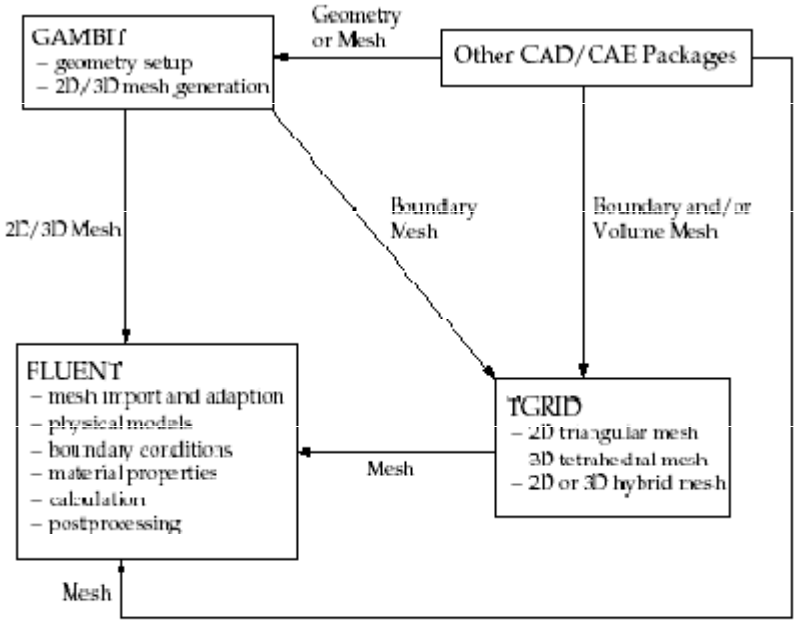

Figure 2-1: Basic program structure [2]

2.3 Program capabilities

The FLUENT solver has the following modeling capabilities: **[2]**

- 2D planar, 2D axisymmetric, 2D axi-symmetric with swirl (rotationally symmetric), and 3D flows
- Quadrilateral, triangular, hexahedral(brick), tetrahedral, prism(wedge), pyramid, and mixed element meshes
- Steady-state or transient flows
- Incompressible or compressible flows, including all speed regimes(low subsonic, transonic, supersonic, and hypersonic flows)
- Inviscid, laminar, and turbulent flows
- Newtonian or non-Newtonian flows
- Heat transfer, including forced, natural, and mixed convection, conjugate (solid/fluid) heat transfer, and radiation
- Chemical species mixing and reaction, including homogeneous and heterogeneous combustion models and surface deposition/reaction models

- Free surface and multiphase models for gas-liquid, gas-solid, and liquid-solid flows
- Lagrangian trajectory calculation for dispersed phase (particles/droplets/ bubbles), including coupling with continuous phase; spray modeling
- Cavitation model
- Phase change model for melting/solidification applications
- Porous media with non-isotropic permeability, inertial resistance, solid heat conduction, and porous-face pressure jump conditions
- Lumped parameter models for fans, pumps, radiators, and heat exchangers
- Acoustic models for predicting flow-induced noise
- Inertial (stationary) or non-inertial (rotating or accelerating) reference frames
- Multiple reference frame (MRF) and sliding mesh options for modeling multiple moving frames
- Mixing-plane model for modeling rotor-stator interactions, torque converters, and similar turbomachinery applications with options for mass conservation and swirl conservation
- Dynamic mesh model for modeling domains with moving and deforming mesh
- Volumetric sources of mass, momentum, heat, and chemical species
- Material property database
- Extensive customization capability via user-defined functions
- Dynamic (two-way) coupling with GT-Power and WAVE
- Magneto-hydro-dynamics (MHD) module (documented separately)
- Continuous fiber module (documented separately)
- Fuel cells modules (documented separately)

FLUENT is ideally suited for incompressible and compressible fluid-flow simulations in complex geometries. Fluent Inc. also offers other solvers that address different flow

regimes and incorporate alternative physical models. Additional CFD programs from Fluent Inc. include Airpak, FIDAP, FloWizard, Icepak, MixSim, and POLYFLOW.

2.4 General simulation steps

Before beginning the CFD modeling using FLUENT, careful consideration of the following issues will contribute significantly to the success of the modeling effort. Also, when planning a CFD project, one has to be sure to also take advantage of the customer support provided to all FLUENT users. [2]

Once the important features of the problem to be solved have been determined, the following basic procedural steps will be followed.

1. Defining the modeling goals.
2. Creating the model geometry and grid.
3. Setting up the solver and physical models.
4. Computing and monitoring the solution.
5. Examining and save the results.
6. Considering revisions to the numerical or physical model parameters, if necessary.

2.4.1 Defining the modeling goals

Defining the modeling goals requires selecting a geometry modeler and grid generator. GAMBIT or a separate CAD system can be used for geometry modeling and grid generation. TGrid can also be used to generate volume grids from surface grids imported from GAMBIT or a CAD package. Alternatively, supported CAD packages can be used to generate volume grids for importing into TGrid or into FLUENT.

2.4.2 Creating the model geometry and grid

FLUENT uses unstructured meshes in order to reduce the amount of time spent in generating meshes simplify the geometry modeling and mesh generation process, model more-complex geometries than handling with conventional, multi-block structured meshes, and helps to adapt the mesh to resolve the flow-field features. FLUENT can also use body-fitted, block-structured. FLUENT is capable of handling triangular and quadrilateral elements (or a combination of the two) in 2D, and tetrahedral, hexahedral, pyramid, and wedge elements (or a combination of these) in 3D. This flexibility allows one to pick mesh topologies that are best suited for one particular application.

FLUENT allows to adapt all types of meshes in order to resolve large gradients in the flow field, but one must always generate the initial mesh (whatever the element types used) outside of the solver, using GAMBIT, TGrid, or one of the CAD systems for which mesh import filters exist.

2.4.3 Setting up the solver and physical models

For a given problem, one will need to do the following.

- Importing and check the grid.
- Selecting the numerical solver (e. g., coupled, segregated, unsteady, etc.).
- Selecting appropriate physical models.
    - Turbulence, combustion, multiphase, etc.
- Defining material properties.
    - Fluid
    - Solid
    - Mixture
- Prescribing operating conditions.
- Prescribing boundary conditions at all boundary zones.
- Providing an initial solution.
- Setting up solver controls.
- Setting up convergence monitors.
- Initializing the flow field.

2.4.4 Computing and monitoring the solution

The discretized conservation equations are solved iteratively. A number of iterations are usually required to reach a converged solution.

Convergence is reached when:

1. Changes in solution variables from one iteration to the next are negligible.

Residuals provide a mechanism to help monitor this trend.

2. Overall property conservation is achieved.

The accuracy of a converged solution is dependent upon

1. Appropriateness and accuracy of physical models.
2. Grid resolution and independence,
3. Problem setup

2.4.5 Examining and saving the results

The results must be examined to review solution and extract useful data.

- Visualization tools can be used to answer such questions as
  1. What is the overall flow pattern?
  2. Is there separation?
  3. Where do shocks, shear layers, etc. form?
  4. Are key flow features being resolved?
- Numerical reporting tools can be used to calculate quantitative results
  1. Forces and moments
  2. Average heat transfer coefficients
  3. Surface and volume integrated quantities
  4. Flux balances.

2.4.6 Revising the model

Once the solution is converged, the following questions should be considered when one is analyzing the solution:

- Are physical models appropriate?
  1. Is flow turbulent?
  2. Is flow unsteady?

3. Are there compressibility effects?
4. Are there 3D effects?

- Are boundary conditions correct?
  1. Is the computational domain large enough?
  2. Are boundary conditions appropriate?
  3. Are boundary values reasonable?
- Is grid adequate?
  1. Can grid be adapted to improve results?
  2. Does solution change significantly with adaption, or is the solution grid independent?
  3. Does boundary resolution need to be improved?

2.5 Overview of numerical schemes

FLUENT allows to the choice of either of two numerical methods:

- Segregated solver, and
- Coupled solver. **[2]**

Using either method, FLUENT will solve the governing integral equations for the conservation of mass and momentum, and (when appropriate) for energy and other scalars such as turbulence and chemical species. In both cases a control-volume-based technique is used that consists of:

- Division of the domain into discrete control volumes using a computational grid.
- Integration of the governing equations on the individual control volumes to construct algebraic equations for the discrete dependent variables ("unknowns") such as velocities, pressure, temperature, and conserved scalars.
- Linearization of the discretized equations and solution of the resultant linear equation system to yield updated values of the dependent variables.

The two numerical methods employ a similar discretization process (finite-volume), but the approach used to linearize and solve the discretized equations is different.

2.5.1 Segregated solution method

In the segregated solver, the governing equations are solved sequentially (i.e., segregated from one another). Because the governing equations are non-linear (and coupled), several iterations of the solution loop must be performed before a converged solution is obtained. Each iteration consists of the steps outlined below:

1. Fluid properties are updated, based on the current solution. (If the calculation has just begun, the fluid properties will be updated based on the initialized solution.)

2. The u, v, and w momentum equations are each solved in turn using current values for pressure and face mass fluxes, in order to update the velocity field.

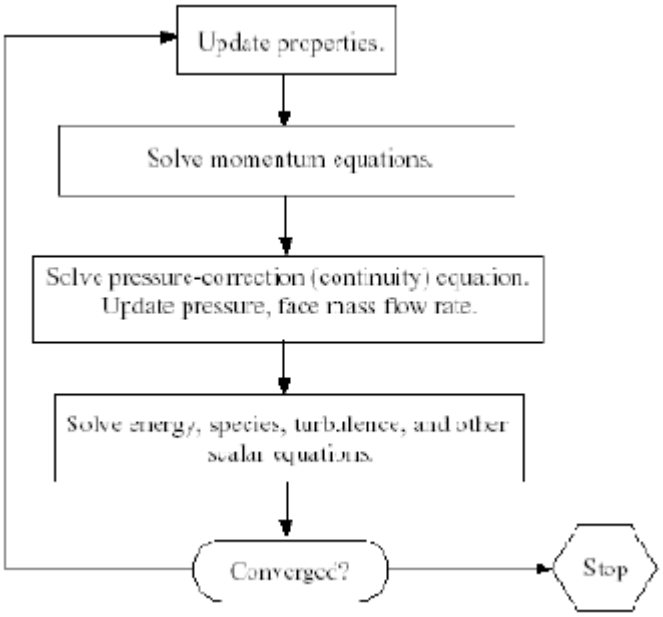

Figure 2-2: Overview of the segregated solution method [2]

3. Since the velocities obtained in Step 2 may not satisfy the continuity equation locally, a “Poisson-type" equation for the pressure correction is derived from the continuity equation and the linearized momentum equations. This pressure correction equation is then solved to obtain the necessary corrections to the pressure and velocity fields and the face mass fluxes such that continuity is satisfied.

4. Where appropriate, equations for scalars such as turbulence, energy, species, and radiation are solved using the previously updated values of the other variables.

5. When interphase coupling is to be included, the source terms in the appropriate continuous phase equations may be updated with a discrete phase trajectory calculation.

6. A check for convergence of the equation set is made. These steps are continued until the convergence criteria are met.

2.5.2 Coupled solution method

The coupled solver solves the governing equations of continuity, momentum, and (where appropriate) energy and species transport simultaneously (i.e., coupled together). Governing equations for additional scalars will be solved sequentially (i.e., segregated from one another and from the coupled set) using the procedure described for the segregated solver. Because the governing equations are nonlinear (and coupled), several iterations of the solution loop must be performed before a converged solution is obtained. Each iteration consists of the steps outlined below:

1. Fluid properties are updated, based on the current solution. (If the calculation has just begun, the fluid properties will be updated based on the initialized solution.)

2. The continuity, momentum, and (where appropriate) energy and species equations are solved simultaneously.

3. Where appropriate, equations for scalars such as turbulence and radiation are solved using the previously updated values of the other variables.

4. When interphase coupling is to be included, the source terms in the appropriate continuous phase equations may be updated with a discrete phase trajectory calculation.

5. A check for convergence of the equation set is made.

These steps are continued until the convergence criteria are met.

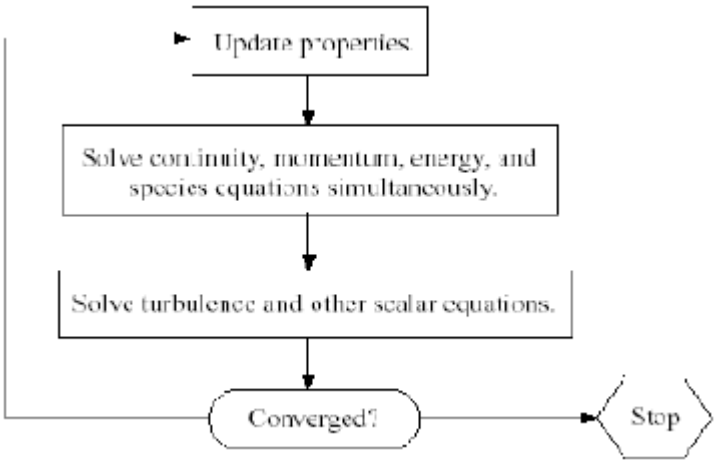

Figure 2-3: Overview of the coupled solution method **[2]**

2.5.3 Linearization: Implicit vs. Explicit

In both the segregated and coupled solution methods the discrete, non-linear governing equations are linearized to produce a system of equations for the dependent variables in every computational cell. The resultant linear system is then solved to yield an updated flow-field solution.

The manner in which the governing equations are linearized may take an “implicit" or “explicit" form with respect to the dependent variable (or set of variables) of interest.

By implicit or explicit we mean the following:

- **Implicit**: For a given variable, the unknown value in each cell is computed using a relation that includes both existing and unknown values from neighboring cells. Therefore each unknown will appear in more than one equation in the system, and these equations must be solved simultaneously to give the unknown quantities.

- **Explicit**: For a given variable, the unknown value in each cell is computed using a relation that includes only existing values. Therefore each unknown will appear in only one equation in the system and the equations for the unknown value in each cell can be solved one at a time to give the unknown quantities.

The segregated approach solves for a single variable field (e.g., pressure) by considering all cells at the same time. It then solves for the next variable field by again considering all cells at the same time, and so on. There is no explicit option for the segregated solver.

The coupled implicit approach solves for all variables (p, u, v, w, T) in all cells at the same time.

The coupled explicit approach solves for all variables (p, u, v, w, T) in one cell at a time.

The segregated solver traditionally has been used for incompressible and mildly compressible flows. The coupled approach, on the other hand, was originally designed for high-speed compressible flows. Both approaches are now applicable to a broad range of flows (from incompressible to highly compressible), but the origins of the coupled formulation may give it a performance advantage over the segregated solver for high-speed compressible flows.

By default, FLUENT uses the segregated solver, but for high-speed compressible flows (as discussed above), highly coupled flows with strong body forces (e.g., buoyancy or rotational forces), or flows being solved on very fine meshes, one may want to consider the coupled implicit solver instead. This solver couples the flow and energy equations, which often results in faster solution convergence. A trade-off involved in the use of the coupled implicit solver is that it requires more memory (1.5 to 2 times) than the segregated solver.

For cases where the use of the coupled implicit solver is desirable, but the machine does not have sufficient memory, one can use the segregated solver or the coupled explicit solver instead. The coupled explicit solver also couples the flow and energy equations, but it requires less memory than the coupled implicit solver. It will, however, usually take longer to reach a converged solution with the coupled explicit solver than with the coupled implicit solver.

2.5.4 Discretization

FLUENT uses a control-volume-based technique to convert the governing equations to algebraic equations that can be solved numerically. This control volume technique consists of integrating the governing equations about each control volume, yielding discrete equations that conserve each quantity on a control-volume basis.

Discretization of the governing equations can be illustrated most easily by considering the steady-state conservation equation for transport of a scalar quantity ϕ. This is demonstrated by the following equation written in integral form for an arbitrary control volume V as follows:

$$\oint \rho \vec{v} \cdot \vec{A} = \oint \Gamma \nabla \cdot \vec{A} + \int \qquad (2.1)$$

where:

ρ =density

$\vec{v}$= velocity vector

$\vec{A}$=surface area vector

Γ =diffusion coefficient for

$\nabla\phi$ =gradient of ϕ S =source of ϕ per unit volume

Equation (2.1) is applied to each control volume, or cell, in the computational domain. The two-dimensional, triangular cell shown in Figure 2.4 is an example of such a control volume. Discretization of Equation (2.1) on a given cell yields

$$\sum \quad \vec{\phi} \quad \vec{} = \sum \quad \Gamma \ (\nabla\phi) \quad \vec{} + S \ V \qquad (2.2)$$

Where

Nfaces= number of faces enclosing g cell

ϕ =value of ϕ convected through face f

$\vec{}$ $\vec{}$= mass flux through the face

$\vec{}$=area of face f

$(\nabla\phi)$ =magnitude of $\nabla\phi$ normal to face f

V= cell volume

The equations solved by FLUENT take the same general form as the one given above and apply readily to multi-dimensional, unstructured meshes composed of arbitrary polyhedra.

By default, FLUENT stores discrete values of the scalar ϕ at the cell centers (c_o and c_1 in Figure 2.4). However, face values ϕ are required for the convection terms in Equation (2.2) and must be interpolated from the cell center values. This is accomplished using an upwind scheme.

Upwinding means that the face value ϕ is derived from quantities in the cell upstream, or "upwind," relative to the direction of the normal velocity V_n Equation (2.2). FLUENT allows one to choose from several upwind schemes:

- First-order upwind,
- Second-order upwind,
- Power law, and
- QUICK.

The diffusion terms in Equation (2.2) are central-differenced and are always second order accurate.

When first-order accuracy is desired, quantities at cell faces are determined by assuming that the cell-center values of any field variable represent a cell-average value and hold throughout the entire cell; the face quantities are identical to the cell quantities. Thus when first-order upwinding is selected, the face value ϕ is set equal to the cell-center value of ϕ in the upstream cell.

The power-law discretization scheme interpolates the face value of a variable, f , using the exact solution to a one-dimensional convection-diffusion equation [9]. When second-order accuracy is desired, quantities at cell faces are computed using a multidimensional linear reconstruction approach. In this approach, higherorder accuracy is achieved at cell faces through a Taylor series expansion of the cell-centered solution about the cell centroid.

For quadrilateral and hexahedral meshes, where unique upstream and downstream faces and cells can be identified, FLUENT also provides the QUICK scheme for computing a higher-order value of the convected variable ϕ at a face. QUICK-type schemes are based on a weighted average of second-order-upwind and central interpolations of the variable.

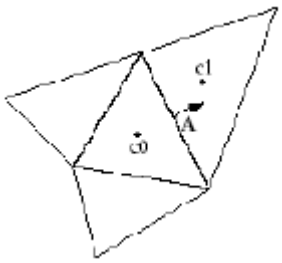

Figure 2-4: Control volume used to illustrate discretization of a scalar**[2]**

Transport equation

The discretized scalar transport equation (Equation (2.2)) contains the unknown scalar variable ϕ at the cell center as well as the unknown values in surrounding neighbor cells.

This equation will, in general, be non-linear with respect to these variables. Because of the nonlinearity of the equation set being solved by FLUENT, it is necessary to control the change of ϕ . This is typically achieved by under relaxation, which reduces the change of ϕ produced during each iteration. In a simple form, the new value of the variable ϕ within a cell depends upon the old value, ϕ , the computed change in ϕ, $\Delta\phi$, and the under-relaxation factor, α, as follows:

$$\phi = \phi \quad + \alpha\Delta\phi \qquad (2.3)$$

When the flow is aligned with the grid (e.g., laminar flow in a rectangular duct modeled with a quadrilateral or hexahedral grid) the first-order upwind discretization may be acceptable. When the flow is not aligned with the grid (i.e., when it crosses the grid lines obliquely), however, first-order convective discretization increases the numerical discretization error (numerical diffusion). For triangular and tetrahedral grids, since the flow is never aligned with the grid, one will generally obtain more accurate results by using the second-order discretization. For quad/hex grids, one will also obtain better results using the second-order discretization, especially for complex flows.

In summary, while the first-order discretization generally yields better convergence than the second-order scheme, it generally will yield less accurate results, especially on tri/tet grids.

For most cases, one will be able to use the second-order scheme from the start of the calculation. In some cases, however, one may need to start with the first-order scheme and then switch to the second-order scheme after a few iterations. For example, when running a high-Mach-number flow calculation that has an initial solution much different than the expected final solution, one will usually need to perform a few iterations with the first-order scheme and then turn on the second-order scheme and continue the calculation to convergence.

For a simple flow that is aligned with the grid (e.g., laminar flow in a rectangular duct modeled with a quadrilateral or hexahedral grid), the numerical diffusion will be naturally low, so one can generally use the first-order scheme instead of the second-order scheme without any significant loss of accuracy.

Finally, if convergence difficulties are encountered with the second-order scheme, it is better to try the first-order scheme instead.

The QUICK discretization scheme may provide better accuracy than the secondorder scheme for rotating or swirling flows solved on quadrilateral or hexahedral meshes. In general, however, the second-order scheme is sufficient and the QUICK scheme will not provide significant improvements in accuracy.

A power law scheme is also available, but it will generally yield the same accuracy as the first-order scheme.

The discretization scheme described for a scalar transport equation is also used to discretize the momentum equations. For example, the x-momentum equation can be obtained by setting $\phi = u$.

There are important issues with respect to the storage of pressure and the discretization of the pressure gradient term; these are addressed next.

FLUENT uses a co-located scheme, whereby pressure and velocity are both stored at cell centers. However, the value of the pressure at the face between cells c_o and c_1, shown in Figure 2.4 is required. Therefore, an interpolation scheme is required to compute the face values of pressure from the cell values.

2.5.5 Pressure interpolation schemes

The default scheme in FLUENT interpolates the pressure values at the faces using momentum equation coefficients. This procedure works well as long as the pressure variation between cell centers is smooth. When there are jumps or large gradients in the momentum source terms between control volumes, the pressure profile has a high gradient at the cell face, and cannot be interpolated using this scheme. If this scheme is used, the discrepancy shows up in overshoots/undershoots of cell velocity.

Flows for which the standard pressure interpolation scheme will have trouble include flows with large body forces, such as in strongly swirling flows, in high- Rayleigh-number natural convection and the like. In such cases, it is necessary to pack the mesh in regions of high gradient to resolve the pressure variation adequately.

Another source of error is that FLUENT assumes that the normal pressure gradient at the wall is zero. This is valid for boundary layers, but not in the presence of body forces or curvature. Again, the failure to correctly account for the wall pressure gradient is manifested in velocity vectors pointing in/out of walls.

Several alternate methods are available for cases in which the standard pressure interpolation scheme is not valid:

- The linear scheme computes the face pressure as the average of the pressure values in the adjacent cells.
- The second-order scheme reconstructs the face pressure in the manner used for second-order accurate convection terms. This scheme may provide some improvement over the standard and linear schemes, but it may have some trouble if it is used at the start of a calculation and/or with a bad mesh.

The second-order scheme is not applicable for flows with discontinuous pressure gradients imposed by the presence of a porous medium in the domain or the use of the VOF or mixture model for multiphase flow.

- The body-force-weighted scheme computes the face pressure by assuming that the normal gradient of the difference between pressure and body forces is constant.This works well if the body forces are known a priori in the momentum equations (e.g., buoyancy and axisymmetric swirl calculations).

- The PRESTO! (PREssure STaggering Option) scheme uses the discrete continuity balance for a "staggered" control volume about the face to compute the "staggered" (i.e., face) pressure. This procedure is similar in spirit to the staggered-grid schemes used with structured meshes. Note that for triangular and tetrahedral meshes, comparable accuracy is obtained using a similar algorithm. The PRESTO! Scheme is available for all meshes, including but not limited to, tetrahedral, triangular, hexahedral, quadrilateral, and hybrid meshes.

For most cases the "standard" scheme is acceptable, but some types of models may benefit from one of the other schemes:

- For problems involving large body forces, the body-force-weighted scheme is recommended.

- For flows with high swirl numbers, high-Rayleigh-number natural convection, high-speed rotating flows, flows involving porous media, and flows in strongly curved domains, use the PRESTO! Scheme.

- For compressible flows, the second-order scheme is recommended.

- The second-order scheme is used for improved accuracy when one of the other schemes is not applicable.

2.5.6 Discretization of the continuity equation

The SIMPLE (Semi-Implicit Method for Pressure-Linked Equations) family of algorithms is used for introducing pressure into the continuity equation.

In order to proceed further, it is necessary to relate the face values of velocity, *vn* , to the stored values of velocity at the cell centers. Linear interpolation of cellcentered velocities to the face results in unphysical checker-boarding of pressure. FLUENT uses a procedure similar to that outlined by Rhie and Chow to prevent checkerboarding. The face value of velocity is not averaged linearly; instead, momentum-weighted averaging, using weighting factors is performed.

2.5.7 Density interpolation schemes

For compressible flow calculations (i.e., calculations that use the ideal gas law for density), FLUENT applies upwind interpolation of density at cell faces. (For

incompressible flows, FLUENT uses arithmetic averaging.) Three interpolation schemes are available for the density upwinding at cell faces:

- First-order upwind (default),
- Second-order-upwind, and
- QUICK.

The first-order upwind scheme sets the density at the cell face to be the upstream cell-center value. This scheme provides stability for the discretization of the pressure-correction equation, and gives good results for most classes of flows.

The first-order scheme is the default scheme for compressible flows. The second-order upwind scheme provides stability for supersonic flows and captures shocks better than the first-order upwind scheme. The QUICK scheme for density is similar to the QUICK scheme used for other variables.

The first-order upwind scheme (the default) provides stability for the discretization of the pressure-correction equation, and gives good results for most classes of flows. If one is calculating a compressible flow with shocks, the first-order upwind scheme may tend to smooth the shocks; one should use the second-order- upwind or QUICK scheme for such flows. For compressible flows with shocks, using the QUICK scheme for all variables, including density, is highly recommended for quadrilateral, hexahedral, or hybrid meshes.

2.5.8 Choosing the pressure-velocity coupling method

FLUENT provides four methods for the pressure-velocity coupling in the segregated solver:

- SIMPLE,
- SIMPLEC,
- PISO, and
- Fractional Step (FSM) (for time-dependant flows using the Use Non- Iterative Time Advancement option (NITA)).

Steady-state calculations will generally use SIMPLE or SIMPLEC, while PISO is recommended for transient calculations.

PISO may also be useful for steady-state and transient calculations on highly skewed meshes.

Pressure-velocity coupling is relevant only for the segregated solver; one will not specify it for the coupled solvers.

SIMPLE is the default, but many problems will benefit from the use of SIMPLEC, particularly because of the increased under-relaxation that can be applied, as described below.

For relatively uncomplicated problems (laminar flows with no additional models activated) in which convergence is limited by the pressure-velocity coupling, one can often obtain a converged solution more quickly using SIMPLEC. With SIMPLEC, the pressure-correction under-relaxation factor is generally set to 1.0, which aids in convergence speed-up. In some problems, however, increasing the pressure-correction under-relaxation to 1.0 can lead to instability due to high grid skewness. For such cases, one will need to use one or more skewness correction schemes, use a slightly more conservative under-relaxation value (up to 0.7), or use the SIMPLE algorithm. For complicated flows involving turbulence and/or additional physical models, SIMPLEC will improve convergence only if it is being limited by the pressure-velocity coupling. Often it will be one of the additional modeling parameters that limits convergence; in this case, SIMPLE and SIMPLEC will give similar convergence rates.

The PISO algorithm with neighbor correction is highly recommended for all transient flow calculations, especially when one wants to use a large time step. For problems that use the LES turbulence model, which usually requires small time steps, using PISO may result in increased computational expense, so SIMPLE or SIMPLEC should be considered instead. PISO can maintain a stable calculation with a larger time step and an under-relaxation factor of 1.0 for both momentum and pressure. For steady-state problems, PISO with neighbor correction does not provide any noticeable advantage over SIMPLE or SIMPLEC with optimal under-relaxation factors.

PISO with skewness correction is recommended for both steady-state and transient calculations on meshes with a high degree of distortion. When one uses PISO neighbor correction, under-relaxation factors of 1.0 or near 1.0 are recommended for all equations. If one uses just the PISO skewness correction for highly-distorted meshes (without neighbor correction), set the under-relaxation factors for momentum and pressure so that they sum to 1 (e.g., 0.3 for pressure and 0.7 for momentum).

For most problems, it is not necessary to disable the default coupling between neighbor and skewness corrections. For highly distorted meshes, however, disabling the default coupling between neighbor and skewness corrections is recommended.

The Fractional Step Method (FSM) is available when one chooses to use the NITA scheme (i.e., the Use Non-Iterative Time Advancement option in the Solver panel). With

the NITA scheme, the FSM is slightly less computationally expensive compared to the PISO algorithm. Whether one selects FSM or PISO depends on the application. For some problems (e.g., simulations that use VOF), FSM could be less stable than PISO.

In most cases, the default values for the solution controls are enough to set a robust convergence of the internal pressure correction sub-iterations due to skewness. Only very complex problems (e.g., moving deforming meshes, sliding interfaces, and the VOF model) could require a reduction of relaxation for pressure up to a value of 0.7 or 0.8.

CHAPTER THREE

FLOW GOVERNING EQUATIONS

3.1 Introduction

The flow of air in the solar chimney power plant is caused by natural convection due to solar radiation. The governing equations used in the simulation consist of the Reynolds' Averaged Navier-Stokes (RANS) equations along with others as follow: **[2]**

- Continuity equation,
- Navier-Stokes equations,
- Energy equation,
- Turbulence equations,
- Radiation transfer equation.

These equations will be discussed in this chapter in a little bit detailed manner.

3.2 The continuity equation

The equation for conservation of mass, or continuity equation, can be written as follows:

$$\frac{}{} + \Delta.(\quad)\vec{} = \qquad (3.1)$$

Equation (3.1) is the general form of the mass conservation equation and is valid for incompressible as well as compressible flows. The source S_m is the mass added to the continuous phase from the dispersed second phase (e.g., due to vaporization of liquid droplets) and any user-defined sources.

For 2D axisymmetric geometries, the continuity equation is given by

$$\frac{}{} + \frac{}{}(\quad) + \frac{}{}(\quad) + \frac{}{} = \qquad (3.2)$$

Where x is the axial coordinate, r is the radial coordinate, v_x is the axial velocity, and v_r is the radial velocity.

3.3 Navier-Stokes equations

Conservation of momentum in an inertial (non-accelerating) reference frame is described

By

$$\frac{\partial}{\partial t}(\rho \vec{v}) + \nabla \cdot (\rho \vec{v}\vec{v}) = -\nabla p + \nabla \cdot (\bar{\bar{\tau}}) + \rho \vec{g} + \vec{F} \quad (3.3)$$

Where P is the static pressure, $\bar{\bar{\tau}}$ is the stress tensor (described below), and $\vec{g}$ and $\vec{F}$ are the gravitational body force and external body forces (e.g., that arise from interaction with the dispersed phase), respectively. $\vec{F}$ also contains other model-dependent source terms such as porous-media and user-defined sources.

For 2D axisymmetric geometries, the axial and radial momentum conservation equations are given by

$$\frac{\partial}{\partial t}(\rho v_x) + \frac{1}{r}\frac{\partial}{\partial x}(r \rho v_x v_x) + \frac{1}{r}\frac{\partial}{\partial r}(r \rho v_r v_x) = -\frac{\partial p}{\partial x} + \frac{1}{r}\frac{\partial}{\partial x}\left[r\mu\left(2\frac{\partial v_x}{\partial x} - \frac{2}{3}(\nabla \cdot \vec{v})\right)\right] + \frac{1}{r}\frac{\partial}{\partial r}\left[r\mu\left(\frac{\partial v_r}{\partial x} + \frac{\partial v_x}{\partial r}\right)\right] + F_x \quad (3.4)$$

And

$$\frac{\partial}{\partial t}(\rho v_r) + \frac{1}{r}\frac{\partial}{\partial x}(r \rho v_x v_r) + \frac{1}{r}\frac{\partial}{\partial r}(r \rho v_r v_r) = -\frac{\partial p}{\partial r} + \frac{1}{r}\frac{\partial}{\partial x}\left[r\mu\left(\frac{\partial v_r}{\partial x} + \frac{\partial v_x}{\partial r}\right)\right] + \frac{1}{r}\frac{\partial}{\partial r}\left[r\mu\left(2\frac{\partial v_r}{\partial r} - \frac{2}{3}(\nabla \cdot \vec{v})\right)\right] + 2\mu\frac{v_r}{r^2} + \frac{2}{3}\frac{\mu}{r}(\nabla \cdot \vec{v}) + \rho\frac{v_z^2}{r} + F_r \quad (3.5)$$

3.4 Turbulence equations

Turbulent flows are characterized by fluctuating velocity fields. These fluctuations mix transported quantities such as momentum, energy, and species concentration, and cause the transported quantities to fluctuate as well. Since these fluctuations can be of small scale and high frequency, they are too computationally expensive to simulate directly in practical engineering calculations. Instead, the instantaneous (exact) governing equations can be time-averaged, ensemble-averaged, or otherwise manipulated to remove the small scales, resulting in a modified set of equations that are computationally less expensive to solve. However, the modified equations contain additional unknown variables, and turbulence models are needed to determine these variables in terms of known quantities. FLUENT provides the following choices of turbulence models: **[2]**

- Spalart-Allmaras model
- k- models
    - Standard k- model
    - Renormalization-group (RNG) k- model

- Realizable k- modeḷ

➢ k- modelṣ

- Standard k- modeḷ
- Shear-stress transport (SST) k- modeḷ

➢ -f model

➢ Reynolds stress model (RSM)

➢ Detached eddy simulation (DES) model

➢ Large eddy simulation (LES) model

Choosing a turbulence model

➢ It is an unfortunate fact that no single turbulence model is universally accepted as being superior for all classes of problems.

➢ The choice of turbulence model will depend on considerations such as;

- The physics encompassed in the flow,
- The established practice for a specific class of problem,
- The level of accuracy required,
- The available computational resources, and
- The amount of time available for the simulation.

To make the most appropriate choice of model for an application, one needs to understand the capabilities and limitations of the various options.

Time-dependent solutions of the Navier-Stokes equations for high Reynolds-number turbulent flows in complex geometries which set out to resolve all the way down to the smallest scales of the motions are unlikely to be attainable for some time to come. Two alternative methods can be employed to render the Navier-Stokes equations tractable so that the small-scale turbulent fluctuations do not have to be directly simulated:

➢ Reynolds-averaging (or ensemble-averaging) and

➢ Filtering.

Both methods introduce additional terms in the governing equations that need to be modeled in order to achieve a "closure" for the unknowns.

The Reynolds-averaged Navier-Stokes (RANS) equations

- Govern the transport of the averaged flow quantities, with the whole range of the scales of turbulence being modelled.
- Greatly reduces the required computational effort and resources,
- Widely adopted for practical engineering applications.
- Includes the models
    - Spalart-Allmaras,
    - k- and its variants,
    - k- and its variants,
    - -f model, and
    - The RSM.

Filtering

The large eddy simulation (LES) is categorized under the Filtering method. In LES

- Large eddies are explicitly computed (resolved)
- Error introduced by turbulence modelling can be reduced by modelling less of turbulence
- Eddies that are smaller than the size of the filter (mesh size in case of Fluent) are removed
- Significant amount of compute resources is required

The Detached Eddy Simulation (DES) model couples the RANS and LES models. The LES region is normally associated with the high-Re core turbulent region where large turbulence scales play a dominant role. In this region, the DES model recovers the pure LES model based on a one-equation sub-grid model. Close to the wall, where viscous effects prevail, the standard RANS model is recovered.

As a general guideline, the Reynolds-Averaged conventional turbulence models are recommended for practical calculations.

Reynolds (ensemble) averaging

In Reynolds averaging, the solution variables in the instantaneous (exact) Navier-Stokes equations are decomposed into the mean (ensemble-averaged or time-averaged) and fluctuating components.

For the velocity components:

$$= \bar{} + \prime$$

Where $\bar{}$ and $\prime$ are the mean and fluctuating velocity components (i = 1; 2; 3).

Likewise, for pressure and other scalar quantities:

$$= + \prime$$

. Where denotes a scalar such as pressure, energy, or species concentration. Substituting expressions of this form for the flow variables into the instantaneous continuity and momentum equations and taking a time (or ensemble) average (and dropping the over bar on the mean velocity, $\bar{}$) yields the ensemble-averaged momentum equations.

A common method employs the Boussinesq hypothesis to relate the Reynolds stresses to the mean velocity gradients.

The Boussinesq hypothesis is used in:

- The Spalart-Allmaras model,
- The k- models, and
- The k- models.

The advantage of this approach is the relatively low computational cost associated with the computation of the turbulent viscosity, . In the case of the Spalart-Allmaras model, only one additional transport equation (representing turbulent viscosity) is solved. In the case of the k- and k- models, two additional transport equations (for the turbulence kinetic energy, k, and either the turbulence dissipation rate, , or the specific dissipation rate ( ) are solved, and is computed as a function of k and . The disadvantage of the Boussinesq hypothesis as presented is that it assumes is an isotropic scalar quantity, which is not strictly true.

The alternative approach, embodied in the RSM, is to solve transport equations for each of the terms in the Reynolds stress tensor. An additional scale-determining equation (normally for) is also required. This means that five additional transport equations are required in 2D flows and seven additional transport equations must be solved in 3D.

It is better to see the RANS equations in a little bit detail for selecting a more convenient model for our specific problem.

- **The Spalart-Allmaras model**
  - It is simple,
  - Solves only one additional equation,
  - Gives good result for boundary layers with adverse pressure gradient and in turbo machinery applications,
  - It is a low Reynolds number model,
  - Applicable for course mesh resolution where accurate turbulent flow computations are not critical,
  - Is less sensitive to numerical errors.
- **The standard k- model**
  - Solves two additional equations,
  - Determines turbulent velocity and length scales independently,
  - Widely applicable in practical engineering calculations,
  - Is robust, economical, and reasonably accurate for wide range of turbulent flows and heat transfer simulations.
- **The RNG k- model**
  - Is a refined standard k- model,
  - Additional term in the equation to improve the accuracy of rapidly strained flows,
  - The effect of swirl on turbulence is included,

- Turbulence Prandtl number is given analytical formula unlike in the case of standard k- model where user-defined constants are used,
- Can be used for low Reynolds number flows, but standard k- model is a high Reynolds number flow model,
- Is more accurate and reliable than the standard k- model.

➢ **The Realizable k- . model**

- Is a refined standard k- model,
- Contains new formulations for ,
- . o equation is derived from an exact equation for mean-square vorticity fluctuation,
- The term “realizable" means that the model satisfies certain mathematical constraints on the Reynolds stresses, consistent with the physics of turbulent flows,
- It more accurately predicts the spreading rate of both planar and round jets,
- It is also likely to provide superior performance for flows involving rotation, boundary layers under strong adverse pressure gradients, separation, and recirculation,
- Provides the best performance of all the k- model versions for several validations of separated flows and flows with complex secondary flow features.

➢ **The standard k- . model**

- Incorporates modifications for low-Reynolds-number effects, compressibility, and shear flow spreading,
- Predicts free shear flow spreading rates for far wakes, mixing layers, and plane, round, and radial jets, and is thus applicable to wall-bounded flows and free shear flows.

➢ **The shear-stress transport (SST) k- . model**

- Is a refined standard k- model,

- Blends the robust and accurate formulation of the k- model in the nearwall region with the free-stream independence of the k- model in the far field using blending functions,
- Incorporates a damped cross-diffusion derivative term in the equation,
- The definition of the turbulent viscosity is modified to account for the transport of the turbulent shear stress,
- The modeling constants are different,
- Is more accurate and reliable for a wider class of flows (e.g., adverse pressure gradient flows, airfoils, transonic shock waves) than the standard k- model.

The RNG k- turbulence modeling is selected for simulation of the solar chimney because of the following reasons:

- A model requiring smaller computing resource is needed since the solar chimney is large in size,
- The geometry is not complicated,
- The flow involves bend,
- The flow arises mainly due to natural convection heat transfer in the collector.

The governing RNG k- model turbulence equations will be presented in the following section.

The RNG k- . turbulence model equations

The RNG-based k- turbulence model is derived from the instantaneous Navier-Stokes equations, using a mathematical technique called "renormalization group" (RNG) methods.

The analytical derivation results in a model with constants different from those in the standard k- model, and additional terms and functions in the transport equations for k and .

Transport equations for the RNG k- . model:

k-equation:

$$\frac{\partial}{\partial}(\quad)+\frac{\partial}{\partial}(\quad)=\frac{\partial}{\partial}\quad\quad\frac{\partial}{\partial}+\quad+\quad-\quad-\quad+ \tag{3.6}$$

-equation:

$$\frac{\partial}{\partial}(\quad)+\frac{\partial}{\partial}(\quad)=\frac{\partial}{\partial}\quad\quad\frac{\partial}{\partial}+\quad-(\quad+\quad)-\quad\frac{\partial}{\partial}-\quad+ \tag{3.7}$$

Where the model constants are obtained in **[17].**

3.5 Radiation transfer equations

FLUENT provides five radiation models, which allow one to include radiation, with or without a participating medium, in the heat transfer simulations:

- Discrete transfer radiation model (DTRM)
- P-1 radiation model
- Rosseland radiation model
- Surface-to-surface (S2S) radiation model
- Discrete ordinates (DO) radiation model

Heating or cooling of surfaces due to radiation and/or heat sources or sinks due to radiation within the fluid phase can be included in the model using one of these radiation models.

In addition to these radiation models, FLUENT also provides a solar load model that allows one to include the effects of solar radiation in the simulation.

Radiative transfer equation

The radiative transfer equation (RTE) for an absorbing, emitting, and scattering medium

at position $\vec{r}$ in the direction $\vec{s}$ is

$$\frac{\partial I(\vec{r},\vec{s})}{\partial s}+(a+\sigma_s)I(\vec{r},\vec{s})=an^2\frac{\sigma T^4}{\pi}+\frac{\sigma_s}{4\pi}\int_0^{4\pi}I(\vec{r},\vec{s}')\Phi(\vec{s}.\vec{s}')\,d\Omega' \tag{3.8}$$

where

$\vec{r}$ = *position vector* $\vec{s}$ = *direction vector*

$\vec{s}'$ = *scattering direction vector* s = *path length*

a = *absorption coefficient* n = *refractive index*

$\vec{\sigma}$ *=scattering coefficient* σ *=Stefa Boltzmann con t*

I *=radiation intensity* T*=local temperature*

Φ *=phase angle* Ω *=solid angle*

(+) is the optical thickness or opacity of the medium . The refractive index n is important when considering radiation in semi-transparent media. Figure3.1 illustrates the process of radiative heat transfer.

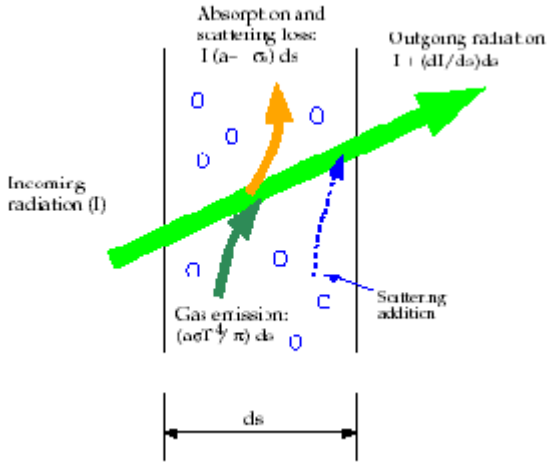

Figure 3-5: Radiative heat transfer **[2]**

Choosing a radiation model

For certain problems, one radiation model may be more appropriate than the others. When deciding which radiation model to use, the following need to be considered:

- **Optical thickness**: The optical thickness L is a good indicator of which model to use in the problem. Here, L is an appropriate length scale for the domain. For flow in a combustor, for example, L is the diameter of the combustion chamber. If L>>1, the best alternatives are the P-1 and Rosseland models. The P-1 model should typically be used for optical thickness > 1. For optical thickness > 3, the Rosseland model is cheaper and more efficient. A second-order discretization scheme is also recommended for high optical thickness cases. The DTRM and the DO model work across the range of optical thickness, but are substantially more expensive to use. So one should use the “thick-limit" models, P-1 and Rosseland, if the problem allows it. For optically thin problems (L<1), only the DTRM and the DO model are appropriate.

- **Scattering and emissivity**: The P-1, Rosseland, and DO models account for scattering, while the DTRM neglects it. Since the Rosseland model uses a temperature slip condition at walls, it is insensitive to wall emissivity.

- **Particulate effects**: Only the P-1 and DO models account for exchange of radiation between gas and particulates.

- **Semi-transparent walls (interior and exterior):** Only the DO model allows one to model semi-transparent walls of various types (e.g., glass).

- **Specular walls**: Only the DO model allows specular reflection (e.g., for dust-free mirror).

- **Partially-specular walls**: Only the DO model allows specular reflection (e.g., dusty mirror).

- **Non-gray radiation**: Only the DO model allows one to compute non-gray radiation using a gray band model.

- **Localized heat sources**: In problems with localized sources of heat, the P-1 model may over-predict the radiative fluxes. The DO model is probably the best suited for computing radiation for this case, although the DTRM, with a sufficiently large number of rays, is also acceptable.

- **Enclosure radiative transfer with non-participating media**: The surface-to-surface (S2S) model is suitable for this type of problem. The radiation models used with participating media may, in principle, be used to compute the surface-to-surface radiation, but they are not always efficient.

The DO model will be used for the simulation of the solar chimney power plant, since it is the only method used to model semi-transparent walls, and will be discussed next.

The Discrete Ordinates (DO) radiation model

The discrete ordinates (DO) radiation model solves the radiative transfer equation (RTE) for a finite number of discrete solid angles, each associated with a vector direction $\vec{}$fixed in the global Cartesian system (x; y; z). The person using the software controls the fineness of the angular discretization. The DO model does not perform ray tracing. The DO model transforms equation (3.8) into a transport equation for radiation intensity in the spatial coordinates (x; y; z). The DO model solves for as many transport equations as there are directions $\vec{}$. The solution method is identical to that used for the fluid flow and energy equations.

The implementation in FLUENT uses a conservative variant of the discrete ordinates model called the finite-volume scheme and its extension to unstructured meshes.

The DO model equations

The DO model considers the radiative transfer equation (RTE) in the direction $\vec{}$as a field equation. Thus, equation (3.8) is written as

$$\nabla \cdot ((\vec{},) \vec{} \vec{} + (\quad + \quad) (\vec{},) \vec{} = \quad \frac{}{} + \frac{}{} \int \quad (\vec{},) \Phi \square \quad \vec{s}.\vec{s} \quad d\Omega \qquad (3.9)$$

CHAPTER FOUR

ENERGY BALANCE AND DRAUGHT EQUATIONS

This part of the thesis helps to understand what is going under the simulation of the plant and how the equations under the previous chapter are used. The equations are used to determine the temperature and pressure distribution throughout the collector of the chimney power plant. **[4]**

4.1 ENERGY BALANCE

4.1.1 Energy equation for air

Consider the elementary controlled volume of collector air shown in Figure: 4.1

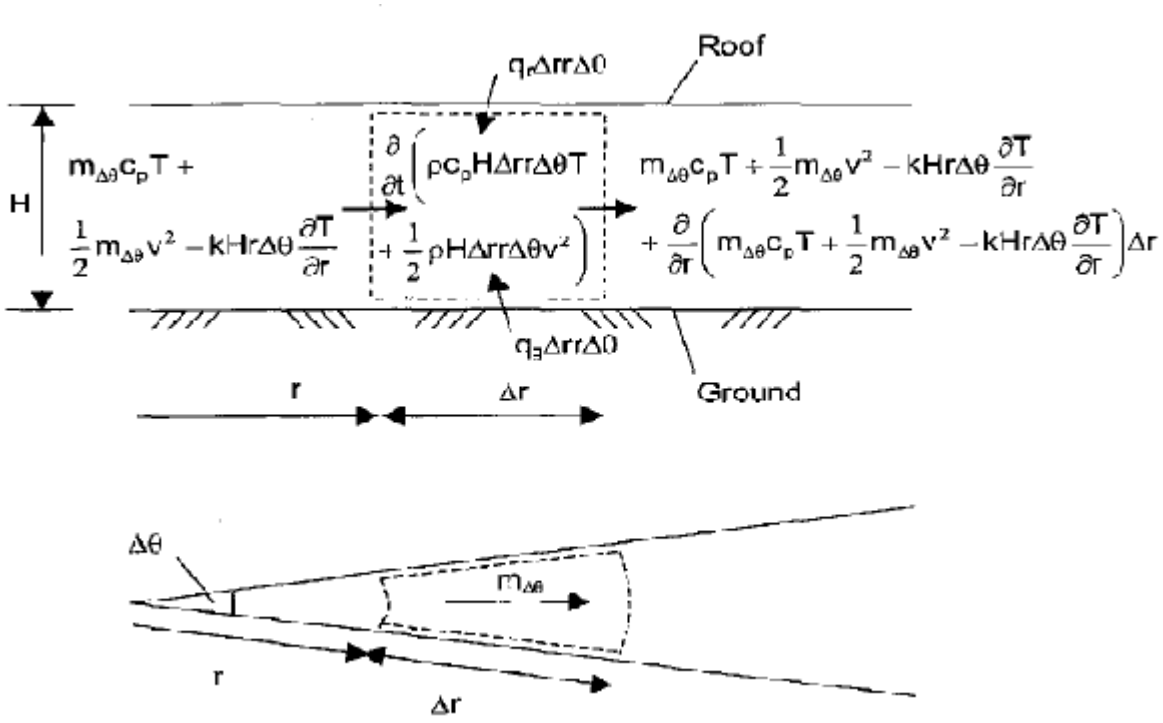

Figure. 4-1: The energy equation applied to an elementary controlled volume of air

Assuming a constant temperature distribution in the vertical plane the energy equation applicable to this control volume can be written as follows:

Δ + Δ − Δ + Δ Δ + Δ Δ = Δ + Δ −

Δ + − Δ + Δ −

− Δ Δ − + Δ Δ (4.1)

Where $_{\Delta}$ is the mass flow that passes through the control volume. Changes in the kinetic energy and conduction terms are negligible and it can be assumed that the specific heat remains essentially constant. With these approximations (4.1) is simplified to read

$$+ = \frac{\Delta}{\Delta} - + \frac{}{\Delta} \frac{\Delta}{} + - ( ) \quad (4.2)$$

According to the perfect gas law =—. Since changes in absolute pressure are essentially negligible in the collector, substitution of the expression for in to the last term of equation (4.2) results in its elimination leading to the following relation

$$+ = \frac{\Delta}{\Delta} - + \frac{}{\Delta} \frac{\Delta}{} \quad (4.3)$$

Applying the conservation of mass to the control volume of air as shown in Figure: 4.1 yields the following equation:

$$_{\Delta} = _{\Delta} + \frac{\Delta}{} \Delta + \frac{(\Delta)\Delta}{} \quad (4.4)$$

Substitute =— into equation 4.4 and find

$$\frac{\Delta}{} = -\Delta \quad — — \quad (4.5)$$

For fully developed flow the convective heat entering the control volume from the underside of the roof can be written as

$$= h (-) \quad (4.6)$$

Where h is given by the relation

$$h = \frac{( )}{. . (\cdot)} \quad (4.7)$$

Where

$$\text{Re} = 2 \quad (4.8)$$

If the surface of the roof is assumed to be smooth the Darcy friction factor is given by

$$= (1.82 - 1.64) \quad (4.9)$$

Similarly, the convective heat entering the control volume from the ground with roughness can be written as

$$= h \quad - \tag{4.10}$$

Where h is given by equation (4.7) with being given by

$$= 0.3086 \quad \frac{\cdot}{} + \frac{}{} \tag{4.11}$$

Substituting equation (4.5), (4.6) and (4.10) into equation (4.3) yields for fully developed flow

$$\frac{\Delta}{\Delta} + \quad = h \quad - \quad + h(\quad - \quad) \tag{4.12}$$

Applying this to the entire annulus (i.e. the control volume formed by increasing the inner angle to 2) we find

$$+ \quad = h \quad - \quad + h(\quad - \quad) \tag{4.13}$$

Repeat the process for the region of developing flow near the inlet of the collector where the heat transfer coefficients are defined with respect to the free stream temperature yields

$$+ \quad = h \quad - \quad + h(\quad - \quad) \tag{4.14}$$

Where h and h are now given by the developing flow equations as given by Kroger and Buys namely:

$$h = 0.0032 \cdot 1 \quad \cdot \quad - \quad \frac{\cdot \quad \cdot}{\cdot \quad \cdot} \tag{4.15}$$

For a smooth surface and

$$h = 0.0032 \cdot 1 \quad \cdot \quad - \quad \times \frac{\cdot \quad \cdot}{\cdot \quad \cdot} \tag{4.16}$$

With

= —— (4.17)

4.1.2 Energy equation for the ground

Consider an elementary control volume as shown in the Figure 2 in the ground of the collector.

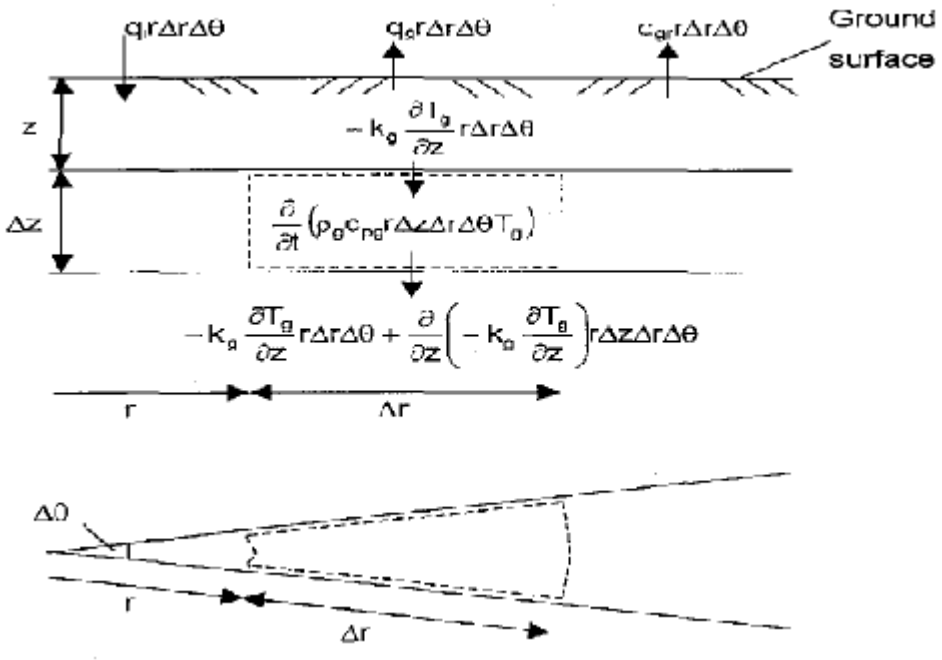

Figure 4-2: Energy equation applied to an elementary control volume of ground.

Since the temperature gradient with respect to varying depth is orders of magnitude higher than in the radial direction a one-dimensional analysis will be appropriate. The energy equation applicable to the elementary control volume shown in Figure: 4.2 is written as follows

— Δ Δ =— — Δ Δ Δ (4.18)

For constant , and this becomes

— = — (4.19)

— = + − (4.20)

at z=0, and at z=∞

$$\frac{}{} = 0 \tag{4.21}$$

Because of the transient nature of the model, the initial condition will be given as some initial temperature. The most accurate way to define initial conditions is to allow the model to run using approximate initial values for as it takes to reach a sustained convergence, and to use the output of this preliminary run s the initial conditions of the actual run.

The fraction of solar radiation entering the surface of the ground is given by

$$= (\quad) + (\quad) \tag{4.22}$$

and are beam and diffuse radiation components of the total radiation such that

$$+ = \tag{4.23}$$

The radiative heat flux between the ground and the roof is given by

$$= \frac{}{} \quad (\quad - \quad) \tag{4.24}$$

To facilitate the discretisation of equation (4.20), equation (4.24) can be written as

$$= h \quad (\quad - \quad) \tag{4.25}$$

Where the radiative heat transfer coefficient is given by

$$h = \frac{}{} \quad - \quad + \tag{4.26}$$

Substituting equation (4.10), (4.22) and (4.25) into equation (4.20) we find a new expression for the surface boundary condition in the region of fully developed flow at z=0, namely

$$\frac{}{} = h \quad - \quad + h \quad - \quad - (\quad) \quad - (\quad) \tag{4.27}$$

For the region of developing flow the boundary condition can be written as

$$\frac{}{} = h \quad - \quad + h \quad - \quad - (\quad) \quad - (\quad) \tag{4.28}$$

4.1.3 Energy equation for the roof

Consider an elementary control volume in the roof of the collector as shown in the Figure: 4.3. In this control volume the axial heat fluxes are orders of magnitude higher than the radial conduction fluxes and so the terms for the latter are negligible. It can also be shown that in order to determine the surface fluxes, the mean temperature of the roof can be used as an approximation of the surface temperature and so only one control volume will be used in the axial direction in the roof.

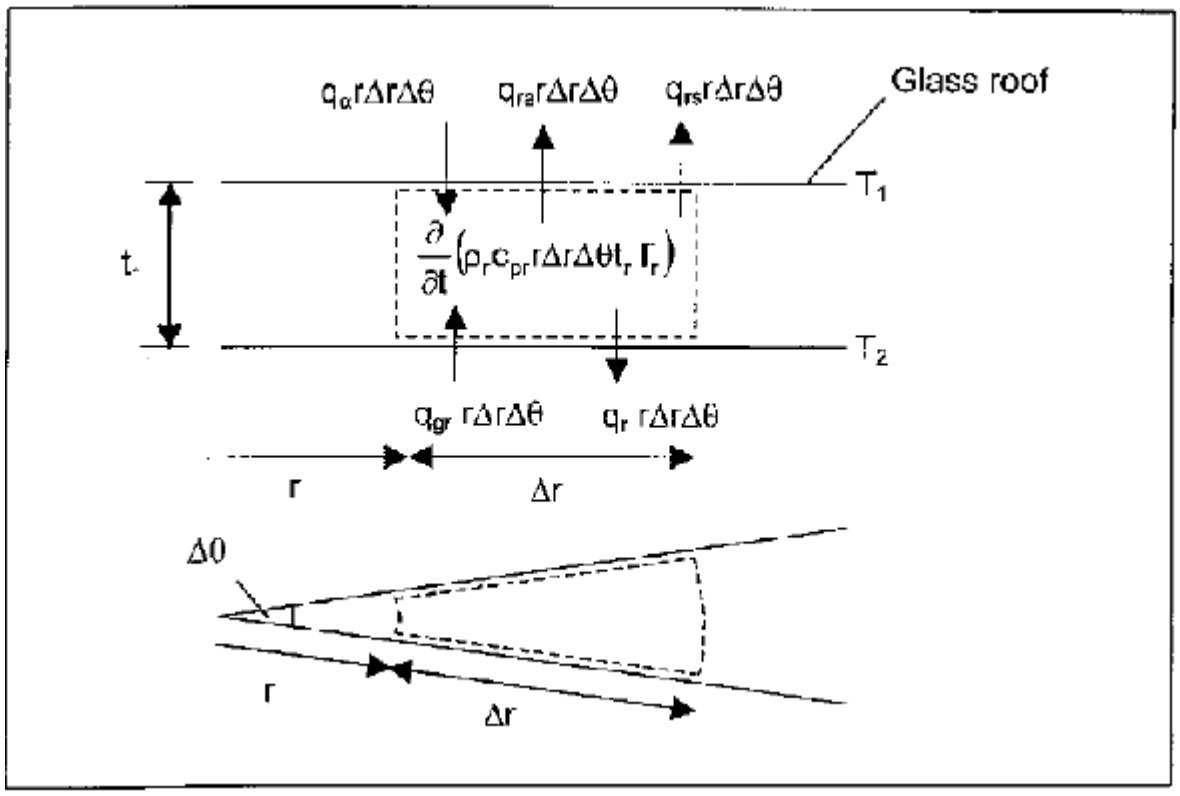

Figure 4-3: Energy equation applied to an elementary roof control volume.

The energy equation applicable to the roof control volume can thus be written as follows:

$$+ \quad - \quad - \quad - \qquad \Delta \ \Delta = (\qquad \Delta \ \Delta \ ) \tag{4.29}$$

For constant , and this can be written as

$$+ \quad - \quad - \quad - \quad = \qquad \tag{4.30}$$

Where is the fraction of solar radiation that is absorbed by the roof and is given by:

$$= (1 - \quad)(1 - \quad) \ + (1 - \quad)(1 - \quad) \tag{4.31}$$

The convective heat flux between the roof and the ambient air is given by

$$= h \quad (\quad - \quad) \tag{4.32}$$

Where h is the convective heat transfer coefficient between the roof and the ambient air. This can be found using the relation suggested by Duffle and Beckman namely

$$h \quad = 5.7 + 3.8 \tag{4.33}$$

The radiative heat flux between the roof and the ambient air can be found using the equation

$$= \qquad - \tag{4.34}$$

$$= h \quad (\quad - \qquad) \tag{4.35}$$

$$h \quad = \qquad + \qquad + \tag{4.36}$$

Where is an approximation for the product of the product of the apparent temperature of the sky and the emissivity thereof. The value of can be found using the relation suggested by swinbank

$$= 0.0552 \qquad \cdot \tag{4.37}$$

Substituting equation (4.6), (4.25), (4.31), (4.32) and (4.35) into equation (4.30) for the region of fully developed flow we find

$$(1- \quad)(1 - \qquad) \quad + (1 - \quad)(1 - \qquad) \quad + h \qquad - \qquad - h \qquad - \qquad -$$
$$h \; (\quad - \quad) - h \quad (\quad - \quad) = \qquad \text{—} \tag{4.39}$$

4.2 Draught equations (System pressure changes)

4.2.1 Collector inlet pressure drop

The total pressure outside the collector inlet is P_a. As the air is drawn towards the collector it undergoes a decrease in pressure due to its acceleration and a loss at the collector inlet. This collector inlet pressure drop is given by

$$\Delta \quad = - \qquad + - \tag{4.40}$$

Where the subscript I refers to the condition in the collector inlet as shown in the Figure 1.1. For a well-rounded inlet the value of the loss coefficient is approximately zero while a value of unit is more approximate for the case of the sharp edged inlet. Any possible

error in this approximation will be negligible since the inlet pressure drop is orders of magnitude smaller than the total pressure drop in the system.

4.2.2 Collector drag pressure drop

The collector roof is supported above the surface of the ground by the collector supports. These are positioned on radii with a radial pitch p_r and spaced tangentially on these radii p_t apart as shown in the Figure 4.4

To find the radial pressure gradient due to the drag effects of the collector supports on the air in the collector consider the force exerted by each support on the air given by

$$= \qquad 2 \tag{4.41}$$

Where V is the local free stream velocity and is given by

$$= \quad (2 \qquad) \tag{4.42}$$

Where H is the height of the collector at radius r and m is the mass flow rate. Substitute equation (4.42) into equation (4.41) and find

$$= \text{—} \quad - \quad \text{—} \tag{4.43}$$

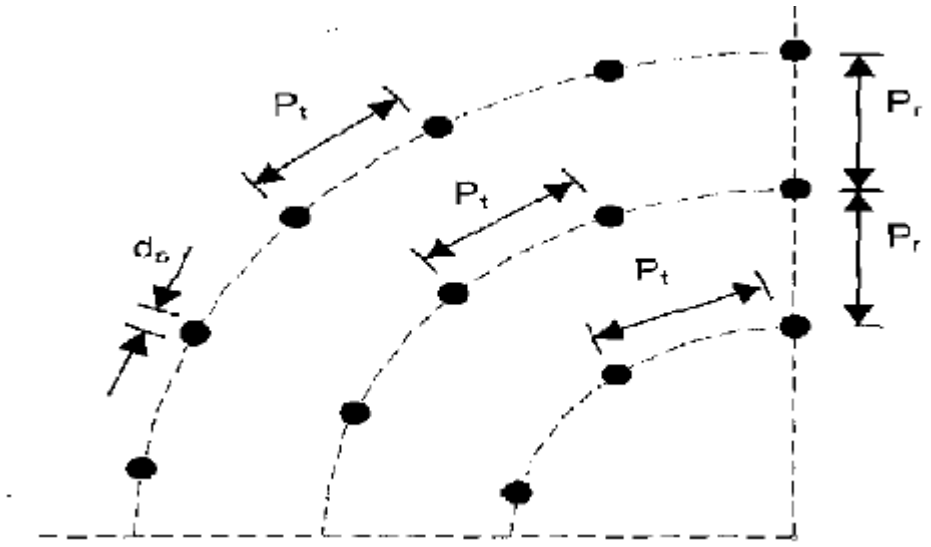

Figure 4-4: Schematic plan view of a portion of the collector showing the position of the collector supports.

With a tangential pitch the number of supports along the circumference at radius r is

$$= (2 \quad) \quad) \tag{4.44}$$

The drag on all the supports at radius r is obtained by multiplying equation (4.43) by equation (4.44)

$$= \quad = \quad (4 \quad) \tag{4.45}$$

This is the force required by the air to move radially inwards through one row of supports. The resultants corresponding pressure difference required is thus given by

$$\Delta \quad = \frac{}{} = \frac{}{} \tag{4.46}$$

Since H is given by

$$H = H \; {}^{r}{}_{r} \tag{4.47}$$

Equation (4.46) can be written as follows

$$\Delta \quad = \frac{(\quad)}{} \tag{4.48}$$

4.2.3 Accelerational pressure drop

The radial pressure gradient due to the momentum changes in the collector (acceleration) can be found as discussed in this section. Consider the control volume shown in Figure: 4.5. The force exerted on the control volume at radius of r is given by

$$= \quad \Delta \tag{4.49}$$

Similarly the force at a radius of r+ Δr is

$$_{\Delta} = - \quad \Delta \; \frac{(}{} \quad \frac{\Delta}{} \Delta \tag{4.50}$$

Applying the partial derivative operator on the right hand side yields

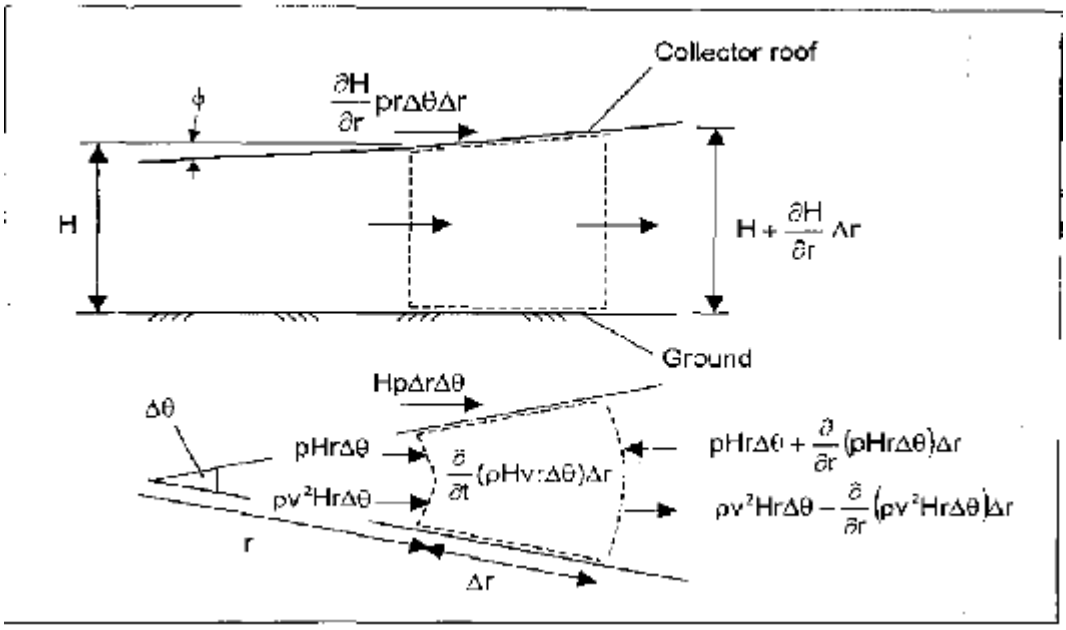

Figure 4-5: Conservation of momentum applied to an elementary control volume of air

$$_{\Delta} = -(\quad + \quad \Delta — (+ \quad \Delta) + — (\quad \Delta)\Delta \tag{4.51}$$

The forces on the side of the control volumes are calculated using the average height and pressure along each side wall. Thus the height and pressure are given by the following relations respectively.

$$= 0.5 \quad +— \Delta \quad + \tag{4.52}$$

$$= 0.5 \quad +— \Delta \quad + \tag{4.53}$$

The sum of the tangential forces acting on the sides is thus

$$= 0.5 \quad +— \Delta \quad + \quad —\Delta \quad + \quad \Delta \tag{4.54}$$

To find the radial component of the forces exerted on the sides this can be multiplied by sine(θ/2). For small angle θ this can be approximated by (θ/2) hence

$$_{,} = 0.5 \quad +— \Delta \quad + \quad —+\Delta \quad + \quad \Delta \quad \Delta \quad /2$$

$$= 0.25 \quad 4 \quad \Delta \quad +—2 \quad \Delta \quad + 2 — \quad \Delta \quad + ——\Delta \quad \Delta \tag{4.55}$$

Once again neglecting the second and third order term this can be simplified to

$$= \quad \Delta \quad \Delta \tag{4.56}$$

There also exist a force on the roof of the control volume that has a radial component.

$$= \quad \Delta \quad -\Delta \quad + \Delta \quad = \quad \Delta \quad \Delta \quad - \quad + 1 \tag{4.57}$$

Since the height gradient is small, the square of the gradient is negligible when compared to unity. The relation for the roof force can thus be approximated as

$$= \quad \Delta \quad \Delta \quad (1) = \quad \Delta \quad \Delta \tag{4.58}$$

Multiplying this by $(\sin(\phi) \approx$ — the force in the radial direction is found to be

$$= - \quad \Delta \quad \Delta \tag{4.59}$$

Summing all the forces in the radial direction we find

$$\sum F = PrH \Delta \theta + HP\Delta \quad \Delta \quad + \frac{\partial H}{\partial r} pr\Delta \quad \Delta \quad - \quad + \quad \frac{\partial P}{\partial r} \quad + \Delta \quad \frac{\partial H}{\partial r} pr\Delta \quad \Delta$$

$$= - \quad \Delta \quad \Delta \tag{4.60}$$

The momentum change across the control volume is given by

$$\Delta \quad = \quad \Delta \quad + (\quad \Delta) \Delta \quad + - (\quad - \quad) \Delta \quad - \quad \Delta \tag{4.61}$$

Equating equation (4.60) and (4.61) and using the relation $_{\Delta} =$ Δwe find

$$- \quad \Delta \quad \Delta \quad = - (\quad \Delta \quad) \Delta \tag{4.62}$$

Or

$$- = - \frac{\Delta}{\Delta} - \tag{4.63}$$

Since $= {}_{\Delta} / \Delta$ and $= /$ equation (4.63) can be written as

$$- = - \frac{\Delta}{\Delta} - \frac{\Delta}{\Delta} \tag{4.64}$$

Since R is constant and P and $_{\Delta}$ remain essentially constant with varaying r, this can be simplified to

$$- = - \frac{\Delta}{\Delta} - - \tag{4.65}$$

$$— = - \frac{\Delta}{\Delta} — \quad \text{———} \tag{4.66}$$

$$— = - \frac{\Delta}{\Delta} \quad — \qquad + (\quad - 1) \tag{4.67}$$

Equation (4.67) can be written in terms of the total mass flow using the relation

$$_{\Delta} = \frac{\Delta}{—} \tag{4.68}$$

Then

$$— = - \frac{\Delta}{\text{———}} \quad — \qquad + (\quad - 1) \tag{4.69}$$

Where m is negative in the solar chimney power plant. Equation (4.69) can be used to approximate the pressure differential over one control volume hence

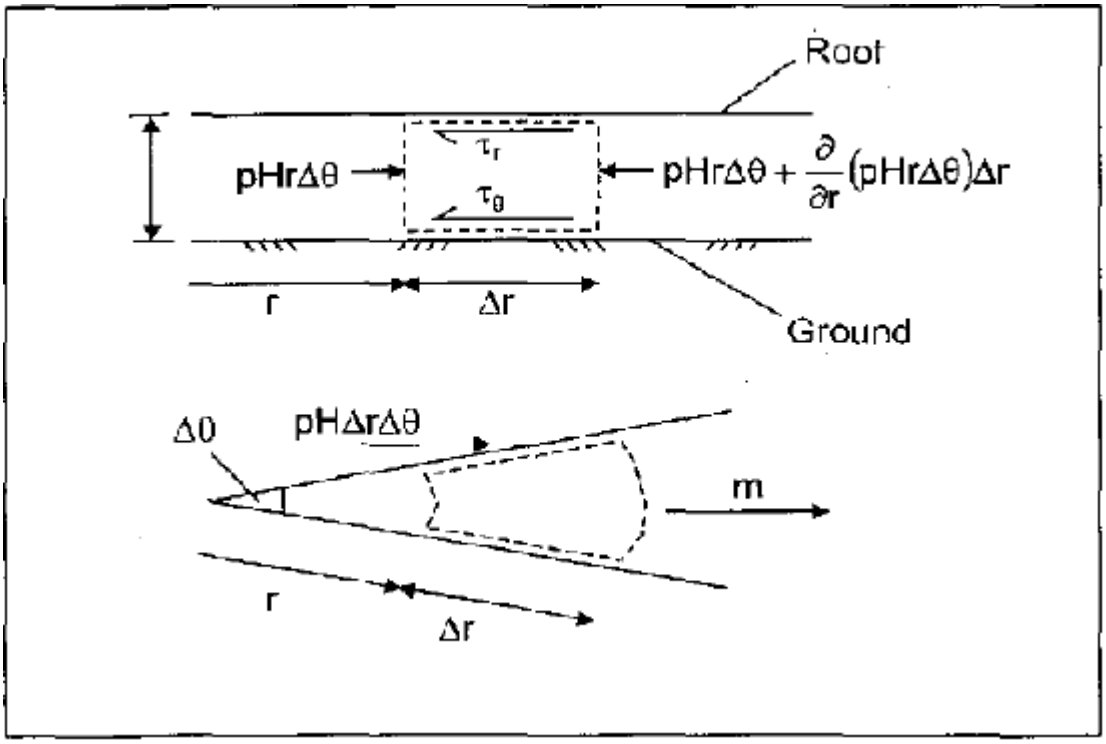

Figure4-6: Momentum equation applied to the air, taking only the frictional pressure drop in account.

$$\Delta \qquad = - \text{————} \quad — \qquad + (\quad - 1) \qquad \Delta \tag{4.70}$$

4.2.4 Collector frictional pressure drop

The radial pressure gradient due to the frictional drag on the ground and the underside of the roof can be found as follows:

Applying the conservation of momentum to the control volume as shown in the Figure: 4.6 considering only the pressure drop due to the shear stresses on the ground and roof and ignoring the change in collector height yields

$$HP\ \Delta\ -HP\ \Delta\ —(HP\ \Delta\ )\Delta\ +HP\Delta\ \Delta\ =\ \Delta\ \Delta\ +(\ \ ) \tag{4.71}$$

Dividing throughout by Δ and neglecting the higher order terms since they are orders of magnitude smaller than the others we find

$$— = -\frac{(\quad)}{\quad} \tag{4.72}$$

Substitute the height as given by equation (4.47) in to equation (4.72) to give

$$— = -— -\ (\ +\ ) \tag{4.73}$$

According to Kroger and Bugs the shear stress exerted by the roof (assuming that it is smooth) on the air in the region of developing flow can be given approximately by

$$= -0.01392\ \cdot(-)\ \cdot \tag{4.74}$$

Where the core velocity is given approximately by

$$V=\frac{}{} \tag{4.75}$$

And where the boundary layer thickness for flow moving radially inwards across a smooth plate is given by

$$(\ ) =\ \{\frac{}{}(—)\ —\ [(—)\ \cdot\ \cdot -\ -\ ]\} \tag{4.76}$$

Similarly the following relation may be used to find the shear stress for developing radial flow over a rough disc

$$= -0.008326\ -\ 1.94\ —\ +1 \tag{4.77}$$

With the boundary layer thickness being by

$$( ) = \quad - \quad - \quad \frac{(-) \quad - \quad}{} + \frac{- \quad -}{}$$

4.78 With b≠ 0.3757, b≠ 0.453 and

$$= \frac{}{} \tag{4.79}$$

Substituting equations (4.74) and (4.77) into equation (4.73) we find the pressure gradient due only to frictional forces on the roof and ground for the region of developing flow

$$\Delta \quad = - - \quad 0.01392 \frac{}{} - \quad - \quad \frac{}{(-) \quad -} \quad +$$

$$0.008326 \quad 1.94 \frac{}{} + 1 \frac{}{} - \quad - \quad \times$$

$$\frac{(-) \quad - \quad}{} + \frac{- \quad -}{} \quad \Delta \tag{4.80}$$

Kroger and Buys suggested that for the region of fully developed flow the shear stress on the roof and ground are given by

$$= - \frac{}{} \tag{4.81}$$

And

$$= -0.02975 \quad - \quad 1.75 \frac{}{} + 1 \quad - \tag{4.82}$$

Respectively, substituting equations (4.81) and (4.82) into equation (4.73) we find for the region of fully developed flow

$$\Delta \quad = - - \quad \left\{ 0.02975 \frac{}{} \quad 1.75 \frac{}{} + 1 \quad - + \right\} \Delta \tag{4.83}$$

4.2.5 Chimney inlet pressure drop

The pressure drop caused by friction and momentum changes between the collector outlet and the turbine inlet is given by

$$\Delta = - \quad (4.84)$$

Where is the turbine inlet loss coefficient. The loss coefficient is dependent on the geometry of the region of the plant at the inlet to the turbine and is thus specified in the reference plant specifications.

4.2.6 Turbine pressure drop

The pressure drop over the turbine can be found using the relation $=\ \Delta$ where p and V are the turbine power and volume flow respectively. Thus the turbine pressure drop is given by

$$\Delta = \quad (4.85)$$

4.2.7 Chimney appurtenances drag pressure drop

The approximate pressure drop caused by the appurtenances in the chimney is given by

$$\Delta = - \quad (4.86)$$

where is defined relative to the conditions at the turbine inlet. This coefficient is also dependent on the geometry of the system and is specified in the reference plant specifications.

4.2.8 Chimney friction pressure drop

The approximate pressure drop caused by the frictional drag in the chimney is given by

$$\Delta = \quad (\quad _2) \quad (4.87)$$

Haaland's equation for the Darcy friction facture is best suited to the fully developed turbulent flow with / small i.e.

4.2.9 Chimney accelerational pressure drop

The approximate differential due to the momentum changes in the chimney is given by

$$\Delta \quad = — \quad (\quad - \quad) + — (\qquad) \quad \approx \frac{}{} \quad — - —$$ (4.88)

4.2.10 Chimney exit pressure change(recovery)

The pressure of the air leaving the chimney differs from the ambient pressure at the chimney exit height by

$$\Delta \quad = -$$ (4.89)

Where the chimney outlet pressure less coefficient is given by

$$= -0.28 \qquad + 0.04$$ (4.90)

With the densimetric Froude number being given by

$$= \sqrt{\qquad} \qquad [\quad (\qquad - \quad) \quad]$$ (4.91)

where the subscript refers to the ambient conditions at the elevation of the chimney outlet. The densities at this elevation outside and inside respectively of the chimney are found using the relations

$$= \frac{}{} \quad 1 — \frac{}{\qquad}$$ (4.92)

$$= \frac{}{} \quad 1 — \frac{}{\qquad}$$ (4.93)

the kinetic energy lost at the exit of the chimney is expressed as

$$\text{Dynamic loss} = 0.5$$ (4.94)

Where is the kinetic energy correlation factor. Du preez and Kroger find that for $1/ \quad \leq 3$ at the exits of dry cooling towers is equal to unity. Since the exit of the chimney may be approximated as dry cooling tower exit and is approximately two, the kinetic energy correction factor is taken as unity.

4.3 Pressure driving potential

Having discussed the system pressure losses it is now appropriate to discuss the driving potential of the solar chimney. The driving potential is essentially the difference between pressure potentials caused by the column of cold (ambient) air outside the chimney and the equivalent column of the warm air inside the chimney. This can be written as

$$- \quad (\quad - \quad) \tag{4.95}$$

Since the pressure at the exit plane of the chimney ( ) and the pressure outside the chimney but at the same elevation as the chimney exit ( ) are approximately equal, the driving potential given in expression (4.93) can be reduced to

$$(\quad - \quad) - (\quad - \quad) \approx \quad - \tag{4.96}$$

The values for and are given by the following equations respectively (if it is assumed that an adiabatic lapse rate and isentropic expansion are applicable and if the air is assumed dry).

$$= \quad (1 - 0.00975 \quad / \quad) \cdot \tag{4.97}$$

$$= \quad (1 - 0.00975 \quad / \quad) \cdot \tag{4.98}$$

Once again making use of fact that the exit pressure of the chimney is very close to the ambient pressure at the same height the following is applicable.

$$(1 - 0.00975 \quad / \quad) \cdot = \quad (1 - 0.00975 \quad / \quad) \cdot \tag{4.99}$$

$$= \quad \{(1 - 0.00975 \quad / \quad)/(1 - 0.00975 \quad / \quad)\} \cdot \tag{4.100}$$

This can be rewritten to give as expression for the driving potential as follows,

$$- \quad = \quad [\{(1 - 0.00975 \quad / \quad)/(1 - 0.00975 \quad / \quad)\} \cdot] \tag{4.101}$$

This is the net driving potential in the solar chimney power plant.

The draught available to the turbine is thus the driving potential less the sum pressure drops throughout the system and is given by the draught equation namely

$$\Delta \quad = \quad - \quad - \Delta \quad - \Delta \quad - \Delta \quad - \Delta \quad - \Delta \quad - \Delta \quad - \Delta \quad - 0.5 \tag{4.102}$$

CHAPTER 5

DISCRETISATION OF ENERGY EQUATIONS

In this part the equations derived above will be solved. Because of the nature of the equations a numerical solution will be required. For this reason each one of the energy equations will be descritised to be transformed from differential equations to explicit algebraic equations.

5.1 Control volume convention

A set of control volumes (hereafter a control volume set will refer to the roof, air and ground control volumes whose nodes occur on a particular radius) is shown in Figure 4.1(two neighboring air control volumes are shown in dotted lines as well because they are used in the air calculations). These control volumes are annular in shape and are arranged in horizontal layers. Each control volume is represented by a node occurring on a circular line at the average radius of the control volume. The nodes in the roof and air control volumes are also situated at the average height of the control volumes while the ground control volumes are divided by planes midway between the nodes.

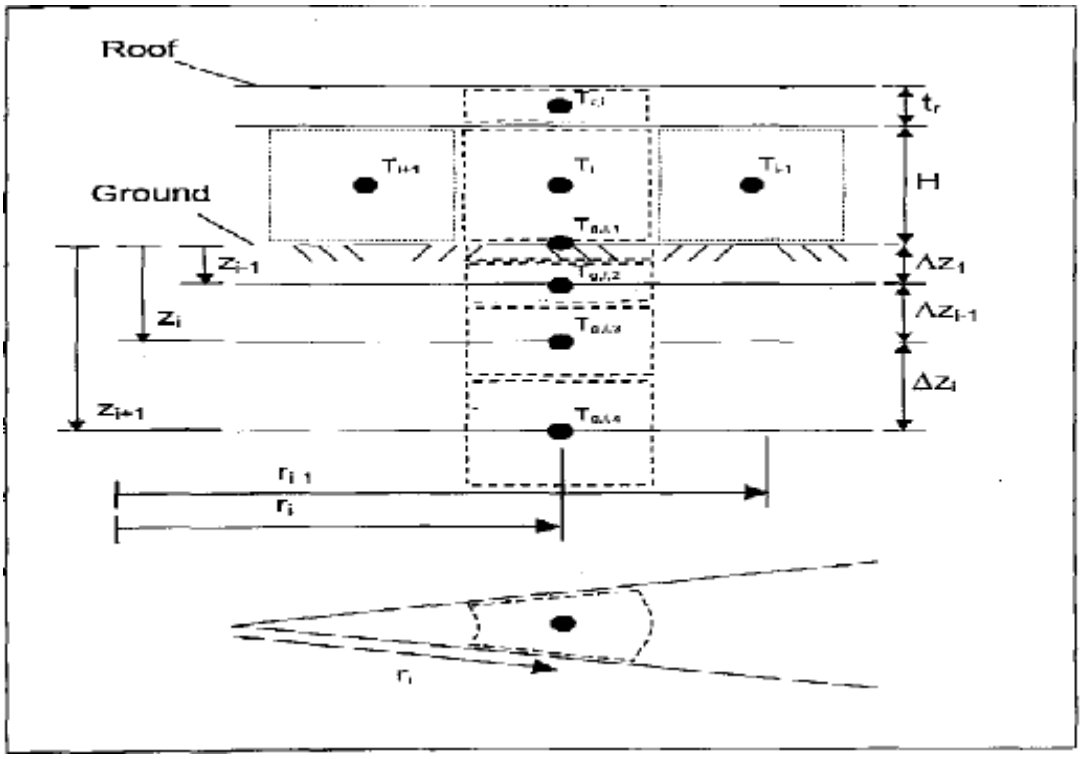

Figure 5-1: A set of control volumes and two neighboring air control volume

5.2 The discritisation schemes

A finite difference scheme is employed to discritese the energy equations. Although a central difference scheme is more accurate than an upwind finite difference scheme the latter is more suitable for the radial temperature gradients in the collector air because it does not cause decoupling. It approximates the gradient at a node with the finite difference between a control volume and its upwind neighbor. The time gradients will be modeled with the finite difference between the present and past property value. Thus the well known scheme namely the backward tome-backward space scheme (BTBS) is employed.

The heat transfer in the ground is of such a nature that simple backward time-central space (BTCS) scheme can be used. This models the temperature gradients with the average difference between the two neighboring control volume and the one question.

5.3 The discretised air equation

The energy equation applicable to the air according to equation (4.13) for the region of fully developed flow given by

$$\rho c \frac{\partial T}{\partial t} + \rho c v \frac{\partial T}{\partial x} = h_{} - + h(-) \tag{5.1}$$

Or applying the BTBS scheme

$$\rho c \frac{T_{,} - T_{,}'}{\Delta t} + \rho c v_{,} \frac{T_{,} - T_{,}'}{\Delta x} = h_{,} - + h_{,} - \tag{5.2}$$

Where the subscripted index refers to the radial position of the point at which the value is taken. (see Figure: 5.1) Manipulating this equation yields

$$= \frac{\dfrac{}{} \quad \dfrac{}{}}{\dfrac{}{} \quad \dfrac{}{}} \tag{5.3}$$

Applying these steps to the region of developing flow results in a similar equation namely

$$= \frac{\dfrac{}{} \quad \dfrac{}{}}{\dfrac{}{} \quad \dfrac{}{}} \tag{5.4}$$

The inlet boundary condition can be implemented by replacing in equation (5.4) with the collector inlet temperature .

5.4 The discretised ground equation

The energy equation applicable to the ground is simple time-dependent one-dimensional conduction equation and is according to equation (4.19)

$$\frac{\partial T}{\partial t} = \frac{\partial}{\partial z}\left(\alpha \frac{\partial T}{\partial z}\right) \tag{5.5}$$

The time derivative can be approximated using a backward difference hence

$$\frac{\partial T}{\partial t} \approx \frac{T_{i,j} - T_{i,j-1}}{\Delta t}, \tag{5.6}$$

Where the subscripted index once again refers to the position (depth) at which the temperature is given. (See Figure: 5.1)

The second derivative applied to the ground temperature with respect to depth (z) is approximated with the central difference scheme. This is done while making provision for the variation of consecutive control volume thicknesses as follows (with the distance between Δ being the distance between the node at and the node below it).

$$\frac{\partial}{\partial z}\left(\alpha \frac{\partial T}{\partial z}\right) \approx \frac{\alpha_{i,j}\left(\frac{T_{i+1,j} - T_{i,j}}{\Delta z_{i+1}}\right) - \alpha_{i-1,j}\left(\frac{T_{i,j} - T_{i-1,j}}{\Delta z_{i}}\right)}{\frac{1}{2}(\Delta z_{i} + \Delta z_{i+1})} \tag{5.7}$$

Applying the second derivative we find

$$\frac{\partial}{\partial z}\left(\alpha \frac{\partial T}{\partial z}\right) \approx \frac{\alpha_{i,j} T_{i+1,j} - \alpha_{i,j} T_{i,j}}{\frac{1}{2}\Delta z_{i} \Delta z_{i+1}} - \frac{\alpha_{i-1,j} T_{i,j} - \alpha_{i-1,j} T_{i-1,j}}{\frac{1}{2}\Delta z_{i} \Delta z_{i+1}} \tag{5.8}$$

Substituting equation (5.6) and (5.8) in to equation (5.5) yields

$$\frac{T_{i,j} - T_{i,j-1}}{\Delta t} = \left[\frac{\alpha_{i,j} T_{i+1,j} - \alpha_{i,j} T_{i,j}}{\frac{1}{2}\Delta z_{i} \Delta z_{i+1}} - \frac{\alpha_{i-1,j} T_{i,j} - \alpha_{i-1,j} T_{i-1,j}}{\frac{1}{2}\Delta z_{i} \Delta z_{i+1}}\right] \tag{5.9}$$

Solving this equation for $T_{i,j}$ yields

$$T_{i,j} = \frac{\frac{\alpha_{i,j} T_{i+1,j}}{\frac{1}{2}\Delta z_{i} \Delta z_{i+1}} + \frac{\alpha_{i-1,j} T_{i-1,j}}{\frac{1}{2}\Delta z_{i} \Delta z_{i+1}} + \frac{T_{i,j-1}}{\Delta t}}{\frac{1}{\Delta t} + \frac{\alpha_{i,j}}{\frac{1}{2}\Delta z_{i} \Delta z_{i+1}} + \frac{\alpha_{i-1,j}}{\frac{1}{2}\Delta z_{i} \Delta z_{i+1}}} \tag{5.10}$$

This equation can be applied to the control volumes in the ground from the second one to the penultimate one. For the first control volume (the just below the surface) the following analysis is applicable. Applying an energy balance over the control volume as shown in the Figure: 5.2 yields for the region of fully developed flow

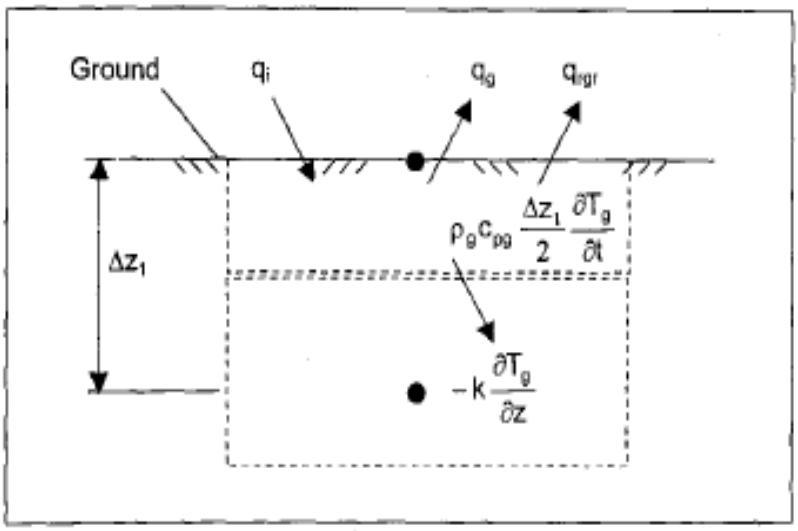

Figure 5-2: An energy balance applied to the ground control volume just below the surface

$$= \quad + \quad - \frac{,}{\Delta} + - \quad \frac{\Delta}{} \frac{}{,} \tag{5.11}$$

This can be approximated using the BTBS scheme as

$$= h \quad , - \quad + h \quad , - \quad + \frac{, \quad ,}{\Delta} + - \quad \frac{\Delta \ (\quad , \quad , \quad),}{} \tag{5.12}$$

Manipulating this gives

$$, = \frac{\frac{,}{\Delta} \quad \frac{\Delta}{} \quad ,}{\frac{\Delta}{} \quad \frac{\Delta}{}} , \tag{5.13}$$

The derivation of an equation for , for the region of developing flow is done in a similar manner to that used to find equation (5.3). The resulting equation follows

$$, = \frac{\frac{,}{\Delta} \quad \frac{\Delta}{} \quad ,}{\frac{\Delta}{} \quad \frac{\Delta}{}} , \tag{5.14}$$

The temperature at the last node , (where is the number of layers used to model the ground) can be found by using the boundary condition given by equation (4.21) namely at $= \infty$

$$\frac{}{} = 0 \tag{5.15}$$

This can be approximated as follows

$$\frac{\quad'\qquad\qquad'\quad}{} = 0 \tag{5.16}$$

Or

$$= \quad' \tag{5.17}$$

5.5 The Discretised roof equation

The equation describing the heat transfer in the roof in the region of fully developed flow is given by equation (4.38) as

$$(1- \quad)(1- \quad) + (1- \quad)(1- \quad) + h \quad - \quad - h \quad - \quad -$$
$$h\,(\quad - \quad) - h\,(\quad - \quad) = \quad \frac{}{} \tag{5.18}$$

Approximating the time gradient with a back difference, equation (5.18) can be written as

$$(1- \quad)(1- \quad) + (1- \quad)(1- \quad) - h \quad - \quad - h \quad -$$
$$) - h\,(\quad - \quad) - h\,(\quad - \quad) = \quad (\quad - \quad' \,)/ \tag{5.19}$$

$$= \frac{(\quad)(\quad) \quad (\quad)(\quad) \qquad\qquad \frac{\qquad'}{}}{\frac{}{}} \tag{5.20}$$

The equivalent equation for the region of developing flow is written as follows

$$= \frac{(\quad)(\quad) \quad (\quad)(\quad) \qquad\qquad \frac{\qquad'}{}}{\frac{}{}} \tag{5.21}$$

CHAPTER SIX

SIMULATION OF THE SOLAR CHIMNEY

This chapter deals with modeling of solar chimney with thermal storage system using FLUENT and compare the expected power output with solar chimney without thermal storage system. The actual structure of the plant is three dimensional, but axisymmetric flow assumption reduces it to two dimensional for both solar chimneys, as shown in Figure 6.1 and Figure 6.2. Complete analysis of the solar chimney consists of designing the structure and modeling flow and heat transfer. The main focus of the thesis is modeling of fluid flow and heat transfer for the evaluation of the power output, seeing the effects of thermal storage system and the position of turbine on the power output.

Soil with depth of 5m is included in the model as shown in Figure 6.1 b. The soil temperature remains constant below about 5m according to Dr. D. L. Nofziger of Department of Plant and Soil Sciences, Oklahoma State University. [1]

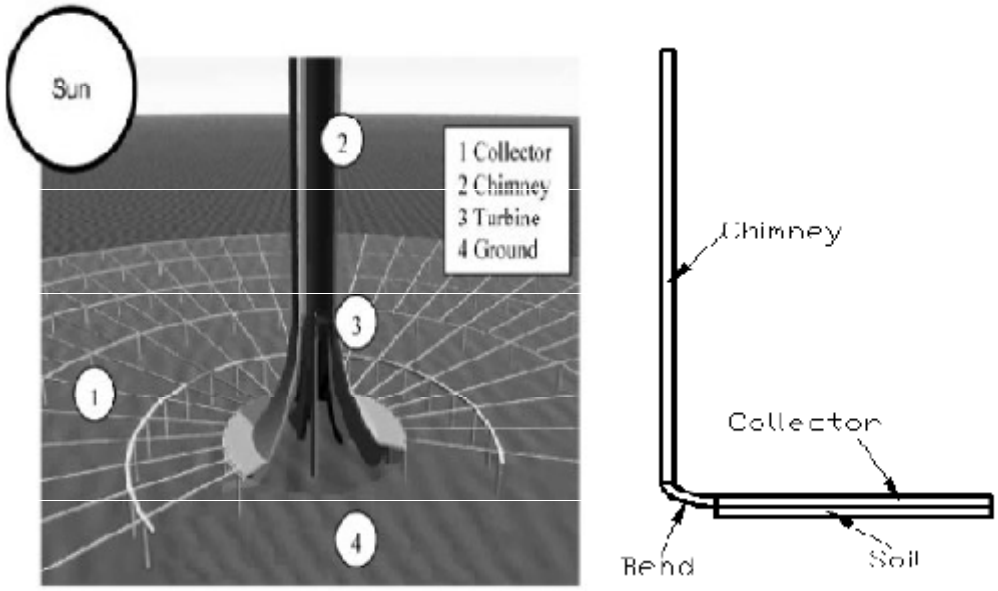

a. 3D Structure [11]

b. Axisymmetric 2D Model for SC without thermal storage system

Figure 6-1: Geometry of the Solar Chimney without thermal storage tank

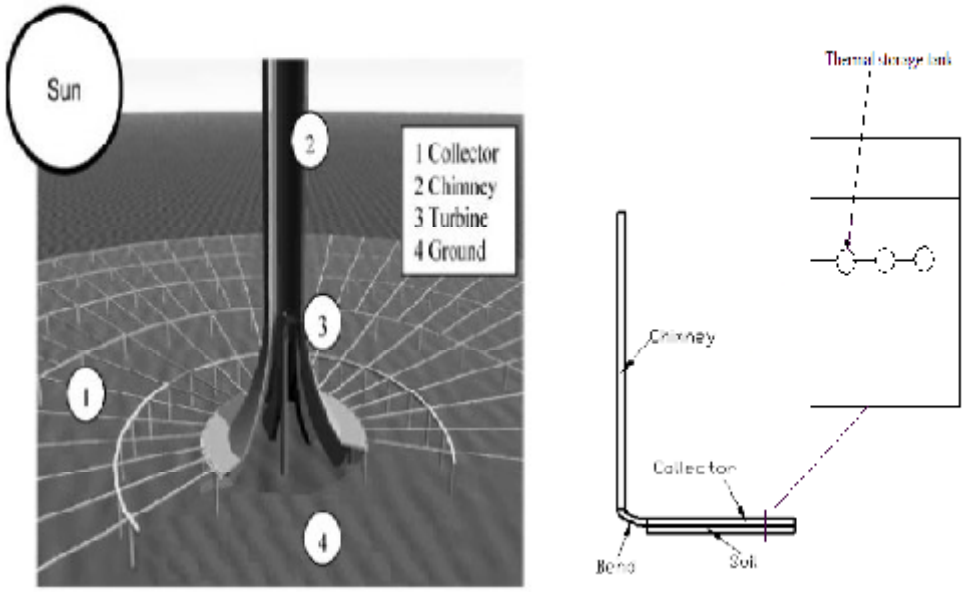

a. 3D Structure b. Axisymmetric 2D Model for SC with thermal storage system

Figure 6-2: Geometry of the Solar Chimney with thermal storage tank

The following simplifying assumptions were made modeling the plant:

- Axisymmetric flow of air and water in the collector and the thermal storage tank respectively is assumed, i.e., non-uniform heating of the collector surface and thermal storage tank in terms of the sun's altitude angle is neglected.
- Frictional losses are not considered. Since the fluid used is air, frictional losses are negligible due to the low viscosity of air.
- The Boussinesque approximation is assumed to be valid. This approximation neglects all variations of properties except for density in the momentum equation.
- It also simplifies the density difference term employing a simplified equation of state.
- Heat loss from the chimney wall and the bend is assumed to negligible.

The general steps followed in the simulation are described below:

- Building geometry on GAMBIT
- Creating geometry,

- Meshing edges and faces,
- Setting boundary conditions and continuum types, and
- Exporting mesh file.
- Preprocessing on FLUENT
- Reading mesh file,
- Checking the grid,
- Smoothing and swapping the grid,
- Displaying the grid,
- Setting models (solver, viscous, energy and radiation),
- Setting materials (air, soil, glass),
- Setting operating conditions,
- Defining boundary conditions,
- Solution control (selecting coupling methods, initializing, residuals, surfaces, iterating), and
- Checking for convergence.
- Post processing on FLUENT
- Displaying results (contours, xy plots, etc)

The power obtained from the solar chimney power plant depends on both chimney height and collector diameter. Therefore, different combinations of these two parts can be constructed. The geometry selected for simulation in this thesis has the dimensions shown in Figure 6.3. This geometry was selected, for comparison purpose; because experimental results of the same geometry are obtained from the prototype constructed in Spain and was previously simulated by Ato Getachew Shunki for the case of Afar using solar chimney power plant without thermal energy storage system. But I will first do the simulation of solar chimney with thermal storage system and then repeat the work done by him for the purpose of check up and comparison with mine.

6.1 Solar chimney with thermal storage systems

For additional thermal storage capacity, water filled black tubes are laid down side by side on the radiation absorbing soil under the collector (Kreetz 1997). The tubes are filled with water once and remain closed thereafter, so that no evaporation can take place.

I will simulate by modeling the system to see the effect of these thermal storage system.

6.1.1 Building geometry on GAMBIT

Since the software Fluent doesn't understand the system unless the axis of the solar chimney is placed on the X axis I had built the geometry by placing the chimney axis on the X axis. Building of the geometry includes the following steps:

a) Creating geometry

Figure 6.3 shows the dimensions of the geometry to be created. The possible steps to be followed are:

- Creating vertices a, b… j and four vertices for each thermal storage tank (pipe of diameter 20cm) at a radial distance of 20cm from each other.
- Creating edges by connecting the vertices,
- Creating faces (chimney, bend, collector, thermal storage tank and soil) using the edges.

Chimney, thermal storage tank (pipes) and bend wall thicknesses were taken to be zero because the heat loss from these walls is assumed to be zero. Glass thickness was also taken to be zero since its absorption is not significant.

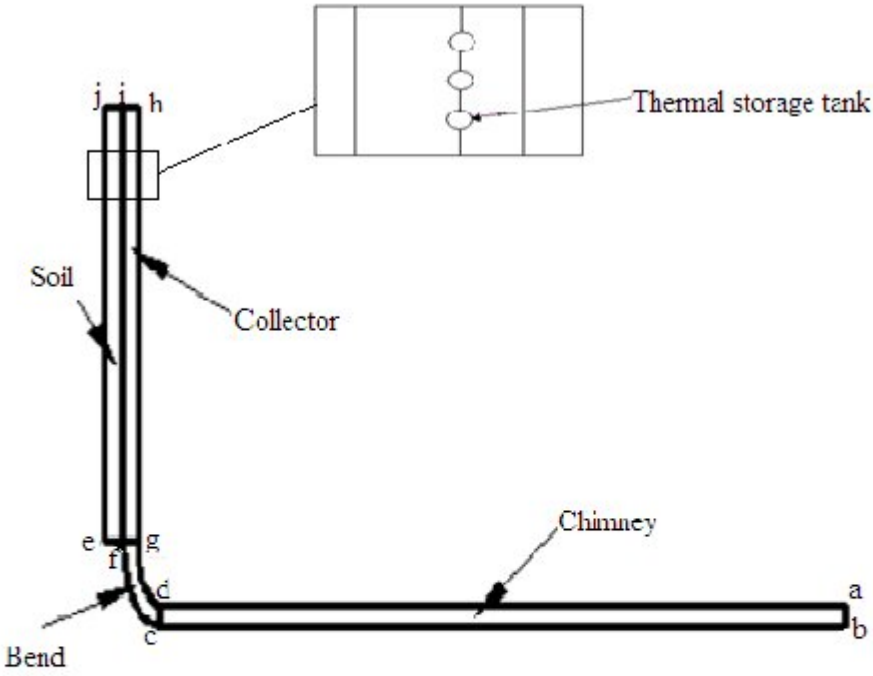

Coordinates

a(195,5)	f(0,13.3)
b(195,0)	g(1.7,13.3)
c(10,0)	h(1.7,120)
d(5,10)	i(0,120)
e(-5,13.3)	j(-5,120)

Figure 6-3: Dimensions of the solar Chimney

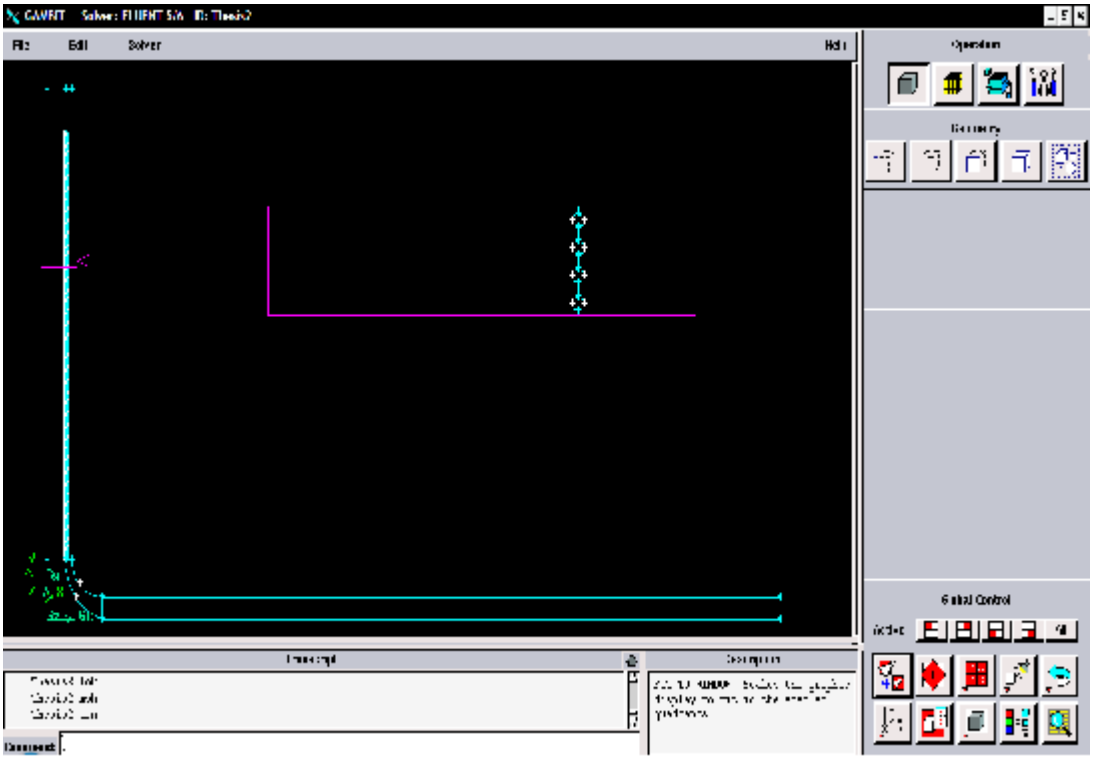

Figure 6-4: The actual geometry that was created

b) Meshing the geometry

FLUENT is finite volume numerical method software. Solutions by numerical methods require meshing of the geometry. The accuracy of the solutions depends on the sizes of the meshes (cells). The smaller the mesh size the more accurate the solution will be. But as the mesh size decreases the number of mesh increases. This results in the requirement of large computing capacity and time. So, one has to make a compromise between these two problems. The meshing process has to proceed until the solution becomes grid independent. Further reduction of mesh size has the disadvantage of requiring more computer memory. In this model, edges of the faces are meshed before meshing the faces. The sizes of the mesh cells near the walls need to be smaller compared to those far from the walls because property gradients are large near walls, Figure 6.5. Faces chimney, soil and collector were meshed using the Quad meshing scheme. The bend and thermal energy storage tank were meshed using the Quad/Tri meshing scheme since it has irregular geometry.

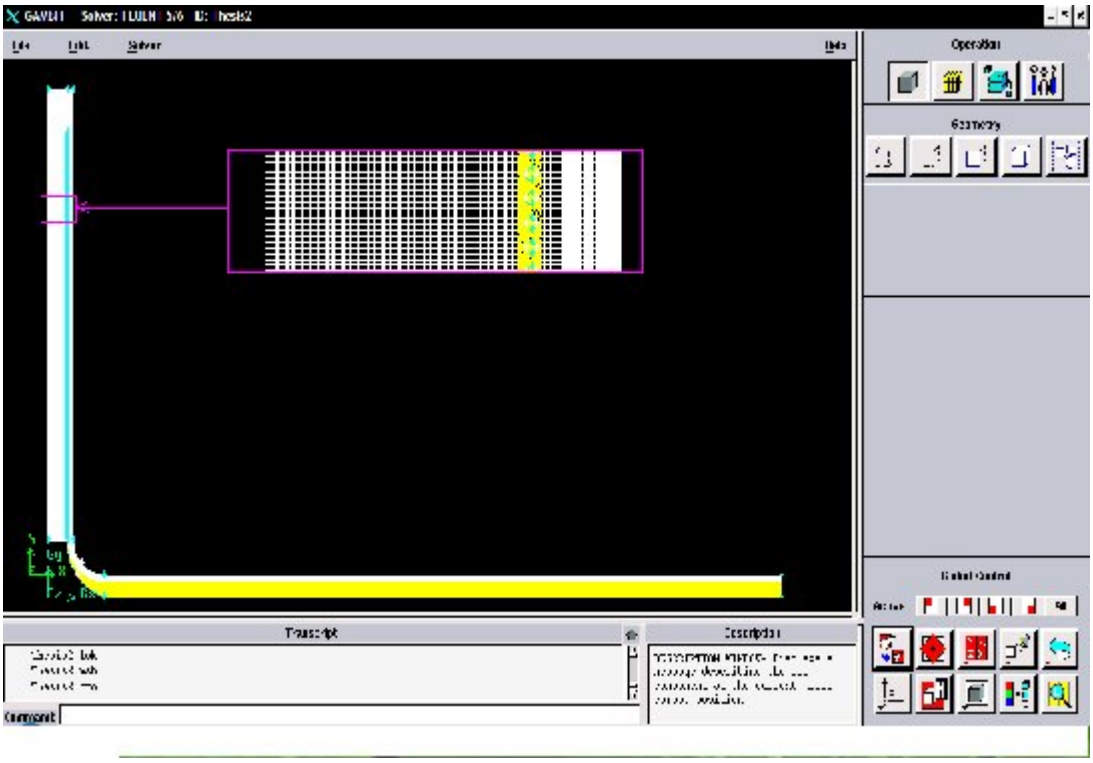

Figure 6-5: Grid of the geometry

c) Setting boundary conditions

Boundary-type specifications define the physical and operational characteristics of the model at those topological entities that represent model boundaries. Five types of boundary conditions were set for the solar chimney. These are wall, pressure inlet, pressure outlet, fan and axis.

Wall boundary conditions are used to bound fluid and solid regions. In viscous flows, the no-slip boundary condition is enforced at walls by default, but one can specify a tangential velocity component in terms of the translational or rotational motion of the wall boundary. Five types of thermal wall boundary conditions are available when solving the energy equation:

- Fixed heat flux
- Fixed temperature
- Convective heat transfer
- External radiation heat transfer
- Combined external radiation and convection heat transfer

Pressure inlet boundary conditions are used to define the fluid pressure at flow inlets, along with all other scalar properties of the flow. They are suitable for both incompressible and compressible flow calculations. Pressure inlet boundary conditions can be used when the inlet pressure is known but the flow rate and/or velocity is not known.

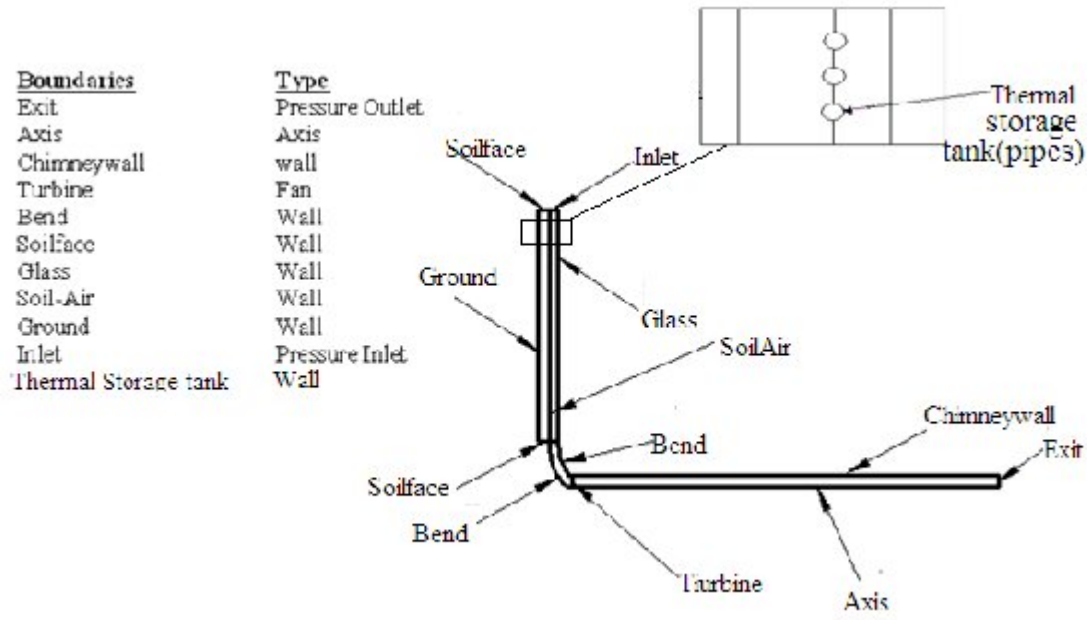

Figure 6-6: Boundary types of the solar chimney

Pressure outlet boundary conditions require the specification of a static (gauge) pressure at the outlet boundary. The value of the specified static pressure is used only when the flow is subsonic. Should the flow become locally supersonic, the specified pressure will no longer be used; pressure will be extrapolated from the flow in the interior. All other flow quantities are extrapolated from the interior.

The ***fan*** model is a lumped parameter model that can be used to determine the impact of a fan/turbine with known characteristics upon some larger flow field. The fan boundary type allows inputting an empirical fan curve which governs the relationship between head (pressure rise/drop) and flow rate (velocity) across a fan/turbine element.

The ***axis boundary*** type must be used as the centerline of an axisymmetric geometry. It can also be used for the centerline of a cylindrical-polar quadrilateral or hexahedral grid. It is not needed to define any boundary conditions at axis boundaries.

d) Setting continuum types

Continuum-type specifications define the physical characteristics of the model within specified regions of its domain. Figure 6.7 shows the types of continuum specified for the solar chimney.

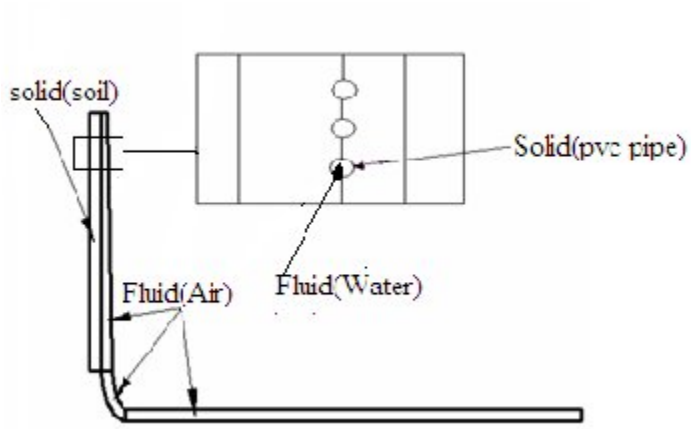

Figure 6-7: Continuum types of the solar chimney

e) Exporting mesh file

FLUENT (the solver) needs models generated on other model developing software like GAMBIT. The models need to be exported so that FLUENT can readily use them for analysis.

6.1.2 Preprocessing on FLUENT

The preprocessing was done according to the following steps for the unsteady state case and we can refer the previous thesis for the steady state case.

a) Reading mesh file

The first step in the preprocessing stage is reading mesh file of the model, which was already exported by model developing software (GAMBIT in this case). From FLUENT's point of view, a mesh file is a subset of a case file. The mesh file contains the coordinates of all the nodes, connectivity information that tells how the nodes are connected to one another to form faces and cells, and the zone types and numbers of all the faces (e.g., wall, pressure-inlet, symmetry). The mesh file does not contain any information on boundary conditions, flow parameters, or solution parameters.

File ➡ Read ➡ Case

b) Displaying grid

During the problem setup or when examining the solution, one may want to look at the grid associated with certain surfaces. The outline of all or part of the domain can be displayed. If any problem is observed in the displayed grid, revision of the model is required.

c) Checking mesh

Once the mesh file is read to FLUENT, it has to be checked before starting the analysis. The grid checking capability in FLUENT provides domain extents, volume statistics, grid topology and periodic boundary information, and (for axisymmetric cases) node position verification with respect to the x axis. The domain extents list the minimum and maximum x, y, and z coordinates in meters. The volume statistics include minimum, maximum, and total cell volume in m^3. A negative value for the minimum volume indicates that one or more cells have improper connectivity. If cells with a negative volume exist the analysis cannot be started and revision of the model is necessary.

d) Smoothing/Swapping grid

Smoothing and face swapping are tools that complement grid adaption, increasing the quality of the final numerical mesh. Smoothing repositions the nodes and face swapping modifies the cell connectivity to achieve these improvements in quality.

e) Setting models

Setting models is a very important step in the preprocessing stage. It is here that the space, time, type of solver and flow governing models (energy, viscous, radiation, etc) are selected.

The axisymmetric, unsteady, segregated solver is chosen from the solver panel.

Solution of the energy equation is activated in the energy panel.

Selecting k-ε in the Viscous Model activates solutions of turbulence equations.

RNG was selected under the k- ε model.

Selecting a radiation model in the radiation model panel enables radiation heat transfer. Discrete Ordinates (DO) was selected under this model.

f) Setting materials

An important step in the setup of the model is defining the materials and their physical properties. Material properties are defined in the Materials panel, where one can enter values for the properties that are relevant to the problem scope defined in the Models panel.

The density variation of air has to be set as Boussinesq with a constant value of 1.2 and the thermal expansion coefficient has to be specified. These are very important when the Boussinesq model is used. For many natural-convection flows, one can get faster convergence with the Boussinesq model than by setting up the problem with fluid density as a function of temperature. This model treats density as a constant value in all solved equations, except for the buoyancy term in the momentum equation:

$$(\quad - \quad) \quad \approx \quad (\quad - \quad) \qquad (6.1)$$

Where is the density of the flow, is the operating temperature, and b is the thermal expansion coefficient. Equation (6.1) is obtained by using the Boussinesq approximation $= (1 - \Delta$)o eliminate from the buoyancy term. This approximation is accurate as long as changes in actual density are small; specifically, the Boussinesq approximation is valid when $(T - To) << 1$.

But the Boussinesq model cannot be used if the temperature variation in the flow field is large.

For solid materials, only density, thermal conductivity and heat capacity are defined. If one is modeling semi-transparent media, radiation properties are also defined.

Table 6.1 shows the most important properties to be set for the materials used in the model.

Table 6-1: Material properties

Properties	**For both SC with and without thermal storage system**			**Only for SC with thermal storage system**	
	Air	**Glass**	**Soil**	**Water**	**PVC pipe**
Density [kg/m3] (Boussinesq)	1.2	2700	2050	998.2	1410
Specific heat capacity [J/kg-K]	1006	840	1840	4182	1000
Thermal conductivity [W/m-K]	0.027	0.78	0.52	0.6	0.16
Viscosity [kg/m-s]	$16.84x10^{-6}$			0.001003	
Thermal expansion coefficient [1/K]	0.00343				
Refractive index[-]	1	1.526		1	1
Emissivity [-]		0.90			
Extinction coefficient[m^{-1}]		23.6			

g) Setting operating conditions

In the unsteady state case the environmental conditions vary with time. These variables are input as boundary conditions using User Defined Functions (UDF). The User Defined Functions are written in C computer programming language. The unsteady state solution in this thesis was obtained taking solar radiation data for months January, April, July and October. The data in Table 6.2 was converted to a graph as shown in the Figure 6-8.

Table 6-2: Data used for transient analysis

Time (hr)	Hourly Total Irradiation(W/m2)			
	January	April	July	October
1	0	0	0	0
2	0	0	0	0
3	0	0	0	0
4	0	0	0	0
5	0	0	0	0
6	0	1.1032	3.2329	0
7	160.75	171.04	158.35	164.9
8	356.44	372.2	340.76	363.61
9	558.42	577.88	526.56	567.97
10	734.68	756.34	687.4	745.93
11	854.94	877.71	796.63	867.19
12	897.63	920.72	835.32	910.21
13	854.94	877.71	796.63	867.19
14	734.68	756.34	687.4	745.93
15	558.42	577.88	526.56	567.97
16	356.44	372.2	340.76	363.61
17	160.75	171.04	158.35	164.9
18	0	1.1032	3.2329	0
19	0	0	0	0
20	0	0	0	0
21	0	0	0	0
22	0	0	0	0
23	0	0	0	0
24	0	0	0	0

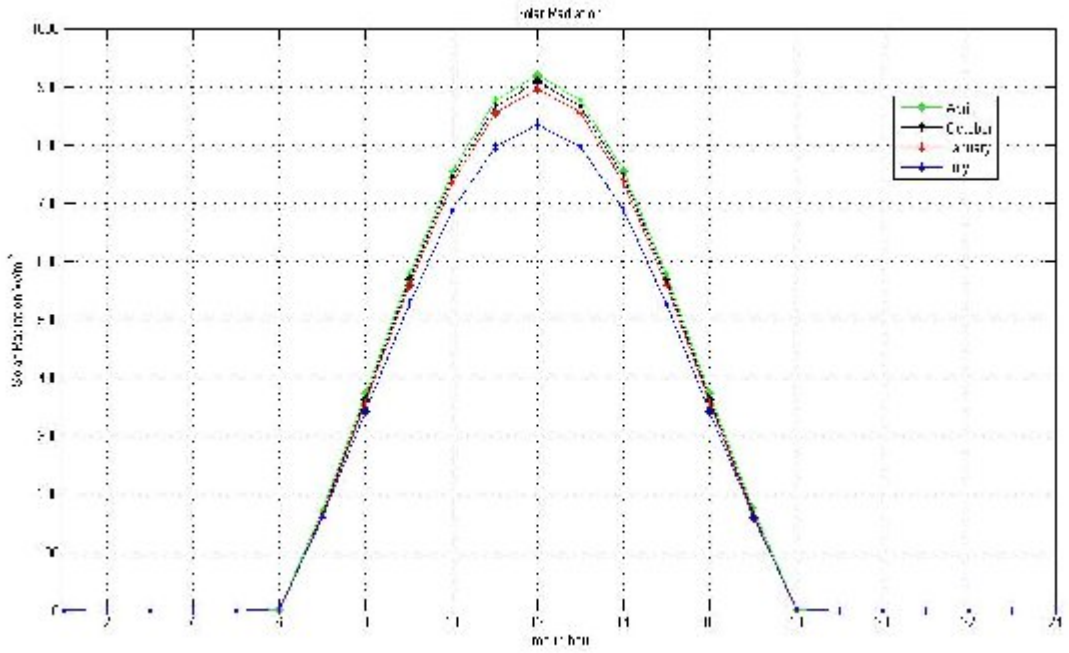

Figure 6-8: Input data of transient analysis

Properties that are used as references are specified in the operating conditions panel. These properties are:

- Operating pressure and its location
- Gravity
- Operating temperature
- Operating density

Operating pressure and its location

Operating pressure is significant for incompressible ideal gas flows because it directly determines the density. One must, therefore, be sure to set the operating pressure appropriately. Operating pressure of 89838.66 Pa = 674.01 mmHg (that of Affar region) is taken in this simulation.

Gravity

Gravity has to be turned on and proper values in the x-, y- and z- directions have to be set for buoyancy driven flows. A value of 9.81 m/s^2 in the axial direction was used in this case.

Operating temperature

Operating temperature has to be specified in the operating properties panel if the Boussinesq model for density variation is used. Operating temperatures vary with time and different values are taken for simulations at different hours.

Operating density

Operating density has to be defined if an incompressible flow is being analyzed. Since the flow is assumed to be compressible in this thesis, there is no need of defining operating density.

h) Defining boundary conditions

Boundary conditions specify the flow and thermal variables on the boundaries of the physical model. They are, therefore, a critical component of the FLUENT simulations and it is important that they are specified appropriately. The boundary conditions applied in this thesis are those shown in Figure 6.6 and Table 6.3. No additional thermal boundary conditions are required for coupled wall boundary conditions, because the solver will calculate heat transfer directly from the solution in the adjacent cells. [9]

Table 6-3: Boundary conditions in detail

Boundary	**Type**	**Boundary condition**
Exit	Pressure outlet	$\Delta p = 0$; $T = T_{ambient} - 0.0065 \times$ *chimney height* Turbulence specification method: Intensity and Hydraulic Diameter; Turbulence Intensity=10%, Hydraulic Diameter=20m Flow Direction:

		Normal to Boundary
Axis	Axis	
Chimney wall	Wall	Fixed heat flux: q=0
Turbine	Fan	Pressure jump: $\Delta p = -\frac{1}{2}\rho v^2$ (from Betz power limit)
Thermal storage tank	wall	Fixed heat flux: q=0
Bend	Wall	Fixed heat flux: q=0
Soil face	Wall	Fixed heat flux: q=0
Soil-Air	Wall	Coupled; roughness height=5cm
Glass	Wall	Convection + Radiation: h=8W/m2K; $T_\infty = T_{ambient}$; Global radiation and beam direction depend on time[The UDF is used under the irradiation panel]
Inlet	Pressure inlet	$\Delta p = 0$; $T = T_{ambient}$; Turbulence specification method: Intensity and Hydraulic Diameter; Turbulence Intensity=10%, Hydraulic Diameter=3.4m Flow Direction: Normal to Boundary
Ground	Wall	Fixed temperature: $T = T_{ambient}$

i) Solution control and checking for convergence

The following are used in the solution control.

- Pressure interpolation scheme: ***Body Force Weighted***.
- Pressure-velocity coupling: ***SIMPLE***
- Up winding schemes for Momentum, Turbulence Kinetic Energy, Turbulence Dissipation Rate, and Energy: ***Second Order Upwind***
- Default under-relaxation factors.

The flow field was initialized using the boundary conditions set at inlet, letting the radial velocity to be 10^{-9}.

Plotting of residuals during the calculation was enabled by letting all the residuals to be 10^{-6} except for energy and DO intensity where the residuals were set to be 10^{-9}.

The mass flow rate at exit was also plotted. This again helps in monitoring the convergence of the solution.

The iteration was started until the solution convergences.

There are three methods to check for convergence of the solution [9]. These are:

1. Monitoring the residuals.

Convergence will occur when the Convergence Criterion for each variable has been reached. If the residuals set above 10^{-6} and 10^{-9} are satisfied, the solution is said to be converged. Figure 6.9 shows that all the scaled residuals are below 10^{-6} and 10^{-9}.

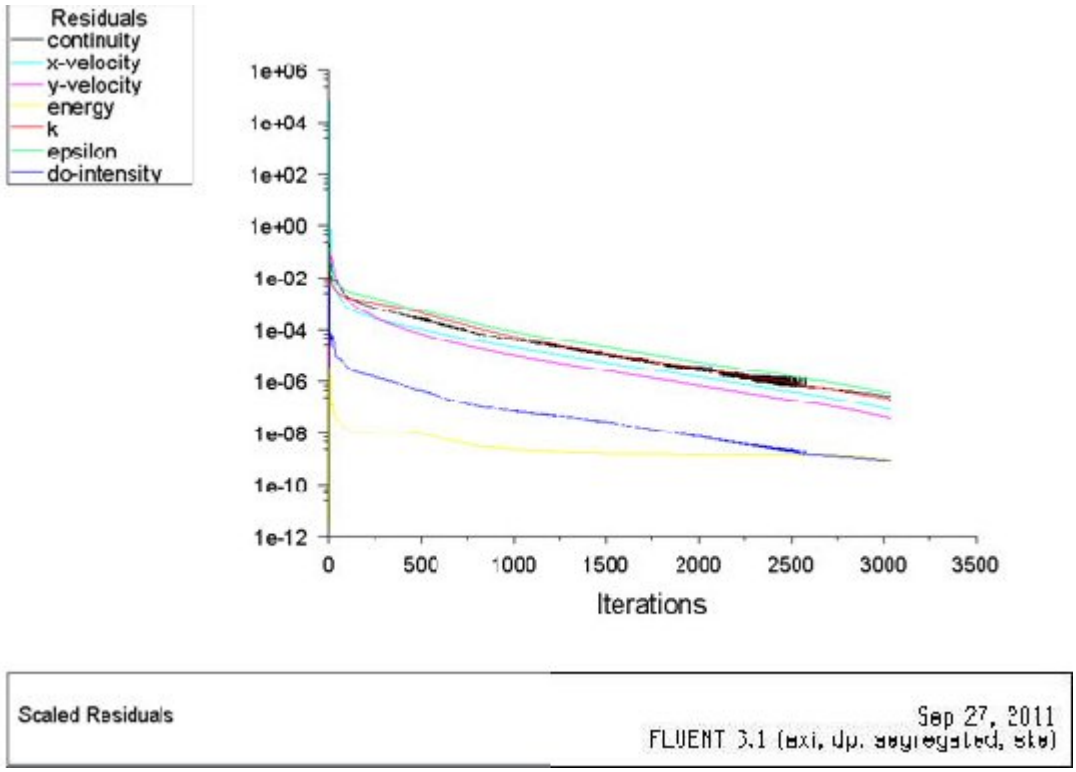

Figure 6-9: Scaled residuals showing convergence

2. Solution no longer changes with more iteration.

Sometimes the residuals may not fall below the convergence criterion set in the case setup. However, monitoring the representative flow variables through iterations may show that the residuals have stagnated and do not change with further iterations. This could also be considered as convergence. Figure 6.10 shows that the exit mass flow rate remains almost unchanged for iterations above about 2000.

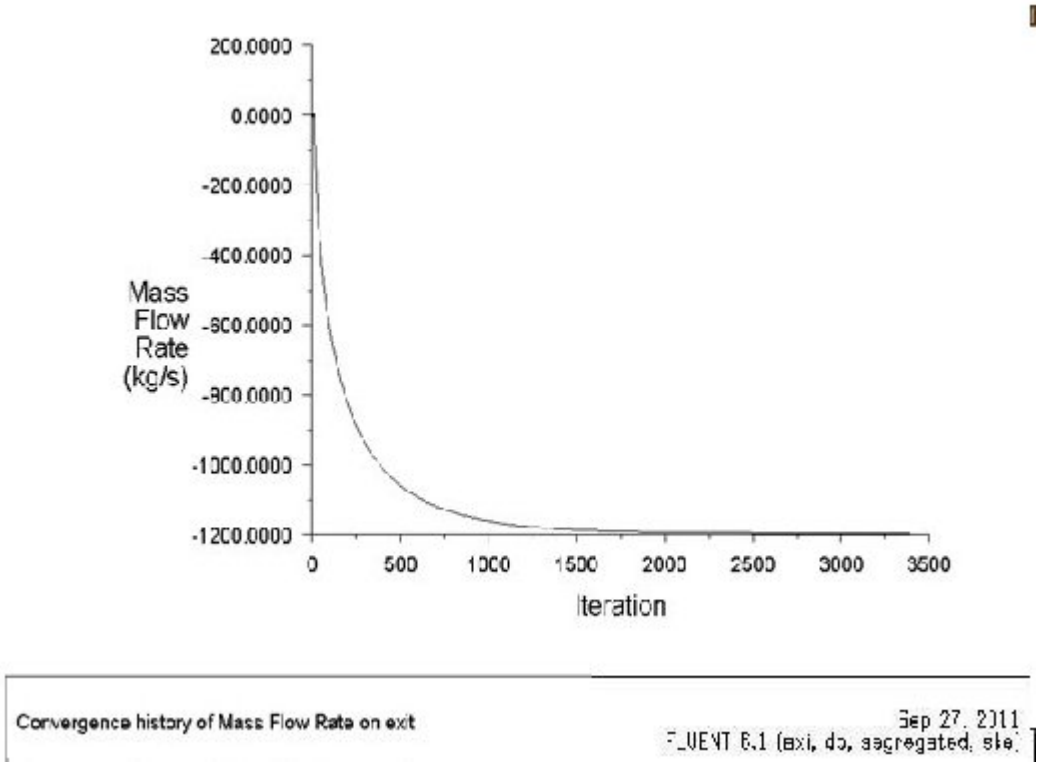

Figure 6-10: Convergence history of exit mass flow rate

3. Overall mass, momentum, energy and scalar balances are obtained.

Checking the overall mass, momentum, energy or scalar balances in the Flux Reports panel is the third way of checking for convergence. The net imbalance should be less than 0.2% of the flux through the domain. For example, the net mass flow rate (kg/s) between the inlet and the exit gives the following result:

Exit: 1254. 3144; **Inlet**: 1254. 3144; **Net mass-flow**: $1.227037065\text{x}10^{-6}$

The percentage net mass flow rate is

$$\frac{-1.227037065\text{x}10}{1254.3144}\text{x}100 = -9.7825\text{x}10 \quad \%$$

Again this shows that the solution has converged.

6.1.3 Post-Processing on Fluent

Once the iteration is completed and converged solutions are obtained, different types of results can be analyzed.

Displaying graphical results

Graphics tools available in FLUENT allow to process the information contained in the CFD solution and to easily view the results. Some of these methods are described below.

1) Displaying contours

FLUENT allows the plotting of contour lines superimposed on the physical domain. Contour lines are lines of constant magnitude for a selected variable (like velocity, temperature, pressure, etc).

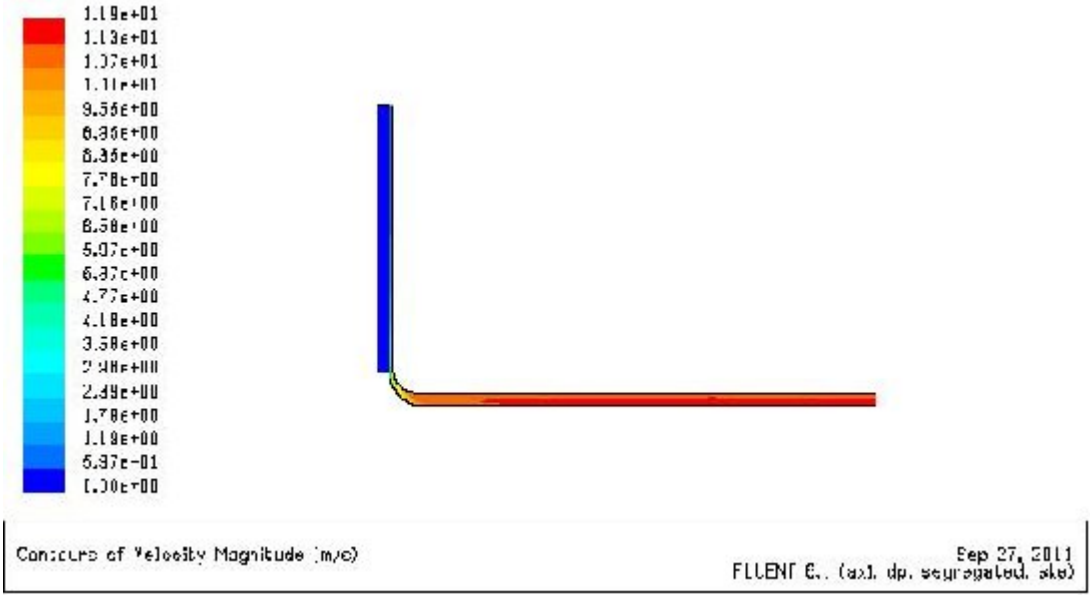

Figure 6-11: Velocity contour

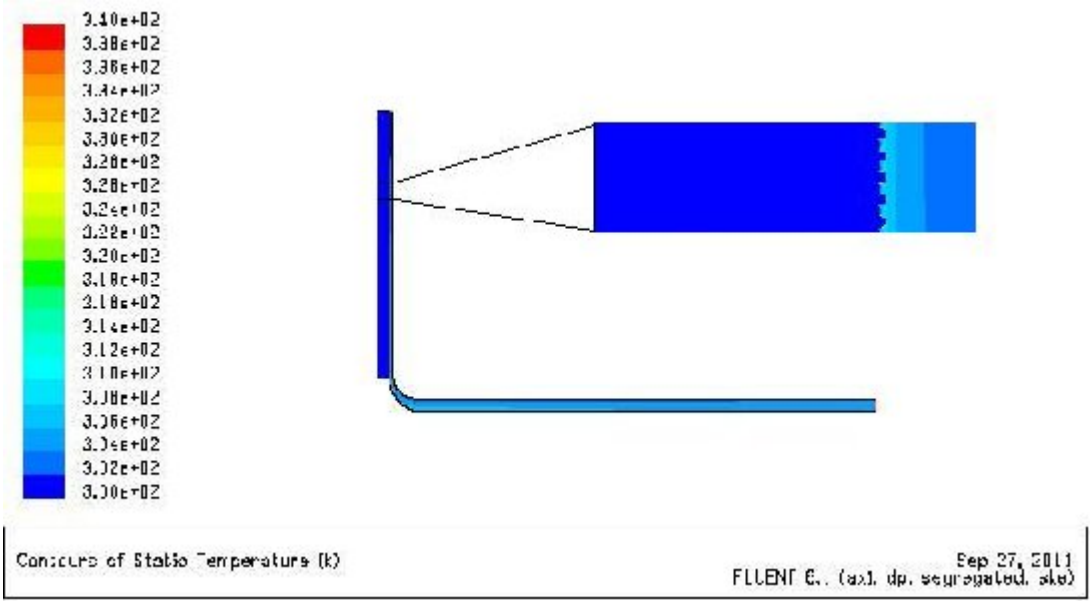

Figure 6-12: Temperature contour

Figure 6.11 and Figure 6.14 show that the velocity gradually increases from collector inlet to the chimney inlet. The velocity gradually increases in the chimney as shown in Figure 6.11 and in Figure 6.14. It can also be seen from Figure 6.12 that the temperature at the ground becomes very high in depth of few units. This indicates that the ground together with thermal storage tank stores energy, which will be used to heat the air when there is no radiation.

2) XY Plots

An XY (abscissa/ordinate) plot is a line and/or symbol chart of data. Virtually any defined variable or function is accessible for this type of plot. Furthermore, one may read in an externally-generated data file in order to compare results with experimental data. If plotting of results on some surfaces is of interest, FLUENT allows creating such surfaces in the grid. Then, the XY-plot facility is used to plot the results.

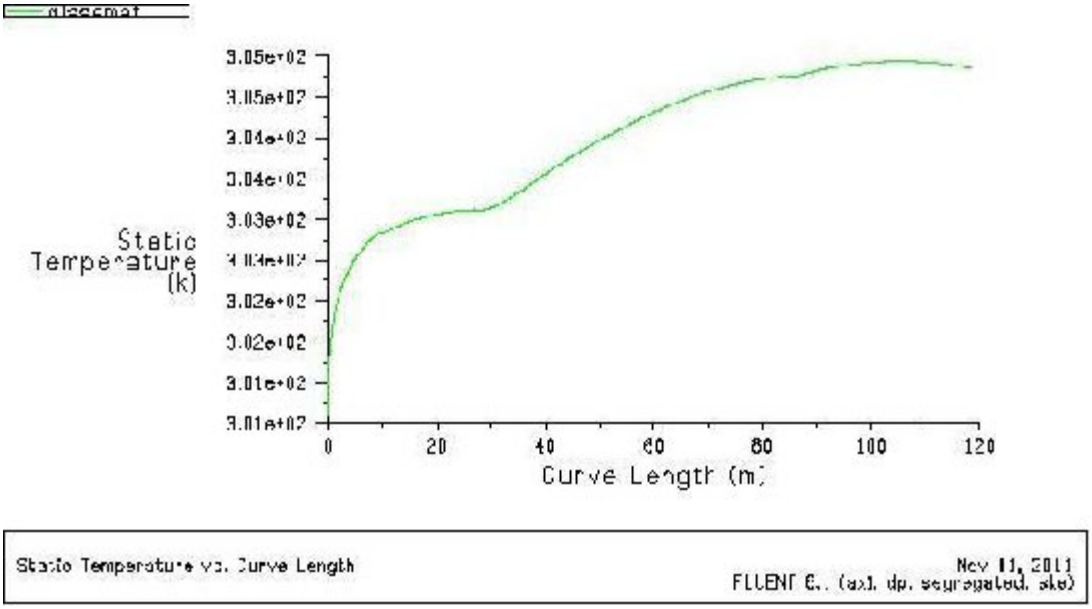

Figure 6-13: Glass temperature variation from collector inlet to collector exit

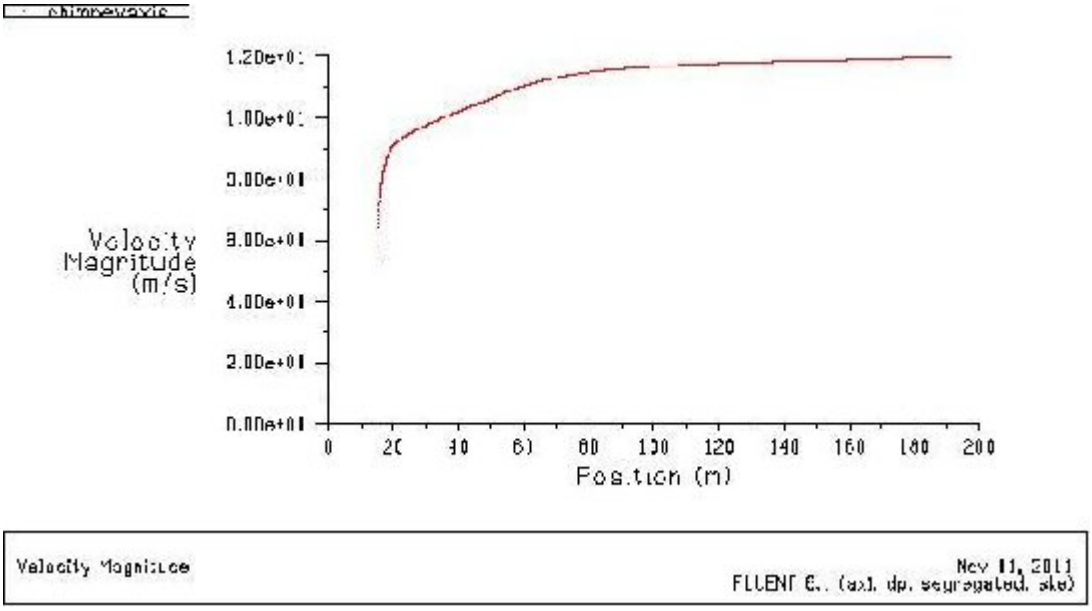

Figure 6-14: Air velocity variation from collector exit to chimney exit

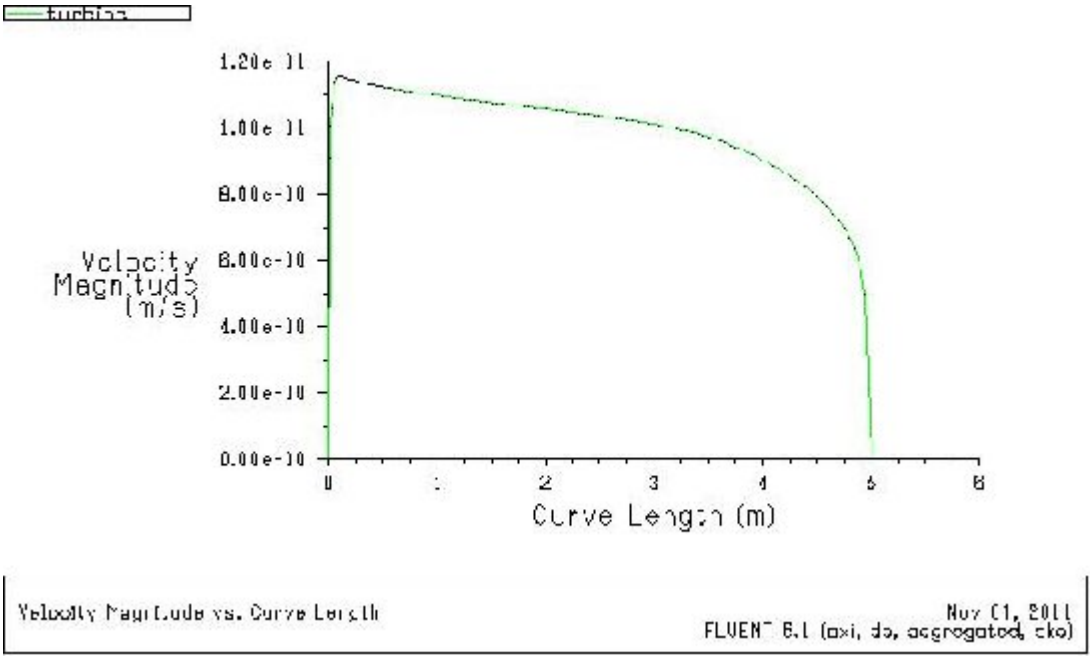

Figure 6-15: Velocity plots at turbine

Figure 6.11 and Figure 6.13 show that the velocity and the temperature of the air increase as it moves from collector inlet to collector outlet. The air velocity shows large increase within few distances from the surfaces of the ground and the glass and then remains almost constant. This is because of the low viscosity of air. Figure 6.15 shows this phenomenon.

6.2 Solar Chimney without thermal energy storage system

The same boundary conditions were used as the solar chimney with thermal storage system except there is no thermal energy storage system (pipe) in case of SC without thermal energy storage system. I have obtained the following outputs.

1) Displaying contours

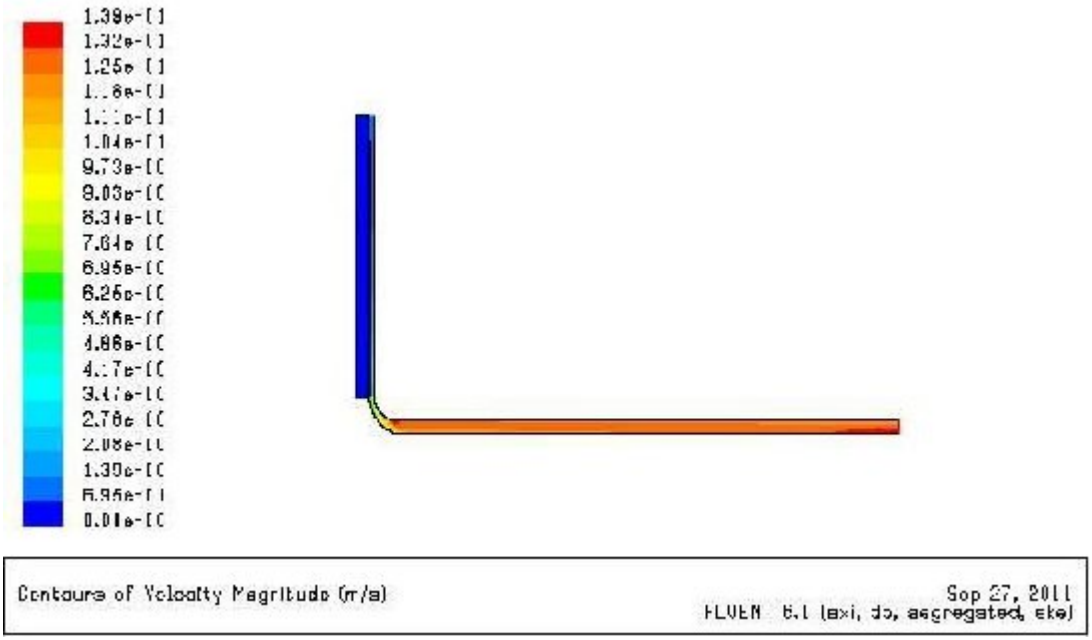

Figure 6-16: Velocity contour

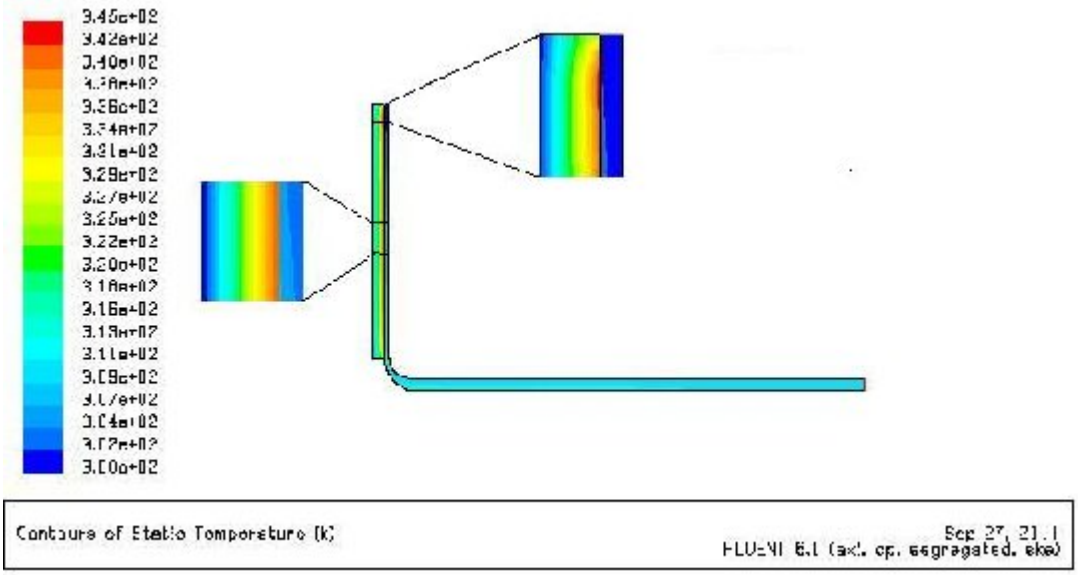

Figure 6-17: Temperature contour

2) XY plot

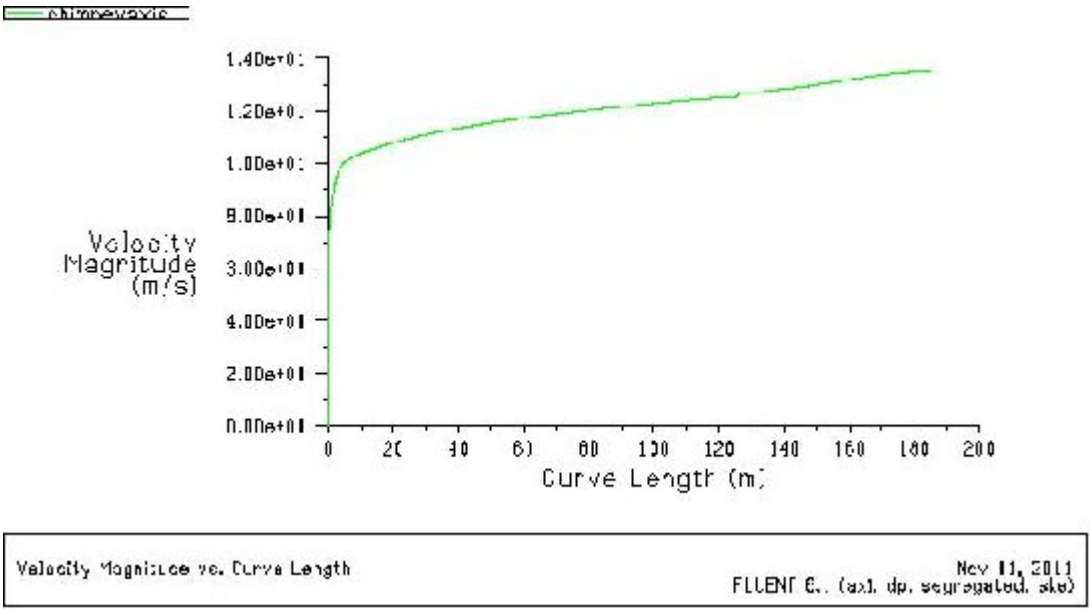

Figure 6-18: Air velocity variation from collector exit to chimney exit

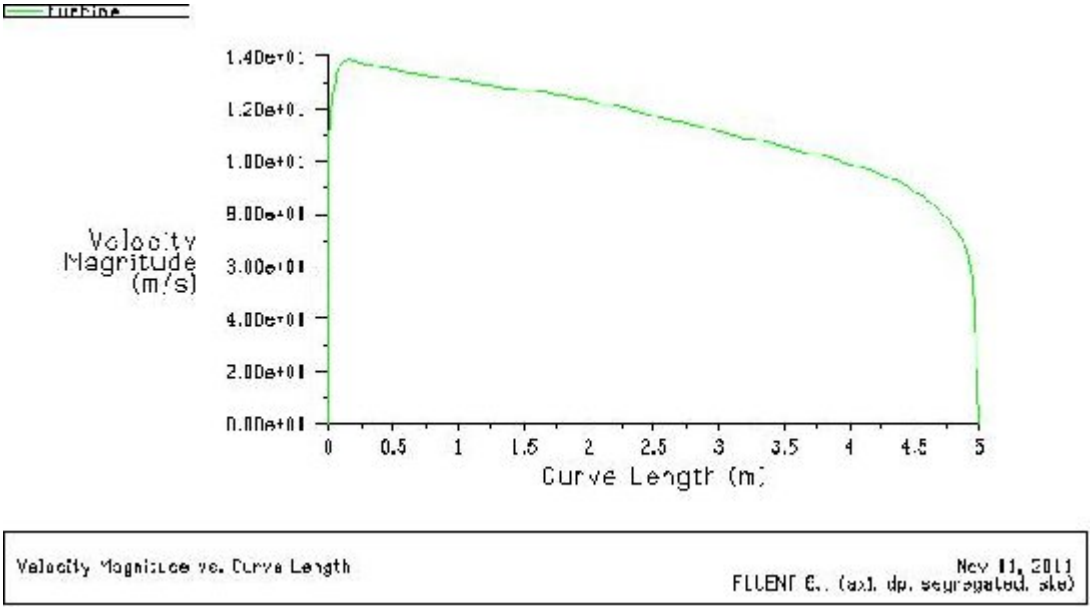

Figure 6-19: Velocity plots at the turbine

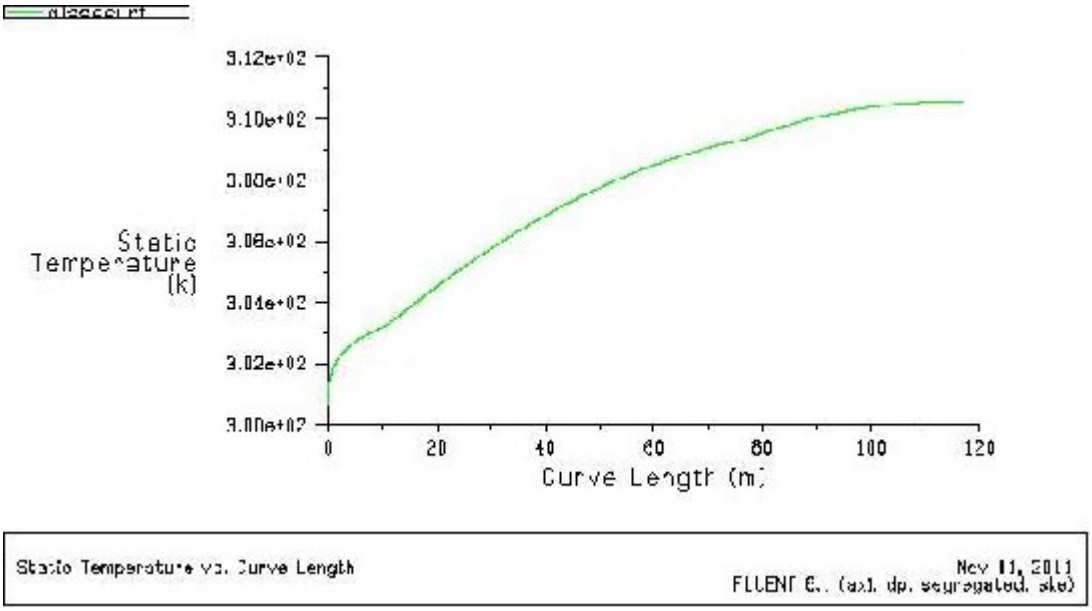

Figure 6-20: Glass Temperature variation from collector inlet to collector exit

The main purpose of taking this data is to see the energy storing effect of the ground and compare the output with experimental results. The outputs obtained are plotted on Figure6.21.

6.3 Analysis of the result

The wind turbine extracts the energy in the air flowing through the chimney. The maximum limit to wind turbine performance was determined by Albert Betz. This is derived by looking at the axial momentum of the air passing through the wind turbine. The air is deflected away from the turbine. This causes the air passing through the rotor plane to have a smaller velocity than the free stream velocity. The degree at which air at the turbine is less than the air far away from the turbine is called the axial induction factor, *a*. It is defined as follows:

≡—— (6-2)

a is the axial induction factor.

is the wind speed far away from the rotor.

is the wind speed at the rotor.

The first step to deriving the Betz limit is applying conservation of axial momentum. As stated above, far away from the turbine, the wind loses speed after the wind turbine. This would violate the conservation of momentum if the wind turbine was not applying a thrust force on the flow. This thrust force manifests itself through the pressure drop across the rotor. The front operates at high pressure while the back operates at low pressure. The pressure difference from the front to back causes the thrust force. The momentum lost in the turbine is balanced by the thrust force.

Axial momentum relates the wake flow to the pressure difference at the rotor. Another equation is needed to relate the pressure difference to the velocity of the flow near the turbine. Here the Bernoulli equation is used between far field flow and the flow near the wind turbine. There is one limitation to the Bernoulli equation. The equation cannot be applied to fluid passing through the wind turbine. Instead conservation of mass is used to relate the incoming air to the outlet air. Betz used these equations and managed to solve the velocities of the flow in the far wake and near the wind turbine in terms of the far field flow and the axial induction factor. The velocities are given below.

= (1 − a) (6-3)

= (1 − 2a) (6-4)

is introduced here as the wind velocity in the far wake. This is important because the power extracted from the turbine is defined by the following equation. However the Betz limit is given in terms of the coefficient of power. The coefficient of power is similar to

efficiency but not the same. Power and the coefficient of power are expressed, respectively, as:

$$= 0.5 \quad (\quad - \quad) \qquad (6\text{-}5)$$

$$\equiv \frac{\quad}{\quad} \qquad (6\text{-}6)$$

Betz was able to develop an expression for Cp in terms of the induction factors. This is done by the velocity relations being substituted into power and power is substituted into the coefficient of power definition. The relationship Betz developed is given below.

$$Cp = 4a(1 - \quad) \qquad (6\text{-}7)$$

The Betz limit is defined by the maximum value that can be given by the above formula. This is found by taking the derivative with respect to the axial induction factor, setting it to zero and solving for the axial induction factor. Betz was able to show that the optimum axial induction factor is one third. The optimum axial induction factor was then used to find the maximum coefficient of power. This maximum coefficient is the Betz limit. Betz was able to show that the maximum coefficient of power of a wind turbine is 16/27. Therefore, the maximum power obtained from the air flow at the turbine is:

$$= \frac{\quad}{\quad} \qquad (6\text{-}8)$$

Where r is air density, *A* is turbine swept area and *v* is air velocity at turbine entrance. Equation (6.8) yields the power in a free flowing stream of air. The electrical power obtained has to be multiplied by the efficiency of the generator, which is usually between 0.75 and 0.90.

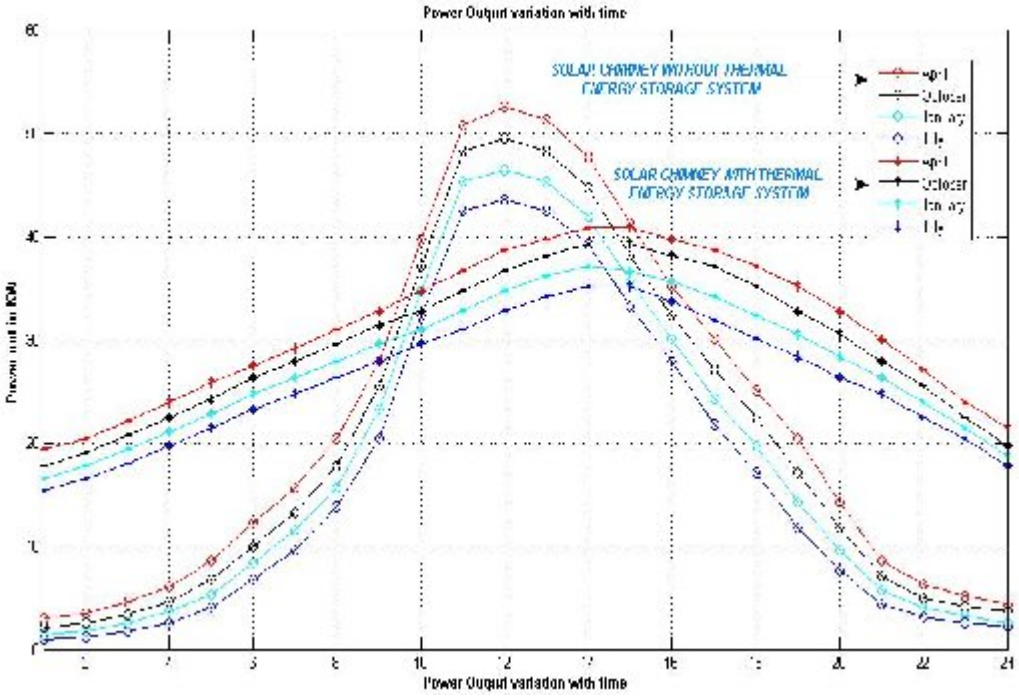

Figure 6-21: Power output variation for both Solar Chimneys with and without thermal energy storage system

The unsteady solution for the solar chimney without thermal energy storage system gave an average power of about 21.231Kw for the data provided at Afar. Figure 6.8 and Figure 6.21 show that solar radiation is zero starting from the 18th hour, but the velocity and so the power has values greater than zero. This is an indication of the fact that the ground stores energy during day time and releases it during night.

But as we can see from the Figure 6.21, the power output drop very rapidly if there is no solar radiation as there is no thermal storage system except the soil(the soil underneath have lease thermal storage effect).

Energy storage in the collector has been explored as a method for re-shaping the power output profile of a solar updraft tower. As shown in Figure 21, the extra thermal mass evens out the power output profile. And it also improves the average power output to 29.65 kW.

At night, when the air in the collector starts to cool down, the water inside the tubes releases the heat that it stored during the day. Heat storage with water works more efficiently than with soil alone, since even at low water velocities – from natural convection in the tubes – the heat transfer between water tubes and water is much higher

than that between ground surface and the soil layers underneath, and since the heat capacity of water is about five times higher than that of soil.

6.4 The effect of varying the position of the turbine

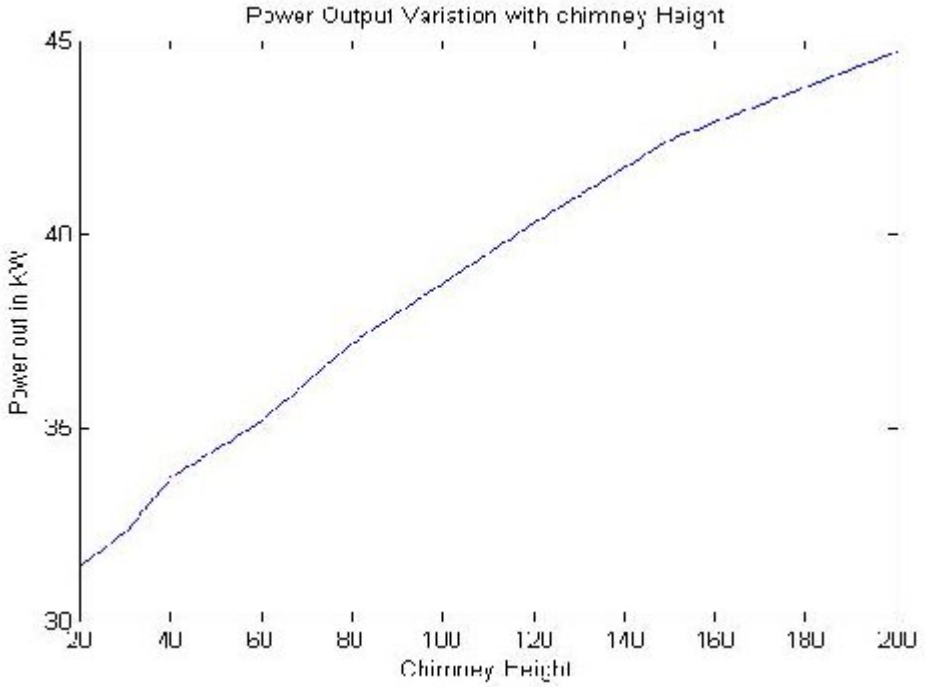

Figure 6-22: Power output variation with chimney height

As we can see from the Figure above as the turbine is positioned at a higher position the velocity will develop more so the power output does. But as the turbine is positioned at a higher position inside the chimney it will complicate the power house and as well the chimney is required to be stronger so this means more investment cost which is uneconomical.

So it is better to put the turbine just at the end of the bend and position the power house inside the bend like the power plant at the Manzanares prototype in Spain.

CHAPTER SEVEN

ECONOMIC ANALYSIS

Solar processes are generally characterized by high initial cost and low operating costs. Thus the basic economic problem is one of comparing an initial known investment with estimated future operating costs. Investments in buying solar energy equipment are important factors in solar process economics. Costs of installing this equipment must also be considered as these can match or exceed the purchase price. Also to be included are costs of structures to support collectors and other alterations made necessary by the solar equipment. The total cost of solar chimney power plant is the sum of the costs of its main components: the chimney, the collector and the power converting units (PCU). These components have sub-components to which costs are associated (Table 7.1). [1]

Table 7-1: Components of the Plant

Component	Sub-components
chimney	Chimney shell
	Ring stiffeners and
	Chimney foundation.
Collector	Glass
	Column system
	Support matrix
Thermal storage tanks(only for SCPP with thermal storage systems)	Pvc pipes of 20cm diameter filled with water
Power conversion unit	Balance of station
	Controls
	Power electronics
	Generators
	Supports
	Central structure and
	Turbines.

The costs associated with these components include material, construction, hoisting and transport costs. The economic analysis of the power plant, therefore, requires the knowledge of these specific costs. To make the cost analysis simple, different detailed

investigations have been made to get unit costs that are independent of the plant size. One of these investigations is that done by Haaf et al. According to this work the chimney cost is proportional to its skin area ($228m^{-2}), the collector cost is proportional to its area ($14 m^{-2}) and power conversion unit cost is proportional to peak power output ($715 kW^{-1} pk). Based on the above assumptions components and total costs were calculated as shown in Table 7.2. The annual operation and maintenance costs were assumed to be about 0.3% of the total investment.

- **For the solar chimney with thermal storage system**

Table 7-2: Components and total costs for solar chimney with thermal storage system

<table>
<tr><td>Height of Chimney 195m
Radius of Chimney 5m
Skin Area of Chimney 2xΠx5x195=6126.1m^2</td><td>228x6126.1=$1396752.1</td><td rowspan="4">Total Investment Cost 1396752.1+615752.2 + 35750+51,094.08 =$2,099,348.38</td></tr>
<tr><td>Outer Radius of Collector 120m
Inner Radius of Collector 20m
Area of Collector Πx(120^2-20^2)= 43982.3m^2</td><td>Cost of Collector 3.5x43982.3=$615752.2</td></tr>
<tr><td>Machinery for 715 days(2year)</td><td>Cost of Machinery 715x50=$ 35750</td></tr>
<tr><td>Thermal storage tanks (Total pipe length =πR$_i$) where R$_i$ =15+0.4*L$_i$ (where L$_i$=1,2,3,4,…200)
Total pipe length = 51,094.08m</td><td>Cost of thermal storage tank=51094.08*$1 =$51,094.08</td></tr>
<tr><td>Operation and Maintenance Cost (0.3%)</td><td colspan="2">0.003x 2,099,348.38= $ 6,298.045</td></tr>
</table>

The following parameters were used to calculate the electricity cost.

- Mean power output: P=29.65 kW,
- Life of plant: N=30 years,
- Inflation rate: f=8%,
- Interest rate: i=6%

The present worth of the operation and maintenance cost is calculated as:

$$= \frac{1+}{-}\ \frac{1+}{1+}\ -1\ = \frac{6{,}298.045}{0.08-0.06}\ \frac{1+0.08}{1+0.06}\ -1\ = \$236809.80$$

The total present worth of the plant will be the sum of the present worth of the operation and maintenance cost and the total investment cost = 236809.80 + 2,099,348.38= **$2,336,158.18**

An equivalent annual cost over the plant lifetime can be calculated according to the following equation.

$$= \frac{(\ \ )}{(\ \ )} = 2336158.18\frac{.\ (\ \ .)}{(\ \ .)} = \$169719.234$$

The annual energy produced by the plant is 29.65x24x365=259734KWh.

The levelized electricity cost will, therefore, be

$$= \frac{}{} = \mathbf{0.65348KWh^{-1}}$$

- **For the solar chimney without thermal storage system**

Table 7-3: Components and total costs for solar chimney without thermal storage system

Height of Chimney 195m Radius of Chimney 5m Skin Area of Chimney 2xΠx5x195=6126.1m^2	228x6126.1=$1396752.1	Total Investment Cost 1396752.1+ 615752.2+ 35750 = $2048254.3
Outer Radius of Collector 120m Inner Radius of Collector 20m Area of Collector Πx(120^2-20^2)= 43982.3m^2	Cost of Collector 3.5x43982.3=$615752.2	
Machinery for 715 days(2year)	Cost of Machinery 715x50=$ 35750	
Operation and Maintenance Cost (0.3%)	0.003x 2048254.3 = $ 6144.7629	

The following parameters were used to calculate the electricity cost.

- Mean power output: P=21.231kW,
- Life of plant: N=30 years,
- Inflation rate: f=8%,
- Interest rate: i=6%

The present worth of the operation and maintenance cost is calculated as:

$$= \frac{1+}{-} - 1 = \frac{6144.7629}{0.08-0.06}\ \frac{1+0.08}{1+0.06} - 1 = \$231046.31$$

The total present worth of the plant will be the sum of the present worth of the operation and maintenance cost and the total investment cost = 231046.31+ 2,048,254.3= **$2,279,300.61**

An equivalent annual cost over the plant lifetime can be calculated according to the following equation.

$$= \frac{(\quad)}{(\quad)} = 2279300.61\frac{.\ (\quad .)}{(\quad .)} = \$165588.7$$

The annual energy produced by the plant is 21.231x24x365=185983.56KWh.

The levelized electricity cost will, therefore, be

$$= \frac{}{} \doteq \mathbf{\$0.89034KWh^{-1}}$$

As it is seen from the analysis if we are going to implement thermal storage system the cost of the plant will increase by about $56857.57 but the levelized energy cost will decrease by $0.23686KWh$^{-1.}$ So, it is economical to implement solar chimney with thermal energy storage than solar chimney without thermal energy storage system. Beyond all the extra thermal mass evens out the power output profile, which do have a great contribution on regulating the power by reducing the great power fluctuation between day and night time.

Generally the electricity cost obtained is very high when compared to the hydroelectric energy and other conventional energy costs in Ethiopia. The cost analysis was based on European context. The cost is expected to decrease in developing countries like Ethiopia because the labor cost and the materials necessary to construct the chimney are cheap.

Even though the cost obtained here is high, cost estimations made for solar chimneys of higher size show that energy cost decreases as size increases as shown in Table 7.4.

Table 7-4: Comparison of electricity cost with Plant size

Capacity (MW)	5	30	100	200
Electricity Cost(€/kWh)	0.21	0.11	0.09	0.07

CHAPTER EIGHT

APPLICABILITY OF SOLAR CHIMNEY IN ETHIOPIA

There is a huge energy resource potential in Ethiopia, which, if utilized, could minimize the present energy crisis prevailing in the country and enhance the process of rural electrification. The total exploitable renewable energy that can be derived annually from primary solar radiation, wind, forest biomass, hydropower, animal waste, crop residue and human waste is about $1{,}959 \times 10^3$ Tcal per year, (EEA, 2002).Out of this, the share of primary solar radiation is about 73.08 percent, while the share of biomass resources is about 12.8 percent (Table 1.1). Studies indicate that for Ethiopia as a whole, the average annual solar radiation reaching the ground is 5.26 kWh/ m^2. The minimum average is estimated to be 4.55 kWh/m^2 in July (the main rainy season) to a maximum average of 5.55 kWh/ m^2 in February and March. The radiation reaching the ground, however, varies significantly from one area to another as well as from season to season.

Table 8-1: Overview of renewable energy resources in Ethiopia

No	**Energy Resources**	**Energy in 10^3 Tcal per year**			
		Potential	**%share**	**Exploitable**	**%share**
1	Primary solar Radiation	1,953,550	99.7	1954	73.08
2	Wind	4,779	0.24	239	8.94
3	Forest Biomass	800	0.005	240	8.97
4	Hydropower	552.1	0.003	138,000	5.16
5	Animal waste	111.28	0.01	33.73	1.26
6	Crop residue	81.36	0.0004	40.63	1.52
7	Human waste	28.18	0.00014	28.18	1.05
Total		1,959,901.93	100.00	2,673.54	100

The above data indicates that Ethiopia is among the naturally solar energy gifted countries, and, therefore, solar energy driven power plants like the solar chimney can be utilized in the country.

Solar updraft towers have many aspects that recommend them for use in remote, isolated communities. Their predictable and steady power output makes them especially suitable for use in smaller communities that require steady power output for use in small-scale industry. In rural areas of Ethiopia connections to the power grid either do not exist of may be unreliable. The development of small-scale industries requires an uninterrupted power output, which can be provided by solar updraft towers.

Solar updraft towers are most efficient at larger sizes; this supports the use of towers for power outputs beyond just the basic provision of electricity for homes. The power output curve of a solar updraft tower can be tuned to provide the appropriate balance of production at different times to satisfy both residential and industrial use.

Solar updraft towers can deliver the required power at as low a price as concentrating solar plants, provided that the towers are built with local parts and labor. This is an additional advantage of solar updraft towers; they can utilize local construction materials, which other types of solar plants cannot. Costs are kept low after construction due to the very low maintenance requirements of the plants.

The low maintenance requirements may also be an important factor in the decision to construct solar updraft towers in remote communities. Specialty replacement parts are not required for these plants; basic maintenance of the collector can be performed by those skilled in construction labor. The feathering turbine of a solar updraft tower is the only complex, actively controlled part in the system, but the turbine can function with the blades set at a fixed angle with a reduction in efficiency. In general, solar updraft towers are very robust.

The fringe benefit of using the collector area for agriculture may also be appealing in some communities.

Overall, solar updraft towers are very suitable for use in remote communities as a power source for both residential and industrial use, based on reliability, cost, and operational factors. They can provide a suitable energy source in many remote areas, including areas that are not currently supplied by conventional means.

CHAPTER NINE

CONCLUSION AND RECOMMENDATION FOR FUTURE WORK

9.1 Conclusions

- As we could see from the analysis the plant efficiency will be improved by using thermal storage tanks. Energy storage in the collector has been explored as a method for re-shaping the power output profile of a solar updraft tower. The most commonly suggested method for creating energy storage is to place extra thermal mass under the collector in the form of black containers of water. Figure 6.2 shows the storage located under the collector.

- As it is seen from the analysis if we are going to implement thermal storage system the cost of the plant will increase by about $56857.57 but the levelized energy cost will decrease by $0.23686KWh$^{-1.}$ So, it is economical to implement solar chimney with thermal energy storage than solar chimney without thermal energy storage system. Beyond all the extra thermal mass evens out the power output profile (As shown in Figure 6.21), which do have a great contribution on regulating the power by reducing the great power fluctuation between day and night time.

- The level of storage used can be adjusted to create a power profile with similar characteristics to the demand profile.

- As the turbine is positioned at higher point of the chimney the power output will increase but the cost of the chimney will increase drastically so the plant cost does. To simplify the plant power house and also chimney it is better to put the plant at the end of the bend or just at the beginning of the chimney and the power house inside the bend.

- Solar chimneys are very suitable for use in remote communities where there is high solar energy capacity; such as Afar and Somalia, as a power source for both residential and industrial use, based on reliability, cost, and operational factors. They can provide a suitable energy source in many remote areas of Ethiopia, including areas that are not currently supplied by conventional means.

9.2 Recommendations for Future Work

In this thesis the effects of thermal storage and the variation of turbine position are considered. The energy storing capacity of the water tubes can be further increased if salt is dissolved in the water and its effect can be investigated further to improve the energy efficiency further. The effect of varying the angle of collector from the ground could be analyzed to obtain the optimum angle.

REFERENCES

[1] Getachew Shunki, Abebayehu Assefa**: Modelling of solar chimney for power generation**: Thesis summitted to the school of graduate studies Addis Abeba University, 2006

[2] **Fluent user's guide**, January 2005

[3] Agust´ın P´erez - Barahona1: **Economic growth and the use of non-renewable energy resources**, 2007

[4] Richard Anthony Hedderwick: **Performance evaluation of solar chimney**, 2000

[5] Bilgen E., Rheault J.: **Solar chimney power plants for high latitudes**, 2005

[6] Marco Aurélio dos Santos Bernardes: **Solar Chimney Power Plants – Developments and Advancements**, *Brazil* 2010

[7] Meyer C M, Technical Journalist: **Towers of power: The solar updraft tower,** 2008

[8] Malima Isabelle Wolf: **Solar Updraft Towers: Their Role in Remote On-Site Generation**, 2005

[9] Ming Tingzhen, Liu Wein,y,z and Xu Guoliang : **Analytical and numerical investigation of the solar chimney power plant systems**, china 2006

[10] Niemann H.-J., F.Lupi, Hoeffer R., Hubert W., Borri C.: **The Solar Updraft Power Plant: Design and Optimization of the Tower for Wind Effects**, Italy 2009

[11] Travis Satsuma, **Solar Updraft Towers**, 2009

[12] Pasumarthi1 N. and Sherif S. A.: **Experimental and theoretical performance of a demonstration solar chimney model part I: mathematical model development,** 1998

[13] Pasumarti1 N. and Sherif2S. A.: **Experimental and theoretical performance of a demonstration solar chimney model part II: experimental and theoretical results and economic analysis,** USA, 1998

[14] Atit Koonsrisuk and Tawit Chitsomboon: **Effect of Tower Area Change on the Potential of Solar Tower,** *2006, Bangkok, Thailand*

[15] Atit Koonsrisuk, Tawit Chitsomboon: **Dynamic similarity in solar chimney modeling**, Thailand 2007

[16] Atit Koonsrisuk, Tawit Chitsomboon : **Partial geometric similarity for solar chimney power plant modeling,** 2009

[17] Joseph Khedari ∗, Ninnart Rachapradit, Jongjit Hirunlabh: **Field study of performance of solar chimney with airconditioned building,** *Thailand*

[18] Jörg Schlaich, Rudolf Bergermann, Wolfgang Schiel, Gerhard Weinrebe : **Design of Commercial Solar Updraft Tower Systems – Utilization of Solar Induced Convective Flows for Power Generation,** Germany 2010

[19] Ingenuin Gasser: **Kinetic and Mean-Field Models in the Socio-Economic Sciences, On a Model for a Solar Updraft Tower ICMS**, Edinburgh, Germany, July 2009

[20] Pretorius J.P. *, Kro¨ger D.G.: **Critical evaluation of solar chimney power plant performance,** South Africa, 2005

[21] von Backstro¨m Theodor W. *, Thomas P.: Fluri : **Maximum fluid power condition in solar chimney power plants – An analytical approach**, South Africa,2006

[22] Fluri T.P., von Backstro¨m T.W.: **Comparison of modelling approaches and layouts for solar chimney turbines**, South Africa July 2007;

[23] Kashiwaa B.A., Kashiwab Corey B.: **The solar cyclone: A solar chimney for harvesting atmospheric water**, 2006

[24] Xinping Zhou a,, Jiakuan Yang a, Fen Wang b, Bo Xiao: **Economic analysis of power generation from floating solar chimney power plant,** PR China,February 2008

[25] Xinping Zhoua, Jiakuan Yanga,_, Bo Xiaoa, Guoxiang Hou : **Simulation of a pilot solar chimney thermal power generating equipment**, China 2006

[26] Xinping Zhou a,*, Jiakuan Yang b, Bo Xiao b, Guoxiang Hou c, Fang Xing b : **Analysis of chimney height for solar chimney power plant**, PR China 2008

[27] Xinping Zhoua; Jiakuan Yangb; Xiaob Bo; Guoxiang Houc; Yingying Wub: **Numerical Investigation of a Compressible Flow through a Solar Chimney,** China 2009

[28] Bacharoudis E., Vrachopoulos M.GR., Koukou M.K., Filios A.E.: **Numerical investigation of the buoyancy-induced flow field and heat transfer inside solar chimneys**, Greece, May 2006

[29] Clever Ketlogetswea, Fiszdonb Jerzy K., Seabea Omphemetse O.: **Solar chimney power generation project—The case for Botswana** , USA 2007

[30] Padki1 M. M. and Sherif2S. A.: **On a simple analytical model for solar chimneys**, USA 1999

[31] Papageorgiou Christos D.: **Floating Solar Chimney versus Concrete Solar Chimney Power Plants**, Greece 2007

[32] Papageorgiou Christos D.: **Carbon Emissions and Floating Solar Chimney Technology**, Greece 2009

[33] Henry Pastohr1, Oliver Kornadt1 and Klaus G.urlebeck: **Numerical and analytical calculations of the temperature and flow field in the upwind power plant**, Germany 2004

[34] Burek S.A.M. a,*, Habeb A.: **Air flow and thermal efficiency characteristics in solar chimneys and Trombe Walls**, UK 2006